A CHARACTERIZATION OF NETWORK PERFORMANCE: THE ROLE OF COMMUNICATION DIRECTIONALITY AND SYSTEM HETEROGENEITY

by
Hasan Giray Oral

A dissertation submitted to Johns Hopkins University in conformity with the requirements for the degree of Doctor of Philosophy

Baltimore, Maryland
August 2020

Abstract

Networked dynamical systems' ability to preserve the system equilibrium in the face of disruptive events or persistent disturbances can be an indication of the convergence efficiency and quantified as a measure of system performance. The performance analysis is usually facilitated by simplifications overlooking certain structural properties of the network that can potentially be significant to actual system behavior. We characterize the performance of networks in relation to these properties, such as communication directionality and system heterogeneity, and unravel their influence on overall performance. We examine performance metrics that quantify an aggregate system effort to maintain and/or restore a network equilibrium; formulated by a general quadratic function ($\mathcal{L}_2$ norm) of the system output. Using this approach, which builds on the widely-used $\mathcal{H}_2$ norm based analysis, we obtain novel closed-form solutions to the performance metrics. We then use them to identify the role of communication directionality and system heterogeneity in network performance.

Particularly, we show that the effect of communication directionality on performance can be characterized by the spectral properties of the weighted Laplacian matrix describing the network interconnection and the output performance matrix. Our results indicate that while this directionality can degrade performance, well-designed feedback can also exploit directionality in certain cases to mitigate this degradation or even lead to improved performance. We also demonstrate that performance is sensitive to the degree of connectivity in networks with directed interconnection, however it does not necessarily improve by increasing this degree of connectivity. We

then derive the asymptotic behavior of performance with respect to network size, and identify additional performance trade-offs associated with large-scale networks with communication directionality. In addition, we investigate system heterogeneity in droop-controlled inverter-based power systems, by relaxing the common assumption of uniformity of inverter control gains. This heterogeneity, which can result from the distribution of power demand between the inverters, can lead to performance limitations. Numerical examples verify and support our theoretical findings. Our results highlight the performance capabilities and limitations due to the structural properties of the network, and can inform judicious feedback design.

Dissertation Readers

Dr. Dennice Gayme (Advisor)
Associate Professor
Department of Mechanical Engineering
Johns Hopkins University

Dr. Enrique Mallada
Assistant Professor
Department of Electrical and Computer Engineering
Johns Hopkins University

Dr. Noah J. Cowan
Professor
Department of Mechanical Engineering
Johns Hopkins University

Dedicated to my parents.

Acknowledgements

I am grateful for my advisor Dr. Dennice Gayme's guidance throughout my Ph.D. research. Without her invaluable support, the contributions of this dissertation would not have been possible. I am also greatly thankful for Dr. Enrique Mallada's support and advising in our joint work. I would also like to thank Dr. Noah J. Cowan for participating in my dissertation readers committee and providing feedback that improved this dissertation.

Many technical discussions with former and current colleagues from both Dr. Gayme's and Dr. Mallada's research groups, as well as collaborations with colleagues outside of the Johns Hopkins University are also greatly appreciated. Especially, I would like to thank Ted Grunberg, Dr. Emma Tegling, Chengda Ji, Dr. Carl Shapiro, Dr. Ismail Hameduddin, Dr. Joel Bretheim, Dr. Devrim Kaba and Charalampos Avraam for their insights. I would also like to thank the Department of Mechanical Engineering and the Whiting School of Engineering for providing the opportunity for pursuing this degree.

I am absolutely grateful for my parents who have always selflessly supported me. Any achievement I might have is thanks to them. This dissertation is dedicated to them.

Contents

List of Tables

List of Figures

Chapter 1

Introduction

Co-operation of multiple agents in order to achieve a common objective is intrinsic to various types of dynamical systems that can be abstracted from biology, sociology, physics and engineering. In its simplest form, this co-operation can be understood as an iterative information exchange between this collection of agents that can eventually converge to an equilibrium. Such systems are generally termed networked dynamical systems.

In certain cases, agents can reach an agreement on their equilibrium state -achieve consensus- which is referred to as network synchronization. Consensus networks, i.e. single, double or higher order integrator systems with a feedback interconnection, represent a broad class of networked dynamical systems and provide a widely used framework for network analysis. In this setting, the 'closed-loop' is determined by state or output feedback based on relative measurements between agents; with the possible addition of feedback based on measurements with respect to an absolute reference frame. For example, the DeGroot model [3] poses the question of synchronization for networked dynamical systems in a simple setting. Each agent receives information from a subset of agents in the network in order to update its state. This model shows that after a sufficient number of iterations, the agents achieve consensus if certain conditions on the network (underlying communication structure) are satisfied. This notion of network synchronization has been studied in various contexts. For example,

achieving consensus (synchronization of states) [3–12] can be understood as an opinion agreement of the agents in social interaction networks or synchronization of the grid frequency in alternating current (AC) power networks.

These consensus protocols are closely related to co-ordination problems such as flocking of vehicles, robots or groups of bird or fish; that are concerned with attaining a desired geometric formation while maintaining a common velocity [13–18]. Naturally, these applications can exhibit equilibrium states that are not necessarily in agreement. Similarly, power networks can exhibit non-synchronous convergence, i.e. the equilibrium values for voltage phase angles [11, 12, 19] and magnitudes [19–21] can be non-uniform. For the purposes of our discussion, the distinction between network convergence and synchronization is insignificant.

In this thesis, we are primarily interested in how 'well' a networked dynamical system can maintain its equilibrium given perturbations to it; namely the network performance. The research questions we study are motivated by engineering systems such as vehicle networks and the electric power grid; however our results are generally applicable to a broader class of systems. In this chapter, we first provide a brief overview of the work on the convergence properties of networks. We then discuss different notions of network performance and related literature. We follow this discussion with a review of the results pertaining to the role of certain network topological characteristics in performance and identify relevant questions for our research motivation. We then provide a summary of our contributions and a detailed overview of our results.

1.1 Background on Network Convergence

Convergence properties of networks have been widely studied, see e.g. [3–29]. Many works investigating convergence in networks build on the principles of the DeGroot model [3], in which each agent in the network updates their state as a weighted

average of their own state with that of their neighbors. This discrete-time model can describe 'first-order' dynamics of agents and can be represented by single-integrator networks in continuous time models [5, 6, 8, 11, 17, 23, 24]. Double-integrator networks [4, 7, 9–11, 13–16, 18], which can use feedback of first and second-order states, can for example represent a class of systems that have inertia as well as damping including vehicle networks and power networks with synchronous generators.

The network structure and constraints imposed on the feedback interconnection are also important parameters in convergence. Namely, the effect of time-delay in communication between agents is considered in [5, 6, 10, 25, 26]. Time-varying network interconnection topologies can represent unreliable communication links or time-dependent sensing constraints [5, 6, 15, 16, 18, 22–24, 26]. In addition, the coupling between the agents can be non-linear, i.e. the feedback received by agents can be given by a non-linear function of relative state measurements [6, 11, 13–18].

We next provide some background for our main research focus of performance evaluation of networks. For a more comprehensive survey of work on convergence in networks, we refer the reader to [30–32].

1.2 Evaluation of Network Performance

Network performance can be defined such that it quantifies a variety of system attributes that are related to convergence properties. For example, in the presence of disturbances that perturb the system from its equilibrium, the network tries to restore this equilibrium or converge to a new one; which leads to transient behavior. In this setting, network performance can be captured in terms of the signal energy associated with these transients; and can be used as a metric of convergence efficiency. Our focus is on this notion of performance. It is standard practice to compute the performance metrics quantifying the total system energy through the $\mathcal{H}_2$ system

norm [33]. A related performance metric is the system gain quantifying the worst-case input amplification which can be an indication of the robust stability of the network; and can be described in terms of the $\mathcal{H}_\infty$ system norm [33, 34].

In networked dynamical systems, these norms can be used to quantify robustness to disturbances and capture a combined effect of agent dynamics and the network topological properties (underlying communication structure). In this work, we develop a novel analysis framework that builds on the $\mathcal{H}_2$ based performance metrics of network dynamical systems in order to characterize the precise effect of certain network topological properties on the overall system performance. Next, we present an overview of the literature related to this class of performance metrics.

1.2.1 Performance as Efficiency of Network Convergence

Network robustness to disturbances can be evaluated using performance metrics that quantify convergence efficiency. These metrics, for example, can be defined in terms of the lack of coherence or the degree of disorder in first order (single-integrator) [1, 35–41] and second order (double-integrator) [1, 42–48] consensus networks. The lack of coherence refers to a network aggregate of the deviation from the synchronous equilibrium state, whereas the degree of disorder may refer to aggregate state errors of agents with respect to nominal values. In this sense, the former can be interpreted as a special case of the latter and also a global performance metric for the network. For spatial formations of agents, the degree of disorder can be specified as short or long range state errors, which respectively quantify the level of cohesion between agents that are relatively close to or distant from each other within the network [1]. For example, these metrics are widely used for vehicle networks but also are applicable to a broader class of systems. Network disorder has been analyzed in terms of the underlying interconnection structure and network size, which can be measured either in terms of the number of agents [1, 38–41, 43, 46, 48] or the spatial dimension of agent

interactions [1, 39–41, 43].

Robustness metrics of power systems are closely related to the degree of network disorder in formation problems. For example, these metrics can quantify the network incoherence in terms of the real power losses or the deviation from the equilibrium values of voltage phase/frequency or magnitude in transmission and inverter-based networks due to system-wide transients resulting from disturbances [49–60]. The transient resistive losses have been investigated using the linearized swing dynamics of a Kron-reduced transmission network [50], a structure preserving network model of a renewable energy integrated power system [61], as well as a model of droop-controlled microgrids with coupled frequency and voltage dynamics [51].

Certain works build on the framework of standard consensus protocols and power system models by introducing additional control that aims to improve overall system performance. Controllers that have been proposed include dynamic feedback [43, 48, 52–54] and optimization based approaches [55, 56]. Control nodes [62] and virtual inertia placement [63] have been proposed to optimize the synchronization performance in constant voltage transmission grids. Dynamic control strategies such as distributed proportional-integral (PI) control have been shown to reduce transient resistive losses [64]. A dynamic droop control based on lead-lag compensation has also been shown to improve the robustness to measurement noise and delay and eliminate the frequency overshoot (frequency nadir) [53, 65]. It has also been demonstrated that proportional-derivative (PD) control can mitigate high frequency oscillations in transmission networks [66].

We are interested in investigating the underlying effect of network topological characteristics on the overall system performance. Next, we provide background on the literature that relates to this aspect of networks.

1.3 The Role of Network Topological Characteristics in Performance

As previously outlined, a widely utilized approach to quantify performance in systems subjected to distributed disturbances is to select a system output such that the desired metric is defined through the input-output $\mathcal{H}_2$ norm of the system. Certain $\mathcal{H}_2$ based performance metrics for systems whose underlying graphs are undirected can be obtained in closed form, e.g. [1, 42, 50, 53, 56]. Related performance metrics have also been evaluated in terms of the effective resistance of undirected graphs [42, 67, 68], which allows for efficient computational approaches [69].

Much of the existing literature on evaluating the performance in systems with directed interconnection topologies considers restrictive scenarios on the graph topology (e.g. spatially invariant [70] and nearest-neighbor type interactions [46]; or systems with normal Laplacian matrices [36, 37, 47]) with closed-form solutions obtained only for specific metrics (full state [71], degrees of disorder [1], etc.). The notion of effective resistance has been extended to directed graphs [72, 73] within a framework that can be used to compute network incoherence for single-integrator networks.

Closed-form expressions for more general quadratic performance metrics of double-integrator networks over undirected graphs formulated in terms of the $\mathcal{L}_2$ norm of the system output have also been obtained [59, 60, 74]. An extension to directed graphs with diagonalizable Laplacian matrices was provided for $\mathcal{H}_2$ based metrics [75], however a precise understanding of the role that the underlying network architecture plays is still lacking. This thesis aims to address this problem by proposing a novel framework of computing the general quadratic performance metrics of networks over directed graphs; and revisiting important classes of graph topologies to unravel previously undiscovered properties of network directionality.

In addition to edge directionality, we also study the heterogeneity of nodal param-

eters in networks, specifically in inverter-based power systems. Much of the literature focuses on identical nodal dynamics, which simplifies the analysis significantly while still providing insight into the robustness of droop control [51]. However, this simplified setting prevents the investigation of a number of important situations that can arise in practice. For example, power sharing constraints resulting from a load demand that is heterogeneous across the network lead to heterogeneous droop gains [12, 19]. There has been work in transmission systems with heterogeneous inertias, which provides a step response characterization of the synchronous system frequency [59, 60]. In a similar setting, the interaction between the network topology (undirected) and this synchronous frequency is studied [66]. However, extensions to inverter-based systems which are typically far less uniform by design have yet to be addressed.

1.4 Contributions

As outlined in the previous section, topological characteristics of the network are often overlooked in performance analysis, through simplifications such as the assumption of symmetric feedback coupling between agents (undirected interconnection) and nodal homogeneity of dynamics/control. In this thesis, we relax some of these simplifying assumptions, and show that network topological characteristics can play a significant role in overall system performance. We categorize our contributions into two areas; pertaining to edge directionality and nodal heterogeneity. While the main focus of this work is on understanding the effect of edge directionality on performance; our results on nodal heterogeneity provide useful insights about design trade-offs in inverter-based power systems.

Although the results from the literature represent progress into a wide range of special cases, a unified treatment of general performance metrics over *arbitrary* directed graphs has yet to be developed. This thesis aims to lay the foundations for such a framework via the following contributions:

1. We provide a novel unifying approach to compute a general class of quadratic performance metrics for single and double integrator systems defined over directed graphs that have at least one globally reachable node (Chapter 4).

2. We use the closed-form solutions resulting from this approach to demonstrate that overall network performance is determined by an interaction between network topological characteristics (e.g. edge directionality and connectivity) and the control strategy. In particular, we show that

(a) The effect of edge directionality on performance can be characterized by the respective spectral structures of Laplacian and output matrices, which needs to be accounted for in judicious feedback design (Chapter 5).

(b) While performance is sensitive to the degree of connectivity in directed graphs, the relationship is not monotonic (Chapter 6).

3. Using our novel closed-form solutions within the framework of spatially invariant systems, we derive the asymptotic scalings of performance metrics that quantify local and global degrees of network disorder. In addition, we identify a subclass of spatially invariant systems and performance metrics for which the scaling bounds have infinite value (i.e. the input-output system is unstable) for finite network size (Chapter 7).

By relaxing the assumption of uniform nodal dynamics in droop-controlled inverter-based power systems, we evaluate performance metrics quantifying system robustness for a more realistic scenario with possibly heterogeneous droop control gains. This gain heterogeneity, which can result from power sharing constraints imposed on the inverters at each node, is shown to lead to performance limitations (Chapter 3).

1.5 Overview of the Results

Now we provide a brief overview of our results and the organization of this work. We begin with the results related to power networks with nodal heterogeneity, followed by an introduction to our novel performance analysis framework for directed networks. Then, using this general framework, we investigate the relationship between performance and network topological characteristics such as edge directionality and connectivity. Following a detailed analysis of finite-size networks, we then focus on 'large-scale' directed networks, investigating how performance metrics of disorder scale as the network size grows. We finally present generalizations of our closed-form solutions for quadratic performance metrics to the class of networks over directed graphs that have at least one globally reachable node. These results are presented in the following chapters:

Chapter 3. *Performance of Droop-controlled Microgrids with Heterogeneous Inverter Ratings:* We analyze the overall system robustness in terms of two performance metrics: the frequency and voltage synchronization cost (the signal energy associated with the transient deviation from the synchronous state) and the transient resistive power losses; given distributed impulse disturbances. We derive closed-form solutions for these metrics in terms of heterogeneous droop-control gains and network properties; and investigate performance limitations associated with both frequency and voltage dynamics.

Chapter 4. *A New Analysis Framework for the Quadratic Performance Metrics of Directed Networks:* We develop a novel framework to compute the quadratic performance metrics in closed-form for a general class of networks over arbitrary directed graphs that have at least one globally reachable node. We use a frequency-domain approach and exploit the algebraic properties of the weighted graph Laplacian matrices representing the network interconnection and the output matrices defining

the performance metrics to derive the closed-form solutions. We first provide the closed-form solutions for the performance metrics of single and double-integrator networks over arbitrary directed graphs that have at least one globally reachable node. We then use our framework in the subsequent chapters to analyze important subclasses of directed networks.

Chapter 5. *Effect of Communication Directionality on Performance:* In this chapter, we focus on the subclass of single and double-integrator systems whose feedback interconnection topologies can be described by normal Laplacian matrices. We first provide the simplified closed-form solutions for the general performance metrics of this special class of systems. Then, we present a comparison between systems with directed interconnection and their undirected counterparts (obtained by 'symmetrizing' the directed feedback structure); demonstrating that performance becomes sensitive to control strategy (e.g. availability of state measurements, using feedback in different state variables) for systems with communication directionality.

Chapter 6. *Effect of Connectivity on the Performance of Directed Networks:* In this chapter, we investigate the role of the degree of connectivity in the performance of single and double-integrator networks that have communication directionality. We focus on a more general class of directed graphs compared to the previous chapter; which emit diagonalizable Laplacian matrices, and provide the closed-form solutions for the performance of this class of systems using our general analysis framework from Chapter 4. Then we study the relationship between performance quantified by a specific network coherency metric (aggregate state deviation from the average) and the degree of connectivity associated with various feedback interconnections such as directed cyclic ω-nearest neighbor networks and all-to-one (imploding star) networks.

Chapter 7. *Disorder in Large-scale Networks with Uni-directional Feedback:* Following a detailed analysis of finite-size networks, we then proceed to evaluate the scaling properties of spatially invariant systems with interconnection directionality;

represented by directed toric lattices. We focus on subclasses of such network interconnections and performance metrics that quantify the network disorder. We derive the asymptotic scaling properties of bounds on these performance metrics as the network size grows, for certain combinations of state feedback. In this setting, we also identify other combinations of state feedback for which the scaling bounds have infinite value (i.e. the input-output system is unstable) for finite network size. Our results indicate a trade-off between communication cost and scalability.

We conclude this chapter by providing references to the publications that resulted from our contributions. Particularly, the material in Chapter 3 is based on

- **H. G. Oral** and D. F. Gayme, "Performance of Droop-Controlled Microgrids with Heterogeneous Inverter Ratings," in Proceedings of the 2019 European Control Conference, June 2019, pp. 1398–1405.

The material in chapters 4, 5 and 6 is based on

- **H. G. Oral**, E. Mallada, and D. F. Gayme, "Performance of Single and Double-Integrator Networks over Directed Graphs," arXiv preprint, November 2019, arXiv:1911.00791,

- **H. G. Oral**, E. Mallada, and D. F. Gayme, "Performance of First and Second Order Linear Networked Systems over Digraphs," in Proceedings of the 56^{th} IEEE Conference on Decision and Control, December 2017, pp. 1688–1694.

The material in Chapter 7 is based on

- **H. G. Oral** and D. F. Gayme, "Disorder in Large-Scale Networks with Uni-Directional Feedback," in Proceedings of the 2019 American Control Conference, July 2019, pp. 3394–3401.

Following the presentation of our results, we provide concluding remarks and present possible directions for future work.

The next chapter sets up the preliminaries for the thesis and formalizes the description of the research questions we study.

Chapter 2

Preliminaries and Problem Description

We begin by introducing definitions, mathematical preliminaries and standard results from the literature.

2.1 Stability of Linear Time-Invariant Systems

A linear time invariant-system T can be viewed as a linear mapping from an input $\mathrm{w}(t) \in \mathbb{R}^p$ to an output $y(t) \in \mathbb{R}^q$ and it can be represented by its impulse response function $T(t)$ in the time-domain. Throughout this work, we are interested in causal systems, i.e. the system output does not depend on information from future time, therefore we assume that $T(t) = 0$ for $t < 0$. The output response to an input $\mathrm{w}(t)$ can be computed using the convolution integral:

$$y(t) = \int_0^t T(t-\tau)\mathrm{w}(\tau)d\tau, \quad t \geq 0. \tag{2.1}$$

With a slight abuse of notation, we will use the letters denoting the signals and impulse response functions in the time domain to denote their respective signals and transfer functions in the frequency-domain. Then, we have

$$y(s) = T(s)\mathrm{w}(s), \quad s \in \mathbb{C},$$

where each function is given by the Laplace transform of their time-domain counterparts.

If it admits a time-domain realization, T can also be represented by the state-space equations:

$$\begin{aligned} \dot{\boldsymbol{\phi}}(t) &= \mathcal{A}\boldsymbol{\phi}(t) + \mathcal{B}\mathrm{w}(t), \\ y(t) &= \mathcal{C}\boldsymbol{\phi}(t) + \mathcal{D}\mathrm{w}(t), \end{aligned} \tag{2.2}$$

where $\mathcal{A}$, $\mathcal{B}$, $\mathcal{C}$ and $\mathcal{D}$ are real matrices. Equivalently, the transfer function of $T(s)$ is given by:

$$T(s) = \mathcal{C}(sI - \mathcal{A})^{-1}\mathcal{B} + \mathcal{D}.$$

We are interested in several notions of stability throughout this work, which we present next.

Definition 2.1 (Asymptotic Stability, [76])**.** *The unforced system*

$$\dot{\boldsymbol{\phi}}(t) = \mathcal{A}\boldsymbol{\phi}(t), \quad \boldsymbol{\phi}(0) = \boldsymbol{\phi}_0, \quad t \geq 0 \tag{2.3}$$

is asymptotically stable if $\boldsymbol{\phi}(t) \to 0$ *as* $t \to \infty$ *for arbitrary* $\boldsymbol{\phi}_0$*.*

The following well-known result pertains to the asymptotic stability of the unforced system.

Fact 2.1. *[77] The unforced system in* (2.3) *is asymptotically stable if and only if all of the eigenvalues of* $\mathcal{A}$ *are on the open left-half plane.*

Another important notion of stability is related to the input-output system $T(t)$. The system is called stable if the output $y(t)$ remains bounded for all time, given a bounded input $\mathrm{w}(t)$. The formal definition is as follows.

Definition 2.2 (BIBO Stability, [77])**.** *The realization* (2.2) *of* T *is bounded-input-bounded-output (BIBO) stable if*

$$\sup_{t\geq 0}\|\mathrm{w}(t)\| < \infty \;\Rightarrow\; \sup_{t\geq 0}\|\mathrm{y}(t)\| < \infty.$$

BIBO stability of T is guaranteed by the asymptotic stability of (2.3). But the converse is not always true. In this case, a certain subset of the modes of $\mathcal{A}$ determines stability. This subset is given by all of the modes that can be both controlled by the input w and observed from the output y. In order to make the argument precise, we state the concepts of controllability and observability.

Definition 2.3 (Controllability)**.** *System* (2.2) *is controllable on* $[0, t_f]$ *if there exists a continuous input* $\mathrm{w}(t)$ *such that* $\boldsymbol{\phi}(t_f) = 0$ *for any* $\boldsymbol{\phi}(0) = \boldsymbol{\phi}_0$*.*

Definition 2.4 (Observability)**.** *System* (2.2) *is observable on* $[0, t_f]$ *if* $\boldsymbol{\phi}(0) = \boldsymbol{\phi}_0$ *can be uniquely determined from* $y(t)$*.*

Using these definitions, the following result establishes the connection between BIBO stability of (2.2) and the asymptotic stability of (2.3).

Fact 2.2. *Suppose that realization* (2.2) *is controllable and observable. Then, it is BIBO stable if and only if* (2.3) *is asymptotically stable.*

Next, we provide a brief review of signal and system norms, which is central to the performance analysis in this work.

2.2 Signal and System Norms

The main signal norm that is going to be used in this work is the $\mathcal{L}_2$ norm. It is given by

$$\|y\|_{\mathcal{L}_2} = \left(\int_0^\infty y(t)^* y(t) dt \right)^{1/2}, \tag{2.4}$$

which provides a measure of the total energy of the system response $y(t)$.

For a strictly proper and stable system $T(s)$, its $\mathcal{H}_2$ norm is defined as

$$\|T\|_{\mathcal{H}_2} = \left(\sup_{\epsilon > 0} \frac{1}{2\pi} \int_{-\infty}^{\infty} \mathrm{tr}\left[T(\epsilon + j\omega)^* T(\epsilon + j\omega) \right] d\omega \right)^{1/2} \tag{2.5}$$

and it can be computed by

$$\|T\|_{\mathcal{H}_2} = \left(\frac{1}{2\pi}\int_{-\infty}^{\infty} \mathrm{tr}\left[T(j\omega)^* T(j\omega)\right] d\omega\right)^{1/2} \tag{2.6}$$

in the frequency-domain and

$$\|T\|_{\mathcal{H}_2} = \left(\int_{0}^{\infty} \mathrm{tr}\left[T(t)^* T(t)\right] dt\right)^{1/2} \tag{2.7}$$

in the time-domain [34]. The equivalence of these two computations is due to Parseval's theorem.

Remark 2.1. *We note that for a system that is not BIBO stable (closed right-half-plane poles exist), the definition of the $\mathcal{H}_2$ norm in (2.5) would lead to an infinite value. In general, (2.6) can be used to define a system 2-norm which can be finite for a certain class of unstable systems [78], which is outside of the scope of this work.*

Noting that a strictly proper system has $\mathcal{D} = 0$, the realization (2.2) can be used to evaluate the $\mathcal{H}_2$ norm through the time domain representation in (2.7):

$$\|T\|_{\mathcal{H}_2}^2 = \mathrm{tr}(\mathcal{B}^* X \mathcal{B}), \quad X = \int_0^\infty e^{\mathcal{A}^* t} \mathcal{C}^* \mathcal{C} e^{\mathcal{A} t} dt,$$

where the observability Gramian X can be computed by solving the Lyapunov equation

$$\mathcal{A}^* X + X\mathcal{A} = -\mathcal{C}^*\mathcal{C},$$

when T is BIBO stable. An equivalent computation can be performed by using the controllability Gramian of T.

There is a connection between the $\mathcal{L}_2$ signal norm of the system response in (2.4) and the $\mathcal{H}_2$ norm of system T in (2.7), which can be established through one of the standard interpretations of the $\mathcal{H}_2$ norm [49]. In general, these interpretations illustrate that the $\mathcal{H}_2$ norm can be computed in terms of the system response when the system is subjected to a specific input. We next review two of these interpretations as they provide background for the analysis in the subsequent chapters.

- Consider a white noise input $\mathrm{w}(t)$ with unit covariance, i.e. $E[\mathrm{w}(\tau)\mathrm{w}(t)^*] = \delta(t-\tau)I$. Then the squared $\mathcal{H}_2$ norm of T quantifies

$$\|T\|_{\mathcal{H}_2}^2 = \lim_{t\to\infty} E[y(t)^* y(t)], \tag{2.8}$$

  i.e. the steady-state variance of the system response $y(t)$.

- Consider an impulsive input to a single input channel, i.e. $\mathrm{w}^{(i)}(t) = e_i\delta(t)$ where e_i is the vector with a 1 at the i^{th} entry and zeros elsewhere, $i \in \{1,\dots,p\}$. Then the squared $\mathcal{H}_2$ norm of T quantifies

$$\|T\|_{\mathcal{H}_2}^2 = \sum_{i=1}^{p} \int_0^\infty y^{(i)}(t)^* y^{(i)}(t)dt, \tag{2.9}$$

  where $y^{(i)}(t)$ denotes the system response to $\mathrm{w}^{(i)}(t)$. In other words, the squared $\mathcal{H}_2$ norm of T can be computed as the sum of the squared $\mathcal{L}_2$ norms of the system responses $y^{(i)}(t)$ to an impulse at the i^{th} input channel.

The stochastic interpretation of the $\mathcal{H}_2$ norm given in (2.8) can for example be used to compute the steady-state variance of an output signal that measures the deviation from a desired trajectory or equilibrium, in the presence of persistent random disturbances. In contrast, disruptive events can be modeled by impulsive inputs and the $\mathcal{H}_2$ norm computation in (2.9) quantifies the aggregate signal energies of the system responses due to these impulsive inputs. We refer to these interpretations throughout the thesis in order to specify the relationship between the disturbance inputs and the performance metrics.

2.3 Graph Theory

In this section, we introduce basic concepts of graph theory, particularly related to the directionality of graphs, algebraic tools that facilitates the analysis of networked dynamical systems and fundamental properties.

Definition 2.5 (Undirected Graph [79]). *An undirected graph is a pair* $\mathcal{G} = \{\mathcal{V}, \mathcal{E}\}$ *with a set of vertices (nodes)* $\mathcal{V}$ *and a set of edges* $\mathcal{E}$ *containing unordered pairs of the vertices in* $\mathcal{V}$.

Definition 2.6 (Directed Graph [79]). *A directed graph (digraph) is a pair* $\mathcal{G} = \{\mathcal{V}, \mathcal{E}\}$ *with a set of vertices (nodes)* $\mathcal{V}$ *and a set of directed edges* $\mathcal{E}$ *containing ordered pairs of the vertices in* $\mathcal{V}$, *i.e.* $\mathcal{E} \subseteq \mathcal{V} \times \mathcal{V}$.

In line with the definition of a directed graph given above, a weighted digraph can be defined as $\mathcal{G} = \{\mathcal{V}, \mathcal{E}, \mathcal{W}\}$, by introducing a weight associated with each edge. Here, the set of edge weights is given by $\mathcal{W} = \{w_{ij} > 0 \mid (i,j) \in \mathcal{E}\}$. Using the same definition, we set $b_{ij} = b_{ji}$ for a weighted undirected graph, since $(i,j) \in \mathcal{E}$ if and only if $(j,i) \in \mathcal{E}$.

The following definitions of the neighbors of a given node in the graph is useful for the algebraic representations of a graph.

Definition 2.7 (In-and-out-neighbors [79]). *For a node* $i \in \mathcal{V}$ *the in-neighbor set is given by* $\mathcal{N}^{in}(i) = \{j \in \mathcal{V} \mid (j,i) \in \mathcal{E}\}$ *and its out-neighbor set is given by* $\mathcal{N}^{out}(i) = \{j \in \mathcal{V} \mid (i,j) \in \mathcal{E}\}$.

Based on the number of neighbors and edge weights, we assign degrees to each node.

Definition 2.8 (Weighted In-and-out-degrees [79]). *The weighted out-degree (in-degree) is given by the sum of the weights associated with the out-neighbors (in-neighbors) of a node. We write*

$$d_{out}(i) = \sum_{j \in \mathcal{N}^{out}(i)} w_{ij}, \qquad d_{in}(i) = \sum_{j \in \mathcal{N}^{in}(i)} w_{ji}, \qquad i \in \mathcal{N}.$$

For an unweighted graph, the same definitions hold with unit edge weights, hence degrees are given by the number of neighbors.

Using these definitions, we can state algebraic representations of graphs [79]. $\mathcal{G}$ can be represented by a square, entry-wise non-negative matrix A called the *adjacency* matrix which is given by

$$[A]_{ij} = \begin{cases} w_{ij} \in \mathcal{W}, & (i,j) \in \mathcal{E} \\ 0, & (i,j) \notin \mathcal{E} \end{cases}, \qquad i,j \in \mathcal{N}.$$

Using the adjacency matrix and the weighted out-degrees of the nodes, the *weighted graph Laplacian* matrix can be defined as

$$L = \text{diag}\left(d_{out}(i)\right)_{i\in\mathcal{N}} - A,$$

which is given entry-wise as

$$e_{ij} := [A]_{ij}, \quad [L]_{ij} = \begin{cases} \sum\limits_{j\in\mathcal{N}\setminus\{i\}} e_{ij}, & i = j \\ -e_{ij}, & i \neq j \end{cases}, \qquad i,j \in \mathcal{N}.$$

An equivalent definition based on the weighted in-degrees can also be used for both matrices. We list some important properties of the weighted graph Laplacian:

- Rows of L sum to zero (i.e. $L\mathbf{1} = 0$, with $\mathbf{1} = \begin{bmatrix} 1 & \dots & 1 \end{bmatrix}^\intercal$). Therefore, zero is an eigenvalue of L.
- Columns of L sum to zero (i.e. $\mathbf{1}^\intercal L = 0$) if and only if G is weight-balanced (i.e. $d_{out}(i) = d_{in}(i)$ for all $i \in \mathcal{N}$) [79].
- Denote the eigenvalues of L by λ_i for $i \in \mathcal{N}$. Then, $\text{Re}[\lambda_i] > 0$ if and only if $\lambda_i \neq 0$, i.e. non-zero eigenvalues of L lie on the open right-half plane [79].

The algebraic multiplicity of zero as an eigenvalue of L can be characterized based on the connectivity of $\mathcal{G}$ [79]. As a simplifying assumption, we are only interested in the case in which the algebraic multiplicity is one, however results can be generalized. The following definitions are useful for the discussion.

Definition 2.9 (Directed Path and Cycle [79])**.** *A directed path is an ordered sequence of nodes* $\{k_1, \dots, k_p\} \subseteq \mathcal{N}$ *such that* $(k_i, k_{i+1}) \in \mathcal{E}$ *for* $i = 1, \dots, p-1$*. A directed path is called a cycle if every element of* $\{k_2, \dots, k_{p-1}\}$ *is unique and* $k_1 = k_p$*.*

Definition 2.10 (Globally Reachable Node [79]). *A node $i \in \mathcal{N}$ is globally reachable if a directed path to i exists from every node $j \in \mathcal{N} \setminus \{i\}$.*

The following result characterizes the class of graphs for which the algebraic multiplicity of the zero eigenvalue of the weighted Laplacian matrix is one.

Fact 2.3 ([79]). *The algebraic multiplicity of the zero eigenvalue of the weighted graph Laplacian L is one if and only if $\mathcal{G}$ contains at least one globally reachable node.*

An implication of this result is that strongly connected directed graphs (every node is globally reachable) and connected undirected graphs have this property.

We next introduce the class of networked dynamical systems that will be studied in this work.

2.4 Single and Double-Integrator Networks

A large class of networked dynamical systems can be abstracted in the form of (2.2), where the system matrix $\mathcal{A}$ depends on an interconnection (feedback) between the agents in the network. Assuming that $\mathcal{A}$ represents the closed-loop dynamics, this realization can be used to investigate system performance, by computing system norms from a disturbance input w to a performance output y.

Consider a network of n agents represented by a weighted directed graph $\mathcal{G}$. The agents are denoted by the nodes in $\mathcal{N} = \{1, ..., n\}$ and the network (feedback) interconnection between agents is represented by the directed edges in $\mathcal{E} = \{(i, j) \mid i, j \in \mathcal{N}, i \neq j\}$ and the associated edge weights in $\mathcal{W}$. The definition of $\mathcal{E}$ implies that there are no self-loops in the graph.

We consider two types of nodal (agent) dynamics. The first one is a single-integrator system of the form

$$\dot{x}_i = u_i + \mathrm{w}_i,$$

at each $i \in \mathcal{N}$, where the control input is given by a weighted combination of relative state measurements of i with respect to its out-neighbors:

$$u_i = -\sum_{j=1}^{n} e_{ij}(x_i - x_j),$$

and w_i denotes the disturbance to the i^{th} agent. This results in the well-known single-integrator (first order consensus) network

$$\dot{x} = -Lx + \mathrm{w}. \tag{2.10}$$

This type of dynamics arises in many areas of networked dynamical systems such as biological networks or social influence networks.

The second type of system is governed by double-integrator dynamics of the form

$$\ddot{x}_i = u_i + \mathrm{w}_i,$$

where the control input is given by

$$u_i \;=\; -\,k_p x_i \;-\; \gamma_p \sum_{j=1}^{n} e_{ij}^{(x)}(x_i - x_j) \;-\; k_d \dot{x}_i \;-\; \gamma_d \sum_{j=1}^{n} e_{ij}^{(v)}(\dot{x}_i - \dot{x}_j) \qquad \forall i \in \mathcal{N}.$$

Adopting the terminology from vehicle networks, we refer to the first two terms in the control input as position feedback and the last two terms as velocity feedback. Each type of feedback has two components based on absolute and relative state measurements. In this case, there are possibly two different feedback interconnection topologies for each type of relative state feedback, defined over directed graphs $\mathcal{G}^{(x)}$ and $\mathcal{G}^{(v)}$. Here, $k_p, k_d \geq 0$ denote the absolute feedback gains and $\gamma_p, \gamma_d \geq 0$ denote the relative feedback gains. As before, w_i denotes the disturbance to the i^{th} agent. Defining $v := \dot{x}$, the double-integrator (second order consensus) network can be expressed in matrix form as

$$\begin{bmatrix} \dot{x} \\ \dot{v} \end{bmatrix} = \begin{bmatrix} 0 & I \\ -k_p I - \gamma_p L^{(x)} & -k_d I - \gamma_d L^{(v)} \end{bmatrix} \begin{bmatrix} x \\ v \end{bmatrix} + \begin{bmatrix} 0 \\ I \end{bmatrix} \mathrm{w}. \tag{2.11}$$

This type of dynamics can be used to study a broad class of networked systems such as vehicular networks or power networks.

Next, we briefly discuss a general formulation of performance metrics for this class of networked systems.

2.5 Performance Metrics

Performance metrics that are quadratic in the state variables are widely used to evaluate system robustness to disturbances. In this thesis we focus on the analysis of such metrics through a general output norm based approach in order to gain insight into how network topological properties such as communication directionality and system heterogeneity affect performance.

We are interested in performance metrics of the form

$$P = \|y\|_{\mathcal{L}_2}^2 = \int_0^\infty y(t)^* y(t) dt, \tag{2.12}$$

i.e. metrics formulated as the signal energy of a performance output $y(t)$, when the system is subject to an impulse input

$$\mathrm{w}(t) = \mathrm{w}_0 \delta(t) \tag{2.13}$$

with an arbitrary direction vector $\mathrm{w}_0 \in \mathbb{R}^n$. Similar metrics appear in [59] for networks over undirected graphs. Substitution of (2.13) and (2.1) into (2.12) gives

$$P = \int_0^\infty \mathrm{w}_0^* T(t)^* T(t) \mathrm{w}_0 dt, \tag{2.14}$$

therefore the performance metric P is given by a modified version of the $\mathcal{H}_2$ norm given by (2.7), which is 'weighted' by the input direction w_0. We note that (2.14) is finite if and only if $T(t)$ is BIBO stable. We will later discuss conditions that guarantee the IO stability of $T(t)$.

We now show that for a special case of the impulse input (2.13), the performance metric (2.14) can be computed using the $\mathcal{H}_2$ norm of $T(t)$. Although this connection is closely related to the standard interpretation in (2.9) [49], for completeness we provide a short proof below. This relationship will be used in the upcoming sections.

Proposition 2.1. *Consider a strictly proper system T, a random impulse input (2.13) with $E\left[\mathrm{w}_0\mathrm{w}_0^*\right] = I$ and zero initial condition. Then $\|T\|_{\mathcal{H}_2}^2 = E\left[\|y\|_{\mathcal{L}_2}^2\right]$.*

Proof. Assuming zero initial condition, the output is given by $y(t) = \mathcal{C}e^{\mathcal{A}t}\mathcal{B}\mathrm{w}_0$. Then

$$\begin{aligned} E\left[\|y(t)\|_{\mathcal{L}_2}^2\right] &= E\left[\mathrm{tr}\int_0^\infty \mathcal{C}e^{\mathcal{A}t}\mathcal{B}\mathrm{w}_0\mathrm{w}_0^*\mathcal{B}^*e^{\mathcal{A}^*t}\mathcal{C}^*dt\right] \\ &= \mathrm{tr}\int_0^\infty \mathcal{C}e^{\mathcal{A}t}\mathcal{B}\mathcal{B}^*e^{\mathcal{A}^*t}\mathcal{C}^*dt \;=\; \|T\|_{\mathcal{H}_2}^2. \end{aligned}$$

□

The squared $\mathcal{H}_2$ norm can be computed in terms of the sum of the squared $\mathcal{L}_2$ norms of each system response to an impulsive input at a single input channel, as given by the interpretation in (2.9). Proposition (2.1) provides a similar computation for the $\mathcal{H}_2$ norm, which is given by the expected value of the squared $\mathcal{L}_2$ norm of the system response to impulsive inputs at every input channel. These inputs have random directions that are spatially uncorrelated and of uniform magnitude.

Since we are focusing on nodal dynamics governed by integrators, we are interested in quantifying as performance the energy associated with states of different order. For example, for $C \in \mathbb{R}^{q\times n}$, the performance output

$$y = Cx \tag{2.15}$$

will be used to quantify the performance of the single-integrator network (2.10) and the double-integrator network (2.11) for metrics related to the position state x. For the double-integrator network (2.11), the performance output

$$y = Cv, \tag{2.16}$$

which quantifies performance metrics related to the velocity state v, will also be considered.

We will analyze system performance in terms of general metrics defined by the outputs (2.15) and (2.16). Widely used performance metrics of networked systems such as vehicle networks and power systems lie within this framework.

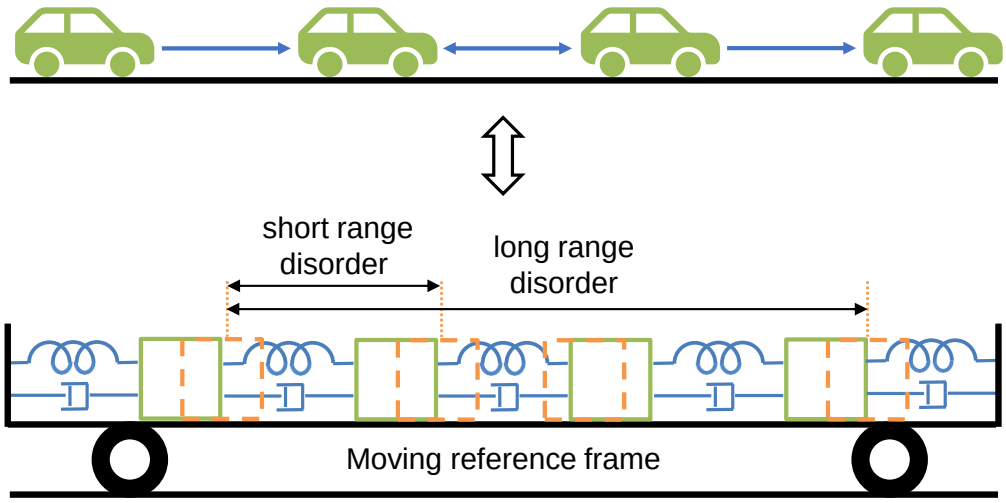

Figure 2-1. (Top) One-dimensional network (platoon) of vehicles with relative state feedback. **(Bottom)** Abstraction of the vehicle network as a sequence of masses coupled by linear springs and dampers on a moving reference frame. Disturbances can perturb the equilibrium and the system's effort to restore this equilibrium can be quantified through performance metrics of short range or long range disorder [1].

For example, consider a one-dimensional network (platoon) of vehicles given in Figure 2-1 (top). Through relative state feedback, a desired formation of vehicles can be achieved with a constant platoon velocity and desired spacing between vehicles. As illustrated in Figure 2-1 (bottom), this formation can be viewed as a sequence of masses coupled by linear springs and dampers over a reference frame moving at constant velocity. If this equilibrium is perturbed by disturbances, each vehicle deviates from the desired formation which is counter-balanced by an effort from the system to mitigate this deviation and restore the network equilibrium. This effort can be captured through the signal energy of the resulting transients; formulated as performance metrics quantifying a system aggregate of state deviations of agents from the equilibrium [1] and can be seen as a measure of network 'disorder'. As shown in Figure 2-1 (bottom), these metrics can quantify short range or long range disorder, depending on the proximity of state error measurements.

A class of performance metrics pertaining to power systems can also be described in analogy with the notion of disorder in vehicle networks. Consider an equivalent

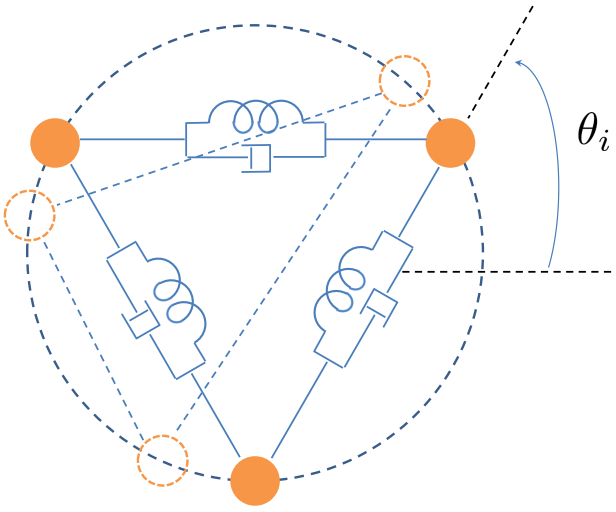

Figure 2-2. Coupled oscillators on a rotational reference frame and a perturbation to their equilibrium (figure is adapted from [2]).

model of a Kron-reduced (loads are lumped into line impedances) power network given in Figure 2-2. Generation units injecting power into the network can be modeled as coupled oscillators constrained to a rotational reference frame. At steady-state, the system attains constant nodal phase angle differences (determines the power-flow between nodes) and a common grid frequency. The effort required to restore the equilibrium after it is perturbed by disturbances can be evaluated for example in terms of performance metrics quantifying transient ressistive line losses [50] and the frequency synchronization cost [59]. The former can be formulated using a position-based performance output of the form (2.15) and the latter using a velocity-based output of the form (2.16).

In the next chapter, we focus on droop-controlled inverter-based power networks and investigate the effect of heterogeneous inverter ratings on performance. Then, we evaluate the role of communication directionality in network performance in the remainder of the thesis.

Chapter 3

Performance of Droop-controlled Microgrids with Heterogeneous Inverter Ratings

In this chapter we study the performance of a certain family of networks that exhibit heterogeneity of nodal parameters. Namely, we analyze the robustness of droop-controlled microgrids (inverter-based power systems) with heterogeneously rated inverters modeled by both frequency and voltage dynamics.

We consider two performance metrics in the presence of distributed impulse disturbances. The first one quantifies the total transient frequency and voltage deviations from the synchronous state while the other quantifies the associated total transient resistive losses. Both metrics are captured through the $\mathcal{L}_2$ norm of the system output. We derive closed-form solutions for these metrics in terms of the heterogeneous droop gains and properties of the network for the case of highly inductive lines (i.e. decoupled frequency and voltage dynamics). We show that the transient deviations from synchrony prevail even in the hypothetical case of infinite droop gains (i.e. infinite control action), which points to the importance of inertia in further mitigating these oscillations. We also show that if disturbances are uniform the transient resistive losses are a monotonically decreasing function of the active power droop gains regardless of network topology. On the other hand, these losses depend on both the reactive

power droop gains and the network topology due to the voltage dynamics. Numerical examples further analyzing the losses reveal that they can be amplified by high droop gain heterogeneity. These simulations also provide insights into how non-uniform line susceptances affect judicious selection of the droop gains for decreasing the losses.

The remainder of the chapter is organized as follows. Section 3.1 describes the system model, performance metrics and the structural assumptions undertaken. Section 3.2 provides our main results characterizing the system performance based on total transient frequency and voltage deviations as well as resistive losses. Section 3.3 provides numerical examples. Section 3.4 concludes the chapter.

3.1 Problem Formulation

3.1.1 Linearized Model of the Microgrid Dynamics

We adopt the framework in [19, 51] and consider a Kron-reduced network [80] of inverters over a weighted, undirected, and connected graph $\mathcal{G} = \{\mathcal{N}, \mathcal{E}\}$. Here $\mathcal{N} = \{1, ..., N\}$ is the set of nodes representing the inverters and $\mathcal{E} = \{\mathcal{E}_{ik}\}$ is the set of edges representing the lines.

The active and reactive power injections P_i and Q_i into the network at node i are given by

$$P_i = -g_{ii}V_i^2 + \sum_{i\sim k} g_{ik}V_iV_k\cos\theta_{ik} + b_{ik}V_iV_k\sin\theta_{ik}, \tag{3.1a}$$

$$Q_i = b_{ii}V_i^2 + \sum_{i\sim k} g_{ik}V_iV_k\sin\theta_{ik} - b_{ik}V_iV_k\cos\theta_{ik}, \tag{3.1b}$$

where V_i and θ_i are the respective nodal voltage magnitude and phase angle and $\theta_{ik} := \theta_i - \theta_k$ if $i \sim k$ (i.e. $\mathcal{E}_{ik} \in \mathcal{E}$). The conductance and susceptance of each line are respectively denoted by g_{ik}, $b_{ik} > 0$. Here $g_{ii} = \bar{g}_i + \sum_{i\sim k} g_{ik}$, and $b_{ii} = \bar{b}_i + \sum_{i\sim k} b_{ik}$ with shunt conductance and susceptance $\bar{g}_i$ and $\bar{b}_i$, respectively. We assume that shunt elements are purely inductive [21], i.e. $\bar{g}_i = 0$, and $\bar{b}_i \geq 0$. Assuming small

deviations from the equilibrium, the first-order Taylor series expansions of (3.1a) and (3.1b) around $(V_i^* = V_k^* = 1, \theta_{ik}^* = 0)$ lead to

$$\Delta P_i \approx \sum_{i \sim k} \left(b_{ik} \Delta\theta_{ik} - g_{ik}(\Delta V_i - \Delta V_k) \right), \tag{3.2a}$$

$$\Delta Q_i \approx 2\bar{b}_i \Delta V_i + \sum_{i \sim k} \left(g_{ik} \Delta\theta_{ik} + b_{ik}(\Delta V_i - \Delta V_k) \right), \tag{3.2b}$$

where the 'Δ' terms indicate the deviation of the respective variable from its equilibrium value. In the following, by an abuse of notation we omit the 'Δ' from these variables.

Remark 3.1. *By the choice of $\theta_{ik}^* = 0$ we assume that the phase angle differences are small at equilibrium, which is a common assumption in power systems analysis [50, 51].*

Droop control aims to operate each inverter at a common frequency ω^* and attain the desired nodal voltage magnitude V_i^*, active power P_i^* and reactive power Q_i^* via the following control laws [28]:

$$\omega_i = \omega^* - k_{P_i}(\hat{P}_i - P_i^*), \quad V_i = V_i^* - k_{Q_i}(\hat{Q}_i - Q_i^*), \tag{3.3}$$

where ω_i is the frequency, $\hat{P}_i$ and $\hat{Q}_i$ are the respective active and reactive power measurements, and $k_{P_i} > 0$ and $k_{Q_i} > 0$ are the active and reactive power droop gains at node i. We assume that the power measurements are governed by first order dynamics [51] with time constants τ_{P_i}, τ_{Q_i}. Differentiating (3.3) with respect to time gives the following closed-loop dynamics at each node i

$$\dot{\theta}_i = \omega_i, \quad \tau_{P_i}\dot{\omega}_i = -\omega_i + \omega^* - k_{P_i}(P_i - P_i^*), \tag{3.4a}$$

$$\tau_{Q_i}\dot{V}_i = -V_i + V_i^* - k_{Q_i}(Q_i - Q_i^*). \tag{3.4b}$$

Using equations (3.2), (3.4) and introducing the disturbance input w, the closed-loop dynamics can be written as

$$\dot{x} = Ax + B\mathrm{w}, \tag{3.5}$$

where

$$x := \begin{bmatrix} \theta^T & \omega^T & V^T \end{bmatrix}^T, \quad \mathrm{w} := \begin{bmatrix} (\mathrm{w}^P)^T & (\mathrm{w}^Q)^T \end{bmatrix}^T,$$

$$A := \begin{bmatrix} 0 & I & 0 \\ -T_P^{-1}K_P L_B & -T_P^{-1} & T_P^{-1}K_P L_G \\ -T_Q^{-1}K_Q L_G & 0 & -T_Q^{-1}(C_Q + K_Q L_B) \end{bmatrix}, \quad B := \begin{bmatrix} 0 & T_P^{-1} & 0 \\ 0 & 0 & T_Q^{-1} \end{bmatrix}^T,$$

$K_P := \mathrm{diag}\{k_{P_i}\}$, $K_Q := \mathrm{diag}\{k_{Q_i}\}$, $T_P := \mathrm{diag}\{\tau_{P_i}\}$, $T_Q := \mathrm{diag}\{\tau_{Q_i}\}$, $C_Q = \mathrm{diag}\{c_{Q_i}\}$. Here, $\mathrm{diag}\{\cdot\}$ denotes the diagonal matrix of the scalars in its argument and $c_{Q_i} = 1 + 2\bar{b}_i k_{Q_i}$. We define the weighted Laplacian matrix L_B as: $[L_B]_{ii} := \sum_{i\sim k} b_{ik}$, $[L_B]_{ik} := -b_{ik}$ if $i \sim k$, $[L_B]_{ik} := 0$ otherwise. L_G is defined similarly using the conductances g_{ik}. The eigenvalues of L_B are denoted by $0 = \lambda_1 < \lambda_2 \leq \cdots \leq \lambda_N$.

We will evaluate the system performance in the presence of a distributed impulse disturbance input of the form

$$\mathrm{w}(t) = \delta(t)\mathrm{w}_0, \tag{3.6}$$

where $\delta(t)$ denotes the Dirac delta function and $\mathrm{w}_0 \in \mathbb{R}^N$ defines the input magnitude and direction.

Remark 3.2. *As given by Proposition 2.1 and the interpretations of the $\mathcal{H}_2$ norm in (2.8) and (2.9), the special case of (3.6) in which $E\{\mathrm{w}_0\mathrm{w}_0^T\} = I$ has a connection with a white noise input $u(t)$ with unit covariance, i.e. $E\{u(0)u(t)^T\} = \delta(t)I$. This disturbance input naturally arises in $\mathcal{H}_2$ norm based analysis of power networks [50]. Therefore, (3.6) is a generalization that can model spatially correlated disturbance inputs.*

3.1.2 Performance Metrics

In this section we introduce the two performance metrics that are the subject of this work; the total transient deviation from frequency and voltage synchrony, and the total transient resistive power losses. The former is a measure of the efficiency of system synchronization in the presence of disturbances while the latter can be interpreted as the "cost" of this synchronization.

3.1.2.1 Deviation from Synchrony

In the following analysis we will show that the frequency can be decomposed as

$$\omega(t) = \bar{\omega}(t)\mathbf{1} + \tilde{\omega}(t)$$

in analogy with transmission networks [59], where $\bar{\omega}(t) \in \mathbb{R}$ denotes the synchronous system frequency and $\tilde{\omega}(t) \in \mathbb{R}^N$ denotes deviations from it. As discussed later, a similar decomposition is not always possible for $V(t)$ if the inverter ratings are heterogeneous, therefore we consider voltage deviations from the equilibrium. For the sake of simplicity, we also use the term "synchrony" for the voltage dynamics by an abuse of terminology. Combining these ideas the total transient deviation from synchrony can be quantified by

$$\Pi_{sync} = \int_0^\infty \|\tilde{\omega}(t)\|_2^2 dt + \int_0^\infty \|V(t)\|_2^2 dt =: \|y_{sync}\|_{\mathcal{L}_2}^2, \tag{3.7}$$

where $y_{sync} := \begin{bmatrix}\tilde{\omega}^T & V^T\end{bmatrix}^T$ defines the performance output and $\|\cdot\|_2$ denotes the Euclidean norm. The frequency part of the metric in (3.7) was used in [59] to quantify the deviations from synchrony in a transmission network with heterogeneous generator inertia, subjected to step disturbances.

3.1.2.2 Transient Resistive Power Losses

The instantaneous resistive power loss incurred across each line $\mathcal{E}_{ik}$ is

$$\Pi_{ik}^{loss} = g_{ik}|v_i - v_k|^2, \tag{3.8}$$

where $v_i = V_i e^{\mathrm{j}\theta_i}$ is the complex voltage. Using standard trigonometric identities (3.8) becomes $\Pi_{ik}^{loss} = g_{ik}(V_i^2 + V_k^2 - 2V_iV_k\cos\theta_{ik})$. A second order Taylor series expansion around $(V_i^* = V_k^* = 1, \theta_{ik}^* = 0)$ leads to

$$\Pi_{ik}^{loss} \approx g_{ik}[(V_i - V_k)^2 + (\theta_i - \theta_k)^2]. \tag{3.9}$$

The corresponding total transient resistive power losses are given by

$$\Pi_{loss} = \int_0^\infty \sum_{i\sim k} \Pi_{ik}^{loss}(t)dt.$$

Using (3.9) and re-writing this expression in terms of L_G gives

$$\Pi_{loss} \approx \int_0^\infty \Big[V(t)^T L_G V(t) + \theta(t)^T L_G \theta(t)\Big] dt = \|y_{loss}\|_{\mathcal{L}_2}^2, \tag{3.10}$$

where the output, $y_{loss} := \begin{bmatrix} L_G^{\frac{1}{2}} & 0 & 0 \\ 0 & 0 & L_G^{\frac{1}{2}} \end{bmatrix} x.$

3.1.3 Decoupled Dynamics for Performance Analysis

We will employ the following assumptions from [51], which are common in power system performance analysis.

Assumption 3.1. *The power measurement time constants τ_{P_i} and τ_{Q_i} are uniform across all inverters, i.e. $\tau_{P_i} = \tau_P$ and $\tau_{Q_i} = \tau_Q$ $\forall i \in \mathcal{N}$.*

Assumption 3.2. *Shunt susceptances are uniform across all nodes, i.e. $\bar{b}_i = \bar{b}$ $\forall i \in \mathcal{N}$.*

Assumption 3.3. *The conductance-to-susceptance ratio α is uniform for all edges, i.e. $\alpha := \frac{g_{ik}}{b_{ik}}$ $\forall \mathcal{E}_{ik}$.*

Assumption 3.4. *The transmission lines are inductive, i.e. the conductance-to-susceptance (resistance-to-reactance) ratio α is small, $\alpha \approx 0$.*

Remark 3.3. *Assumption 3.3 is reasonable in this setting due to the increased uniformity in node degrees in Kron-reduced networks [81] and the uniformity of physical line properties in microgrids. Although Assumption 3.4 is not applicable in general, it is reasonable for an inverter-based network since inverter output impedances are highly inductive [21] and can dominate line resistances in a Kron-reduced model. Although the analysis easily extends to the case of non-uniform shunt susceptances, we use Assumption 3.2 for notational simplicity.*

Assumtion 3.3 implies that $L_G = \alpha L_B$ which is then combined with assumptions 3.1, 3.2 and 3.4 so that (3.5) leads to the decoupled phase-frequency and voltage dynamics

$$\begin{bmatrix}\dot{\theta}\\ \dot{\omega}\\ \dot{V}\end{bmatrix} = \begin{bmatrix} 0 & I & 0 \\ -\frac{1}{\tau_P}K_P L_B & -\frac{1}{\tau_P}I & 0 \\ 0 & 0 & -\frac{1}{\tau_Q}(C_Q + K_Q L_B)\end{bmatrix}\begin{bmatrix}\theta\\ \omega\\ V\end{bmatrix} + \\ + \begin{bmatrix} 0 & 0 \\ \frac{1}{\tau_P}I & 0 \\ 0 & \frac{1}{\tau_Q}I\end{bmatrix}\mathrm{w},\ y_{loss} = \sqrt{\alpha}\begin{bmatrix}L_B^{\frac{1}{2}}\theta\\ L_B^{\frac{1}{2}}V\end{bmatrix},\ y_{sync} = \begin{bmatrix}\tilde{\omega}\\ V\end{bmatrix}. \tag{3.11}$$

This decoupling between phase and voltage as well as frequency and voltage will enable us to quantify the individual contributions of frequency and voltage dynamics to the performance metrics in (3.7) and (3.10).

3.2 Performance of Heterogeneously Rated Inverters

In this section, we employ the framework introduced in [59] to investigate the effect of heterogeneous inverter ratings on the performance of droop-controlled microgrids.

3.2.1 Diagonalization of the Closed-Loop System

We begin by defining a parameter called the node rating. When considering frequency and voltage dynamics individually we respectively choose the node ratings as $f_{P_i} := \frac{k_{P_i}}{k_P}$ and $f_{Q_i} := \frac{k_{Q_i}}{k_Q}$ for $i = 1, \ldots, N$ such that they determine the ratio of each droop gain to predetermined constants $k_P > 0$ and $k_Q > 0$.

By taking the Laplace transform of (3.4) and excluding the power flow terms, we define two open-loop transfer functions associated with each node; one corresponding to the phase and the other to the voltage dynamics

$$g_i^P(s) := \frac{k_{P_i}}{\tau_P s^2 + s} \quad \text{and} \quad g_i^Q(s) := \frac{k_{Q_i}}{\tau_Q s + 1}, \quad i = 1, \ldots, N.$$

These can be written in terms of the node ratings as

$$g_i^P(s) = f_{P_i} g_0^P(s) \quad \text{and} \quad g_i^Q(s) = f_{Q_i} g_0^Q(s), \quad i = 1, \ldots, N,$$

where $g_0^P(s)$ and $g_0^Q(s)$ are node-independent reference transfer functions with fixed parameters (independent of k_{P_i} or k_{Q_i}). We specify these reference transfer functions as

$$g_0^P(s) = \frac{k_P}{\tau_P s^2 + s} \quad \text{and} \quad g_0^Q(s) = \frac{k_Q}{\tau_Q s + 1}.$$

Combining the nodal open-loop transfer functions leads to the open-loop transfer function of the system

$$\mathcal{G}(s) := \begin{bmatrix} \text{diag}\{g_i^P(s)\} & \\ & \text{diag}\{g_i^Q(s)\} \end{bmatrix} = \mathcal{F} g(s), \tag{3.12}$$

where $\mathcal{F} := \begin{bmatrix} F_P & \\ & F_Q \end{bmatrix}$, $F_P := \text{diag}\{f_{P_i}\}$, $F_Q := \text{diag}\{f_{Q_i}\}$ and $g(s) := \begin{bmatrix} g_0^P(s) I & \\ & g_0^Q(s) I \end{bmatrix}$.

Based on the state equation in (3.11), the closed loop system is given by the block diagram in Figure 3-1. Here, we introduce the feedback matrix

$$\mathcal{L} := \begin{bmatrix} L_B & \\ & 2\bar{b} I + L_B \end{bmatrix},$$

which determines the power flows emerging from the underlying interconnection graph; as well as the matrix of droop gains $\mathcal{K} := \begin{bmatrix} K_P & \\ & K_Q \end{bmatrix}$. Due to (3.12), $\mathcal{G}(s) = \mathcal{F}^{\frac{1}{2}} g(s) \mathcal{F}^{\frac{1}{2}}$ which along with block manipulations leads to the block diagram in Figure 3-2, where $\Gamma := \begin{bmatrix} \frac{1}{k_P} I & \\ & \frac{1}{k_Q} I \end{bmatrix}$. We use a scaled Laplacian [59] defined by

$$\mathcal{L}_{\mathcal{F}} := \mathcal{F}^{\frac{1}{2}} \mathcal{L} \mathcal{F}^{\frac{1}{2}} = \begin{bmatrix} F_P^{\frac{1}{2}} L_B F_P^{\frac{1}{2}} & \\ & F_Q^{\frac{1}{2}} (2\bar{b} I + L_B) F_Q^{\frac{1}{2}} \end{bmatrix}, \tag{3.13}$$

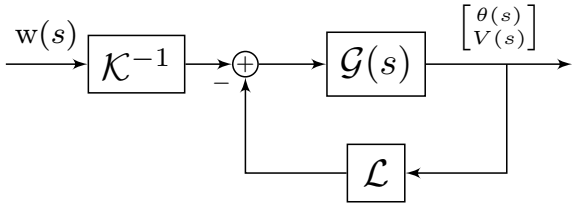

Figure 3-1. Closed-loop microgrid dynamics.

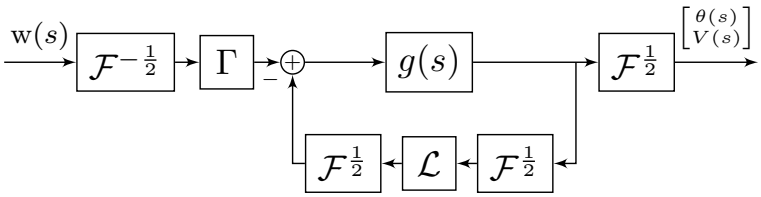

Figure 3-2. Closed-loop dynamics with the open-loop determined by the reference transfer functions and the scaled Laplacians in the feedback.

which is symmetric, therefore orthogonally diagonalizable

$$\mathcal{L}_{\mathcal{F}} := \mathcal{S}\Lambda\mathcal{S}^T, \tag{3.14}$$

where $\mathcal{S} \in \mathbb{R}^{N\times N}$ and $\mathcal{S}\mathcal{S}^T = I$, and $\Lambda \in \mathbb{R}^{N\times N}$ is diagonal. Due to the block diagonal form of (3.13), the decomposition in (3.14) is also block diagonal with

$$\mathcal{S} = \begin{bmatrix} R & \\ & U \end{bmatrix} \quad \text{and} \quad \Lambda = \begin{bmatrix} \Lambda_P & \\ & \Lambda_Q \end{bmatrix},$$

which equivalently results in the orthogonal diagonalizations

$$\mathcal{L}_{\mathcal{F}} =: \begin{bmatrix} L_P & \\ & L_Q \end{bmatrix} = \begin{bmatrix} R\Lambda_P R^T & \\ & U\Lambda_Q U^T \end{bmatrix}. \tag{3.15}$$

This decomposition and block manipulations lead to the diagonalized closed-loop dynamics shown in the block diagram of Figure 3-3 with the transfer function

$$T(s) = \mathcal{F}^{\frac{1}{2}}\mathcal{S}H(s)\mathcal{S}^T\mathcal{F}^{-\frac{1}{2}}.$$

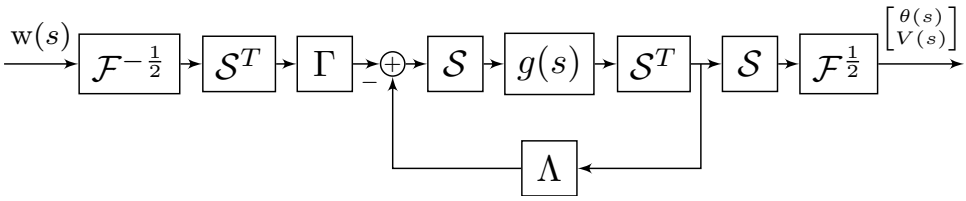

Figure 3-3. Diagonalized Closed-loop dynamics.

The diagonalized transfer function $H(s)$ can be partitioned with respect to phase-frequency and voltage dynamics as

$$H(s) = \begin{bmatrix} H^P(s) & \\ & H^Q(s) \end{bmatrix}.$$

We next describe each of these blocks.

3.2.1.1 Phase-Frequency Dynamics

Since F_P is full rank, L_P is positive semi-definite and rank $N-1$ due to (3.13). Therefore the decomposition in (3.15) leads to $\Lambda_P =: \text{diag}\{\lambda_i^P\}$ and $0 = \lambda_1^P < \lambda_2^P \leq \cdots \leq \lambda_N^P$.

The transfer function from $\text{w}^P(s)$ to $\theta(s)$ in Figure 3-3 is

$$T_{\theta \text{w}^P}(s) = F_P^{\frac{1}{2}} R H^P(s) R^T F_P^{-\frac{1}{2}}, \tag{3.16}$$

where $H^P(s) = \text{diag}\{h_i^P(s)\}$ and for $i = 1, \ldots, N$,

$$h_i^P(s) = \frac{1}{k_P}\left(\frac{g_0^P(s)}{1+\lambda_i^P g_0^P(s)}\right) = \frac{1}{\tau_P s^2 + s + \lambda_i^P k_P}. \tag{3.17}$$

Given the partition $R = \begin{bmatrix} r_1 & R_\perp \end{bmatrix}$, the first eigenvector of L_P can be written as $r_1 = \gamma_P F_P^{-\frac{1}{2}} \mathbf{1}$, with the normalization parameter $\gamma_P = \left(\sum_{i=1}^N f_{P_i}^{-1}\right)^{-\frac{1}{2}}$ and $\mathbf{1} = \begin{bmatrix} 1 & \ldots & 1 \end{bmatrix}^T$. Using (3.16), the phase signal due to input (3.6) is given by

$$\begin{aligned} \theta(s) &=: \bar{\theta}(s)\mathbf{1} + \tilde{\theta}(s) \\ &= \underbrace{F_P^{\frac{1}{2}} r_1}_{=\gamma_P \mathbf{1}} h_1^P(s) r_1^T F_P^{-\frac{1}{2}} \text{w}_0^P + F_P^{\frac{1}{2}} R_\perp \tilde{H}^P(s) R_\perp^T F_P^{-\frac{1}{2}} \text{w}_0^P, \end{aligned} \tag{3.18}$$

where $R_\perp = \begin{bmatrix} r_2 & \ldots & r_N \end{bmatrix}$, $\tilde{H}^P(s) := \text{diag}\{h_i^P(s)\}_{i=2,\ldots,N}$. We note that the frequency signal can be obtained from

$$\omega(s) = s\theta(s) =: \bar{\omega}(s)\mathbf{1} + \tilde{\omega}(s), \tag{3.19}$$

which is characterized by the dynamic terms

$$h_i^{P,\omega}(s) := s h_i^P(s), \quad i = 1, \ldots, N. \tag{3.20}$$

Since $r_1^T R_\perp = 0$, we have $\mathbf{1}^T F_P^{-1} \tilde{\omega}(s) = 0$. Then multiplying the equation above from the left by $\mathbf{1}^T F_P^{-1}$ leads to the expression for the synchronous frequency $\bar{\omega}(t)$

$$\bar{\omega}(t) = \frac{\sum_{i=1}^N f_{P_i}^{-1} \omega_i(t)}{\sum_{i=1}^N f_{P_i}^{-1}} = \frac{\sum_{i=1}^N k_{P_i}^{-1} \omega_i(t)}{\sum_{i=1}^N k_{P_i}^{-1}}.$$

This is analogous to the center of inertia (COI) in transmission networks [59] in the sense that the averaging weights are the inverses of active power droop gains instead of inertias.

The following result proves the stability of the phase-frequency dynamics.

Proposition 3.1. *The phase and frequency deviations $\tilde{\theta}(t)$ and $\tilde{\omega}(t)$ are asymptotically stable.*

Proof. First, observe from (3.18) and (3.19) that the stability of $\tilde{\theta}$ and $\tilde{\omega}$ are respectively determined by $h_i^P(s)$ and $h_i^{P,\omega}(s)$ for $i = 2, \ldots, N$. Then the result follows from (3.17) and (3.20) by noting that $\lambda_i^P > 0$ for $i = 2, \ldots, N$. □

3.2.1.2 Voltage Dynamics

Since F_Q is full rank, L_Q is positive definite and full rank due to (3.13). Therefore the decomposition in (3.15) leads to $\Lambda_Q = \text{diag}\{\lambda_i^Q\}$ and $0 < \lambda_1^Q \leq \lambda_2^Q \leq \cdots \leq \lambda_N^Q$.

The transfer function from $\mathrm{w}^Q(s)$ to $V(s)$ in Figure 3-3 is

$$T_{V\mathrm{w}^Q}(s) = F_Q^{\frac{1}{2}} U H^Q(s) U^T F_Q^{-\frac{1}{2}}, \tag{3.21}$$

where $U = \begin{bmatrix} u_1 & \ldots & u_N \end{bmatrix}$, $H^Q(s) = \text{diag}\{h_i^Q(s)\}$ and

$$h_i^Q(s) = \frac{1}{k_Q}\left(\frac{g_0^Q(s)}{1 + \lambda_i^Q g_0^Q(s)}\right) = \frac{1}{\tau_Q s + \lambda_i^Q k_Q + 1}, \tag{3.22}$$

for $i = 1, \ldots, N$. Using (3.21) the voltage due to input (3.6) is

$$V(s) = F_Q^{\frac{1}{2}} U H^Q(s) U^T F_Q^{-\frac{1}{2}} \mathrm{w}_0^Q = \sum_{i=1}^{N} h_i^Q(s) \xi_i, \tag{3.23}$$

where $\xi_i = \left(u_i^T F_Q^{-\frac{1}{2}} \mathrm{w}_0^Q\right) F_Q^{\frac{1}{2}} u_i \in \mathbb{R}^N$. In contrast to the frequency in (3.19), the voltage signal may not include an inherent synchronous mode characterized by $\mathbf{1}$ if the reactive power droop gains are heterogeneous. This is shown in Proposition 3.2 and for this reason we consider the deviations from the equilibrium voltage as defined by (3.7).

Proposition 3.2. *Suppose that u_i has non-zero entries for all i such that $\xi_i \neq 0$. If $F_Q \neq \zeta I$ for all $\zeta > 0$, then $\xi_i \notin \text{span}\{\mathbf{1}\}$ for all i such that $\xi_i \neq 0$.*

Proof. Using (3.23) consider $\xi_i = \left(u_i^T F_Q^{-\frac{1}{2}} \mathrm{w}_0^Q\right) F_Q^{\frac{1}{2}} u_i \neq 0$. Assume that $\xi_i \equiv \beta_i \mathbf{1}$ and $0 \neq \beta_i \in \mathbb{R}$ for some i such that $\xi_i \neq 0$. Then noting that $u_i = \eta_i F_Q^{-\frac{1}{2}} \mathbf{1}$ for $0 \neq \eta_i \in \mathbb{R}$, we have $\lambda_i^Q u_i = L_Q u_i = \eta_i F_Q^{\frac{1}{2}} (2\bar{b} I + L_B)\mathbf{1} = 2\bar{b} F_Q u_i$, where we used (3.13) and (3.15). This implies that $F_Q = \frac{\lambda_i^Q}{2\bar{b}} I$ since by assumption u_i has non-zero entries. □

The following result proves the stability of the voltage dynamics.

Proposition 3.3. *The voltage $V(t)$ is asymptotically stable.*

Proof. The result follows from (3.22) and (3.23) by noting that $\lambda_i^Q > 0$ for $i = 1, \ldots, N$. □

Next we study the deviations from synchrony.

3.2.2 Deviation from Synchrony

In this subsection, we study the synchronization performance of (3.11). The following lemma provides a preliminary result that will be used in the analysis that follows.

Lemma 3.1. *The metric Π_{sync} in (3.7) is given by*

$$\Pi_{sync} \;=\; z_0^T \Psi z_0,$$

where $z_0 := \begin{bmatrix} (z_0^P)^T & (z_0^Q)^T \end{bmatrix}^T$, $z_0^P = R_\perp^T F_P^{-\frac{1}{2}} \mathrm{w}_0^P$ and $z_0^Q = U^T F_Q^{-\frac{1}{2}} \mathrm{w}_0^Q$. The matrix $\Psi := \begin{bmatrix} \Psi^P & \\ & \Psi^Q \end{bmatrix}$ has the entries

$$\psi_{ij}^P \;=\; \phi_{ij}^P \langle h_{i+1}^{P,\omega}, h_{j+1}^{P,\omega} \rangle, \quad i,j = 1, \ldots, N-1, \tag{3.24}$$

$$\psi_{ij}^Q \;=\; \phi_{ij}^Q \langle h_i^Q, h_j^Q \rangle, \qquad i,j = 1, \ldots, N, \tag{3.25}$$

where ϕ_{ij}^P *and* ϕ_{ij}^Q *respectively denote the entries of* $\Phi^P := R_\perp^T F_P R_\perp$ *and* $\Phi^Q := U^T F_Q U$. *The inner products in* (3.24) *and* (3.25) *are given by*

$$\langle h_i^{P,\omega},\, h_j^{P,\omega} \rangle \;=\; \frac{\lambda_i^P + \lambda_j^P}{2\tau_P(\lambda_i^P + \lambda_j^P) + k_P\tau_P^2(\lambda_i^P - \lambda_j^P)^2}, \tag{3.26}$$

$$\langle h_i^{Q},\, h_j^{Q} \rangle \;=\; \frac{1}{2\tau_Q + k_Q\tau_Q(\lambda_i^Q + \lambda_j^Q)}. \tag{3.27}$$

Proof. See Appendix. □

Note that Π_{sync} depends on the heterogeneous droop gains through the eigenvalues λ_i^P and λ_i^Q. Lemma 3.1 is next used to compute Π_{sync} for homogeneous inverter ratings.

Theorem 3.1 (Homogeneous Inverter Ratings)**.** *Suppose that* $\mathcal{F} = I$. *Then* Π_{sync} *in* (3.7) *is given by*

$$\Pi_{sync} \;=\; \frac{1}{2\tau_P}\sum_{i=2}^{N}(r_i^T \mathrm{w}_0^P)^2 \;+\; \frac{1}{2\tau_Q}\sum_{i=1}^{N}\frac{(u_i^T \mathrm{w}_0^Q)^2}{c_Q + k_Q\lambda_i},$$

where $c_Q = 1 + 2\bar{b}k_Q$. *If in addition* $E\{\mathrm{w}_0\mathrm{w}_0^T\} = I$, *then*

$$E\{\Pi_{sync}\} \;=\; \frac{1}{2\tau_P}(N-1) \;+\; \frac{1}{2\tau_Q}\sum_{i=1}^{N}\frac{1}{c_Q + k_Q\lambda_i}.$$

Proof. $F_P = F_Q = I$ leads to $\Phi^P = I$ and $\Phi^Q = I$ so Ψ_P and Ψ_Q are diagonal due to (3.24), (3.25). Also $z_0^P = R_\perp^T \mathrm{w}_0^P$ and $z_0^Q = U^T \mathrm{w}_0^Q$. Using Lemma 3.1, $\Pi_{sync} = \mathrm{tr}(z_0 z_0^T \Psi)$ which yields the first result via (3.26), (3.27). Assuming $E\{\mathrm{w}_0\mathrm{w}_0^T\} = I$, the second result follows from $E\{(r_i^T \mathrm{w}_0^P)^2\} = E\{r_i^T \mathrm{w}_0^P (\mathrm{w}_0^P)^T r_i\} = 1$ and $E\{(u_i^T \mathrm{w}_0^Q)^2\} = 1$. □

If the disturbances have unit covariance and the inverter ratings are homogeneous, the contribution of frequency dynamics is independent of network topology whereas that of the voltage dynamics depends on the topology through the eigenvalues of L_B. If the disturbance direction is arbitrary, then for given $\|\mathrm{w}_0^P\|_2$, the contribution of frequency dynamics is zero if $\mathrm{w}_0^P \in \mathrm{span}\{\mathbf{1}\}$ and maximal if $\mathrm{w}_0^P \in \mathrm{span}\{\mathbf{1}\}^\perp$ since in the homogeneous case $r_1 = \frac{1}{\sqrt{N}}\mathbf{1}$. Similarly for given $\|\mathrm{w}_0^Q\|_2$, the contribution of voltage dynamics is minimal if $\mathrm{w}_0^Q \in \mathrm{span}\{u_N\}$ and maximal if $\mathrm{w}_0^Q \in \mathrm{span}\{\mathbf{1}\}$.

The next theorem provides an analogous result for heterogeneous inverter ratings.

Theorem 3.2 (Heterogeneous Inverter Ratings)**.** *For given inverter ratings* $\mathcal{F}$*,* Π_{sync} *in* (3.7) *has the asymptotic value*

$$\Pi_{sync} \;\to\; \frac{1}{2\tau_P}\sum_{i=1}^{N-1}\phi_{ii}^P(z_{0i}^P)^2,$$

assuming that $\lambda_i^P \neq \lambda_j^P$ *for* $i \neq j$*, as* $k_P \to \infty$ *and* $k_Q \to \infty$*, i.e. in the limit of large droop gains; and*

$$\Pi_{sync} \;\to\; \frac{1}{2\tau_P}\sum_{i,j=1}^{N-1}\phi_{ij}^P z_{0i}^P z_{0j}^P \;+\; \frac{1}{2\tau_Q}\sum_{i,j=1}^{N}\phi_{ij}^Q z_{0i}^Q z_{0j}^Q,$$

as $k_P \to 0$ *and* $k_Q \to 0$*, i.e. in the limit of small gains.*

Proof. In the limit of $k_P \to \infty$ and $k_Q \to \infty$, (3.24) and (3.25) lead to the fact that Ψ^P is diagonal with $\psi_{ii}^P \to \frac{\phi_{ii}^P}{2\tau_P}$ and $\Psi^Q \to 0$. Similarly, as $k_P \to 0$ and $k_Q \to 0$, $\psi_{ij}^P \to \frac{\phi_{ij}^P}{2\tau_P}$ and $\psi_{ij}^Q \to \frac{\phi_{ij}^Q}{2\tau_Q}$. Using the fact from Lemma 3.1 that $\Pi_{sync} = \mathrm{tr}(z_0 z_0^T \Psi)$ yields the result. □

In these asymptotic expressions the dependence on heterogeneous droop gains is through the entries of Φ^P, Φ^Q and z_0. The dependence on network topology is only through the eigenvectors r_i and u_i of the scaled Laplacians L_P and L_Q; and λ_i^P and λ_i^Q do not appear. For given F_P and F_Q, Π_{sync} in the small gain limit has additional summation terms for $i \neq j$, while these terms are suppressed in the large gain limit. Furthermore, in the limit of large gains there is no deviation from the equilibrium voltage hence the contribution of the voltage dynamics to Π_{sync} is zero. In contrast, frequency deviations cannot be eliminated even with infinite control action. Theorem 3.2 therefore shows that lack of inertia can indeed be problematic in inverter-based systems because even at the large gain limit frequency deviations can grow unboundedly as the disturbance magnitude is increased. Additional inertia would contribute to the time constant term τ_P due to (3.4), and help to mitigate these deviations. Dynamic control strategies can also improve frequency synchronization [53].

3.2.3 Transient Resistive Power Losses

In this subsection, we begin by providing the closed-form solution for the transient resistive losses. In the special cases where disturbance directions have unit covariance and the covariance scales with inverter ratings, we will analyze the dependence of losses on the droop gains k_{P_i} and k_{Q_i}.

Lemma 3.2. *The metric* Π_{loss} *in* (3.10) *is given by*

$$\Pi_{loss} \;=\; \underbrace{\frac{\alpha}{2k_P}\sum_{i=1}^{N-1}\left(z_{0i}^{P}\right)^2}_{=:\,\Pi_{loss}^{P}} \;+\; \underbrace{\frac{\alpha}{2\tau_Q}\sum_{i=1}^{N}\frac{\left(z_{0i}^{Q}\right)^2}{k_Q+\frac{1}{\lambda_i^Q}}}_{=:\,\Pi_{loss}^{Q}} \;-\; \Sigma^Q$$

where the notation is adopted from Lemma 3.1 and

$$\Sigma^Q \;=\; 2\alpha\bar{b}(z_0^Q)^T\Psi_Q z_0^Q. \tag{3.28}$$

Furthermore $\Pi_{loss}\to 0$ *as* $k_P \;\to\; \infty$ *and* $k_Q\to\infty$*, i.e. in the limit of large droop gains for given inverter ratings* $\mathcal{F}$*.*

Proof. See Appendix. □

As Lemma 3.2 indicates, Π_{loss} depends on both the droop gains and the network topology. The dependence on network topology is through the eigenvectors r_i and u_i of the scaled Laplacian for Π_{loss}^P whereas Π_{loss}^Q additionally includes the eigenvalues λ_i^Q. Note that these variables also are functions of the droop gains. Π_{loss} can be eliminated in the hypothetical case of infinite gains, while this is not true for Π_{sync} as shown by theorems 3.1 and 3.2.

We now investigate the effect of network topology and heterogeneous droop gains on the transient resistive losses.

Theorem 3.3. *Suppose that* $E\{\mathrm{w}_0\mathrm{w}_0^T\} = I$. *Then*

$$E\{\Pi_{loss}\} \;=\; \frac{\alpha}{2}\left(\sum_{i=1}^{N} k_{P_i}^{-1} \;-\; \frac{\sum_{i=1}^{N} k_{P_i}^{-2}}{\sum_{i=1}^{N} k_{P_i}^{-1}}\right) + \frac{\alpha}{2\tau_Q}\sum_{i=1}^{N}\frac{u_i^T F_Q^{-1} u_i}{k_Q + \frac{1}{\lambda_i^Q}} \;-\; E\{\Sigma^Q\},$$

where Σ^Q *is given by* (3.28). *If* $E\{\mathrm{w}_0\mathrm{w}_0^T\} = \mathcal{F}$, *then*

$$E\{\Pi_{loss}\} \;=\; \frac{\alpha}{2k_P}(N-1) \;+\; \frac{\alpha}{2\tau_Q}\sum_{i=1}^{N}\frac{\lambda_i^Q - 2\bar{b}u_i^T F_Q u_i}{1 + k_Q\lambda_i^Q}.$$

Proof. Assuming $E\{\mathrm{w}_0\mathrm{w}_0^T\} = I$, we have $E\{(z_{0i}^P)^2\} = r_{i+1}^T F_P^{-1} r_{i+1}$ and $E\{(z_{0i}^Q)^2\} = u_i^T F_Q^{-1} u_i$. Then using $E\{\Pi_{loss}^P\} = \frac{\alpha}{2k_P}\mathrm{tr}\left(R_\perp R_\perp^T F_P^{-1}\right) = \frac{\alpha}{2k_P}\mathrm{tr}\left[\left(I - r_1 r_1^T\right) F_P^{-1}\right]$ and recalling that $r_1 = \gamma_P F_P^{-\frac{1}{2}}\mathbf{1}$ and $\gamma_P = \left(\sum_{i=1}^{N} f_{P_i}^{-1}\right)^{-\frac{1}{2}}$ leads to

$$\begin{aligned} E\{\Pi_{loss}^P\} &= \frac{\alpha}{2k_P}\,\mathrm{tr}\left(F_P^{-1} - \gamma_P^2 F_P^{-1}\mathbf{1}\mathbf{1}^T F_P^{-1}\right) \\ &= \frac{\alpha}{2k_P}\left(\sum_{i=1}^{N} f_{P_i}^{-1} - \frac{\sum_{i=1}^{N} f_{P_i}^{-2}}{\sum_{i=1}^{N} f_{P_i}^{-1}}\right). \end{aligned}$$

Taking $\frac{1}{k_P}$ inside the parenthesis yields the first result. Assuming that $E\{\mathrm{w}_0\mathrm{w}_0^T\} = \mathcal{F}$, we have $E\{z_0^P\,(z_0^P)^T\} = I$ and $E\{z_0^Q\,(z_0^Q)^T\} = I$. Therefore (3.25) and (3.28) lead to

$$E\{\Sigma^Q\} \;=\; 2\alpha\bar{b}\,\mathrm{tr}\,(\Psi_Q) \;=\; 2\alpha\bar{b}\sum_{i=1}^{N} u_i^T F_Q u_i \|h_i^Q(t)\|_{\mathcal{L}_2}^2.$$

Combining (3.33) and Lemma 3.2 completes the proof. □

If the disturbance has unit covariance, $E\{\Pi_{loss}^P\}$ only depends on the active power droop gains and is independent of network topology. In contrast, $E\{\Pi_{loss}^Q\}$ depends on the reactive power droop gains as well as the network topology. Scaling the inverter ratings in accordance with the disturbance magnitude at each node leads to $E\{\Pi_{loss}^P\}$ scaling linearly with network size, while $E\{\Pi_{loss}^Q\}$ still depends both on network topology and droop gains.

Next we show $E\{\Pi_{loss}^P\}$ is monotonically decreasing in the active power droop gains if the disturbance has unit covariance.

Corollary 3.1. *If* $E\{\mathrm{w}_0\mathrm{w}_0^T\} = I$*, then* $E\{\Pi_{loss}^p\}$ *is monotonically decreasing in* k_{P_l} *for* $l = 1, \ldots, N$*, i.e.*

$$\frac{\partial}{\partial k_{P_l}}\left[\frac{\alpha}{2}\left(\sum_{i=1}^{N} k_{P_i}^{-1} - \frac{\sum_{i=1}^{N} k_{P_i}^{-2}}{\sum_{i=1}^{N} k_{P_i}^{-1}}\right)\right] < 0, \quad l = 1, \ldots, N.$$

Proof. See Appendix. □

Since the derivative in each direction is negative, performance is improved by increasing any of the active power droop gains. Therefore, $E\{\Pi_{loss}^p\}$ can be minimized by maximizing all k_{P_i} for given upper limits on these gains. Furthermore, since there is no dependence on network topology, node connectivity does not play a role in the optimal choice of k_{P_i}. On the other hand, the directional derivative in (3.34) *is* a function of the direction k_{P_l}. So, for given heterogeneous gains, the directional descent can be non-uniform. This point will be further investigated in Section 3.3.

We next establish an upper bound on $E\{\Pi_{loss}^q\}$.

Corollary 3.2. *If* $E\{\mathrm{w}_0\mathrm{w}_0^T\} = I$*,*

$$E\{\Pi_{loss}^q\} \;\leq\; \frac{\alpha(2\bar{b} + \lambda_N)k_{Q_N}}{2\tau_Q\left(1 + (2\bar{b} + \lambda_N)k_{Q_N}\right)} \sum_{i=1}^{N} k_{Q_i}^{-1}, \tag{3.29}$$

where $k_{Q_N} := \max_i\{k_{Q_i}\}$.

Proof. See Appendix. □

The bound in (3.29) depends on the network topology only via the maximum eigenvalue of L_B instead of the eigenvalues and the eigenvectors of L_Q. It also asymptotically goes to zero in the limit of large reactive power gains. Although $E\{\Pi_{loss}^q\}$ is not necessarily monotonically decreasing in the gains, for given k_{Q_N} this bound provides a worst case performance value that is decreasing in all $k_{Q_i} \neq k_{Q_N}$.

3.3 Numerical Examples

We now numerically investigate the dependence of the transient resistive losses on the changes in heterogeneous droop gains for $E\{\mathrm{w}_0\mathrm{w}_0^T\} = I$. The parameter values are $\alpha = 0.2$, $\bar{b} = \tau_Q = 1$ in all simulations. The directional derivative (3.34) is plotted with respect to non-uniform active power gains $k_{P_i} \in \{1, \ldots, 50\}$ in Figure 3-4 (left). It can be observed that the steepest descent in $E\{\Pi^P_{loss}\}$ occurs in the direction of the smallest gain. Furthermore, the degree of descent monotonically decreases as the magnitude of the perturbed gain increases. As a result, in this particular example the amount of performance improvement is inversely related to the magnitude of the perturbed gain. Therefore, heterogeneous active power sharing requirements (equivalently heterogeneous inverter ratings F_P) might limit performance, regardless of the network topology and line properties. Analytical exploration of this observation is a direction for future work.

In the case of a complete graph with unit edge weights, which dictates uniform topology dependence of all nodes, a similar behavior is observed from Figure 3-4 (right) for $\frac{\Delta E\{\Pi^Q_{loss}\}}{\Delta k_{Q_i}}$, i.e. the estimation of the directional derivative of $E\{\Pi^Q_{loss}\}$ with respect to $k_{Q_i} \in \{1, \ldots, 50\}$. We estimate this derivative by choosing a perturbation of $\Delta k_{Q_i} = 10^{-5}$. As before, performance improvement is inversely related to the magnitude of the perturbed gain.

We next investigate (for $E\{\mathrm{w}_0\mathrm{w}_0^T\} = I$) how line susceptances affect the rate of change in $E\{\Pi_{loss}\}$ due to a change in each node's droop gain. We only consider $E\{\Pi^Q_{loss}\}$ since $E\{\Pi^P_{loss}\}$ does not depend on the network topology. We consider a complete graph with edge weights drawn from the uniform distribution over the interval $(0, 1]$ and assign uniform gains via $F_Q = I$ and $k_Q = 1$. Using a perturbation of $\Delta k_{Q_i} = 10^{-5}$, $\frac{\Delta E\{\Pi^Q_{loss}\}}{\Delta k_{Q_i}}$ is plotted with respect to the perturbed node i in Figure 3-5. Here the nodes are sorted by increasing weighted degree. The general trend is that

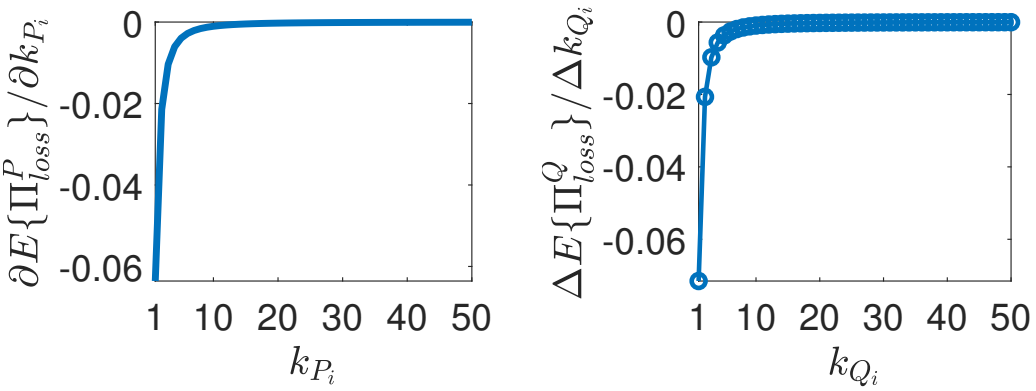

Figure 3-4. Directional derivative of $E\{\Pi^P_{loss}\}$ with respect to k_{P_i} (left), and a numerical estimate of the directional derivative of $E\{\Pi^Q_{loss}\}$ with respect to k_{Q_i} for a complete graph of unit edge weights (right) with $E\{\mathrm{w}_0\mathrm{w}_0^T\} = I$.

a larger performance improvement is observed for unit change in the droop gain as the weighted degree increases. However this relationship is not monotonic. In several instances this general trend is not seen, which can be explained as follows. $E\{\Pi^Q_{loss}\}$ depends on the eigenvalues and eigenvectors of the scaled Laplacian L_Q as well as the inverter ratings F_Q per Theorem 3.3. Since the weighted degrees are non-uniform, each gain perturbation leads to possibly non-uniform perturbations in the eigenvalues and the eigenvectors of L_Q. So, the perturbation terms in $E\{\Pi^Q_{loss}\}$ can result in a non-monotonic relationship with increasing weighted degree.

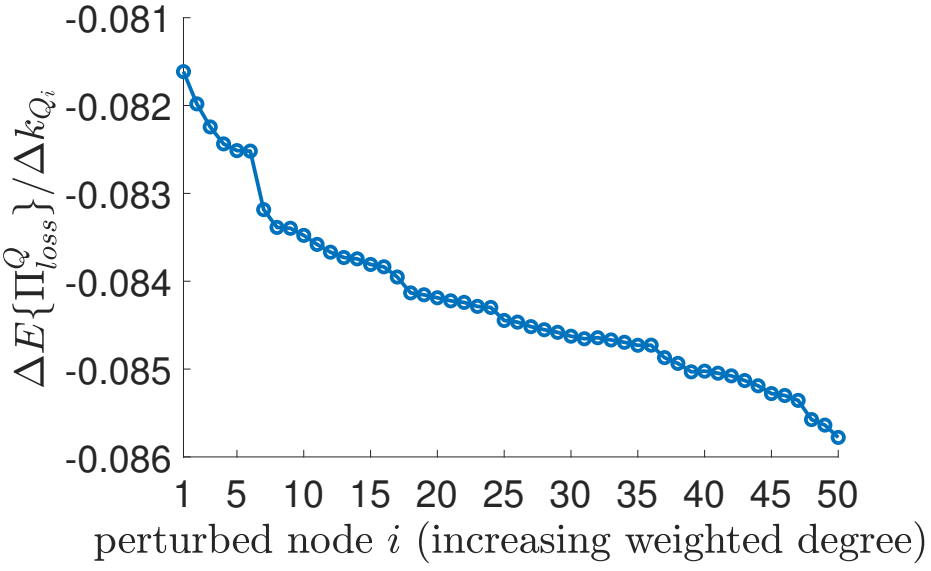

Figure 3-5. A numerical estimate of the directional derivative of $E\{\Pi^Q_{loss}\}$ with respect to k_{Q_i} for a complete graph with edge weights drawn from the uniform distribution over $(0, 1]$, where $E\{\mathrm{w}_0\mathrm{w}_0^T\} = I$.

3.4 Summarizing Remarks

This work generalized previous performance analysis concerning uniform nodal dynamics in droop-controlled microgrids to the case of heterogeneously rated inverters. Our result for the frequency and voltage synchronization performance emphasizes the possible problem of inertia in inverter-based systems. We also demonstrated that the transient resistive losses are sensitive to the heterogeneity in droop gains, hence power sharing requirements can limit performance. Extension to the case of coupled frequency-voltage dynamics is a direction for future work.

3.5 APPENDIX

3.5.1 Proof of Lemma 3.1

Equations (3.24) and (3.25) follow from (3.7), using (3.19) and (3.23) in the time-domain. A realization for (3.20) is given by

$$h_i^{P,\omega} = \left(\begin{array}{c|c} A_i & B_i \\ \hline C_i & 0 \end{array}\right),$$

where $A_i = \begin{bmatrix} 0 & 1 \\ -\frac{k_P}{\tau_P}\lambda_i^P & -\frac{1}{\tau_P} \end{bmatrix}$, $B_i = \begin{bmatrix} 0 \\ \frac{1}{\tau_P} \end{bmatrix}$, $C_i = \begin{bmatrix} 0 & 1 \end{bmatrix}$. The inner product in (3.24) can be computed by [59]

$$\langle h_i^{P,\omega},\, h_j^{P,\omega} \rangle \;=\; \int_0^\infty [h_i^{P,\omega}(t)]^T h_j^{P,\omega}(t) dt \;=\; B_i^T X_{ij} B_j,$$

where X_{ij} is the solution to the Sylvester equation

$$A_i^T X_{ij} + X_{ij} A_j = -C_i^T C_j. \tag{3.30}$$

The inner product $\langle h_i^Q,\, h_j^Q \rangle$ in (3.25) can be similarly computed using the following time-domain realization for (3.22)

$$h_i^Q = \left(\begin{array}{c|c} \frac{-1-k_Q\lambda_i^Q}{\tau_Q} & \frac{1}{\tau_Q} \\ \hline 1 & 0 \end{array}\right). \tag{3.31}$$

3.5.2 Proof of Lemma 3.2

We can rewrite (3.10) as

$$\Pi_{loss} = \alpha \int_0^\infty \Big[\theta(t)^T L_B \theta(t) \; + \\ V(t)^T (2\bar{b} I + L_B) V(t)\Big] dt - 2\alpha\bar{b}\|V\|_{\mathcal{L}_2}^2,$$

which by using (3.18) and (3.23) in the time-domain leads to

$$\Pi_{loss} = \alpha \int_0^\infty \Big[(z_0^P)^T \tilde{H}^P(t) R_\perp^T L_P R_\perp \tilde{H}^P(t) z_0^P \; + \\ (z_0^Q)^T H^Q(t) U^T L_Q U H^Q(t) z_0^Q\Big] dt - 2\alpha\bar{b}\|V\|_{\mathcal{L}_2}^2. \tag{3.32}$$

Here $R_\perp^T L_P R_\perp = \text{diag}\{\lambda_i^P\}_{i=2,\ldots,N} =: \tilde{\Lambda}_P$ and we recall that $U^T L_Q U = \Lambda_Q$ which leads to

$$\begin{aligned} \int_0^\infty \tilde{H}^P(t) \tilde{\Lambda}_P \tilde{H}^P(t) dt &= \text{diag}\{\lambda_i^P \|h_i^P(t)\|_{\mathcal{L}_2}^2\}_{i=2,\ldots,N}, \\ \int_0^\infty H^Q(t) \Lambda_Q H^Q(t) dt &= \text{diag}\{\lambda_i^Q \|h_i^Q(t)\|_{\mathcal{L}_2}^2\}. \end{aligned}$$

The realization of h_i^P in (3.17) is given by $h_i^P = \left(\begin{array}{c|c} A_i & B_i \\ \hline C_i & 0 \end{array}\right)$, where $A_i = \begin{bmatrix} 0 & 1 \\ -\frac{k_P}{\tau_P}\lambda_i^P & -\frac{1}{\tau_P} \end{bmatrix}$, $B_i = \begin{bmatrix} 0 \\ \frac{1}{\tau_P} \end{bmatrix}$, $C_i = \begin{bmatrix} 1 & 0 \end{bmatrix}$. Then $\|h_i^P(t)\|_{\mathcal{L}_2}^2 = B_i^T X_{ii} B_i$ where X_{ii} solves (3.30) for $i = j$, which is a Lyapunov equation. Similarly the realization of h_i^Q in (3.31) leads to

$$\|h_i^P(t)\|_{\mathcal{L}_2}^2 = \frac{1}{2k_P\lambda_i^P}, \; \|h_i^Q(t)\|_{\mathcal{L}_2}^2 = \frac{1}{2\tau_Q\left(1 + k_Q\lambda_i^Q\right)}. \tag{3.33}$$

Substituting these expressions and $\|V\|_{\mathcal{L}_2}^2 = (z_0^Q)^T \Psi_Q z_0^Q$ from Lemma 3.1 into (3.32) yields the first result. Taking the limit of Π_{loss} as $k_P \to \infty$ and $k_Q \to \infty$ and using $\Psi_Q \to 0$ from the proof of Theorem 3.2 leads to the second result.

3.5.3 Proof of Corollary 3.1

The partial derivative of $E\{\Pi^P_{loss}\}$ with respect to k_{P_l} is

$$\begin{aligned}\frac{\partial E\{\Pi^P_{loss}\}}{\partial k_{P_l}} &= \frac{\alpha}{2k_{P_l}^2}\left(-1+\frac{2k_{P_l}^{-1}}{\sum_{i=1}^N k_{P_i}^{-1}}-\frac{\sum_{i=1}^N k_{P_i}^{-2}}{\left(\sum_{i=1}^N k_{P_i}^{-1}\right)^2}\right) \\ &= \alpha\left(\frac{-k_{P_l}\sum\limits_{i=1}^N k_{P_i}^{-2}-k_{P_l}\sum\limits_{j=1}^N\sum\limits_{i=1}^{j-1}(k_{P_i}k_{P_j})^{-1}+\sum\limits_{i=1}^N k_{P_i}^{-1}}{k_{P_l}^3\left(\sum\limits_{i=1}^N k_{P_i}^{-1}\right)^2}\right),\end{aligned} \tag{3.34}$$

where we used the fact that $\left(\sum_{i=1}^N k_{P_i}^{-1}\right)^2 = \sum_{i=1}^N k_{P_i}^{-2} + 2\sum_{j=1}^N\sum_{i=1}^{j-1}(k_{P_i}k_{P_j})^{-1}$. So $\frac{\partial E\{\Pi^P_{loss}\}}{\partial k_{P_l}} < 0$ if and only if

$$\kappa_l := -k_{P_l}\left(\sum_{i=1}^N k_{P_i}^{-2}+\sum_{j=1}^N\sum_{i=1}^{j-1}(k_{P_i}k_{P_j})^{-1}\right)+\sum_{i=1}^N k_{P_i}^{-1} < 0.$$

Partitioning the double summation over a triangular region,

$$\sum_{j=1}^N\sum_{i=1}^{j-1}(k_{P_i}k_{P_j})^{-1} = \sum_{i=1}^{l-1}(k_{P_i}k_{P_l})^{-1}+\sum_{j=l+1}^N(k_{P_l}k_{P_j})^{-1}+\Xi_l,$$

where $\Xi_l = \sum\limits_{j=1}^{l-1}\sum\limits_{i=1}^{j-1}(k_{P_i}k_{P_j})^{-1}+\sum\limits_{j=l+1}^N\sum\limits_{i=1}^{l-1}(k_{P_i}k_{P_j})^{-1}+\sum\limits_{j=l+2}^N\sum\limits_{i=l+1}^{j-1}(k_{P_i}k_{P_j})^{-1}$. Substituting this expression into κ_l gives $\kappa_l = -k_{P_l}\left(\sum\limits_{i\in\{1,\dots,N\}\setminus l}k_{P_i}^{-2}+\Xi_l\right) < 0$, which completes the proof since $l\in\{1,\dots,N\}$ is arbitrary.

3.5.4 Proof of Corollary 3.2

Recalling that $\Sigma^Q = 2\alpha\bar{b}\|V\|^2_{\mathcal{L}_2} \geq 0$, the following holds

$$E\{\Pi^Q_{loss}\} \;\leq\; \frac{\alpha}{2\tau_Q}\sum_{i=1}^N\frac{u_i^T F_Q^{-1}u_i}{k_Q+\frac{1}{\lambda_i^Q}}, \tag{3.35}$$

due to Theorem 3.3. Using the definition of L_Q given by (3.13) and (3.15), one can write for $i=1,\dots,N$

$$\frac{\lambda_i^Q}{u_i^T F_Q u_i} = \frac{u_i^T F_Q^{\frac{1}{2}}(2\bar{b}I+L_B)F_Q^{\frac{1}{2}}u_i}{u_i^T F_Q u_i} \in \text{conv}(\{2\bar{b}+\lambda_j\}),$$

where $\mathrm{conv}(\cdot)$ denotes the convex hull and we used the numerical range of the symmetric matrix $2\bar{b}I + L_B$ [82]. Then $\lambda_i^Q \in \mathrm{conv}\left(\{u_i^T F_Q u_i(2\bar{b} + \lambda_j)\}\right)$, which leads to

$$\lambda_i^Q \leq \max_j \{u_i^T F_Q u_i(2\bar{b} + \lambda_j)\} = u_i^T F_Q u_i(2\bar{b} + \lambda_N).$$

Finally noting that $\lambda_i^Q \leq \max_i\{\lambda_i^Q\} \leq (2\bar{b}+\lambda_N)\frac{k_{Q_N}}{k_Q}$, substituting into (3.35) and using $\sum_{i=1}^N u_i^T F_Q^{-1} u_i = \mathrm{tr}(U^T F_Q^{-1} U) = \mathrm{tr}(F_Q^{-1})$ yields the result.

Chapter 4

A New Analysis Framework for the Quadratic Performance Metrics of Directed Networks

In this chapter, we develop a novel framework to evaluate the performance of directed networks [83]. This is achieved by formulating the performance metrics through the $\mathcal{L}_2$ norm of the system response due to distributed impulse disturbances. Adopting the terminology from vehicular networks, the metrics are defined in terms of either the position or the velocity states of agents. Our novel method of computing these metrics in closed-form stems from exploiting the spectral properties of weighted graph Laplacians and output performance matrices. Using our framework, we first provide closed-form solutions for the general quadratic performance metrics of single and double-integrator networks defined over arbitrary directed graphs.

This novel framework also paves the way for our analytical findings in the subsequent chapters. Particularly, we will revisit important subclasses of systems defined over directed graphs emitting diagonalizable Laplacians. We will then derive and use the closed-form solutions for the performance metrics for this family of graphs, allowing for the investigation of the interplay between the network topology and control strategy and unraveling previously undiscovered system properties. We will also evaluate the scaling properties of performance metrics of networks with interconnection directionality.

4.1 System Models and Performance Metrics

4.1.1 Single and Double-Integrator Networks

Consider n dynamical systems that communicate over a weighted digraph $\mathcal{G} = \{\mathcal{N}, \mathcal{E}, \mathcal{W}\}$ that have at least one globally reachable node. Here, $\mathcal{N} = \{1, ..., n\}$ is the set of nodes and $\mathcal{E} = \{(i,j) \mid i,j \in \mathcal{N},\, i \neq j\}$ is the set of edges with weights $\mathcal{W} = \{b_{ij} > 0 \mid (i,j) \in \mathcal{E}\}$. In the following $b_{ij} = 0$ if and only if $(i,j) \notin \mathcal{E}$.

We consider two types of nodal dynamics. Single integrator systems of the form

$$\dot{x}_i = -\sum_{j=1}^{n} b_{ij}(x_i - x_j) + w_i,$$

at each $i \in \mathcal{N}$, where w_i denotes the disturbance to the i^{th} agent. This results in the well-known consensus network

$$\dot{\mathbf{x}} = -L\mathbf{x} + \mathbf{w}, \tag{4.1}$$

where L denotes the weighted graph Laplacian matrix given by $[L]_{ii} = \sum_{j=1}^{n} b_{ij}$, and $[L]_{ij} = -b_{ij}$ if $i \neq j$, $\forall i,j \in \mathcal{N}$. The second type of system is governed by double-integrator dynamics of the form

$$\ddot{x}_i + k_d\dot{x}_i + k_p x_i = u_i + w_i,$$

where $u_i = -\gamma_p \sum_{j=1}^{n} b_{ij}(x_i - x_j) - \gamma_d \sum_{j=1}^{n} b_{ij}(\dot{x}_i - \dot{x}_j)$ $\forall i \in \mathcal{N}$. Here, $k_p, k_d, \gamma_p, \gamma_d \geq 0$, and w_i denotes the disturbance to the i^{th} system. Defining $\mathbf{v} := \dot{\mathbf{x}}$, the double-integrator dynamics can be expressed in matrix form as

$$\begin{bmatrix} \dot{\mathbf{x}} \\ \dot{\mathbf{v}} \end{bmatrix} = \begin{bmatrix} 0 & I \\ -k_p I - \gamma_p L & -k_d I - \gamma_d L \end{bmatrix} \begin{bmatrix} \mathbf{x} \\ \mathbf{v} \end{bmatrix} + \begin{bmatrix} 0 \\ I \end{bmatrix} \mathbf{w}. \tag{4.2}$$

A necessary condition for (4.2) to reach consensus without disturbance ($\mathbf{w} = 0$) is that at least one of (k_p, γ_p) and at least one of (k_d, γ_d) are non-zero (follows from [9, Theorem 1], see [47, Lemma 3] for a self-contained proof). To ensure that this condition is met, we impose the following assumption throughout the remainder of this thesis.

Assumption 4.1. *System (4.2) has feedback in both state variables (position and velocity), i.e. at least one of (k_p, γ_p) and at least one of (k_d, γ_d) are non-zero.*

4.1.2 Performance Metrics

For $C \in \mathbb{R}^{q \times n}$ that defines the performance metric, the performance output $\mathbf{y}(t)$ in (2.15) will be used to quantify the performance of the single-integrator network (4.1) and the double-integrator network (4.2) for metrics related to the position state $\mathbf{x}$. For the double-integrator network (4.2), the performance output in (2.16) which quantifies performance metrics related to the velocity state $\mathbf{v}$, will also be considered.

We are interested in performance metrics that quantify the squared $\mathcal{L}_2$ norm of the output $\mathbf{y}(t)$, which is of the form in (2.12), when the system is subjected to an impulse input $\mathbf{w}(t)$ of the form in (2.13). Denoting the impulse response function from $\mathbf{w}(t)$ to $\mathbf{y}(t)$ by $T(t)$, the performance metric can be written as given in (2.14), which will be computed in closed-form in the upcoming sections. We also note that the relationship between the output $\mathcal{L}_2$ norm and the system $\mathcal{H}_2$ norm given in Proposition 2.1 will be used to investigate special cases in the subsequent chapters.

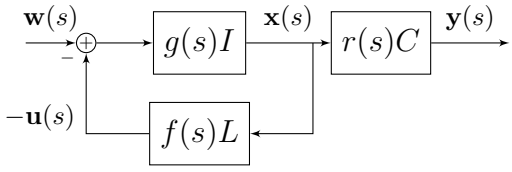

Figure 4-1. Block diagram of the closed-loop system $T(s)$ from the disturbance input $\mathbf{w}(s)$ to the performance output $\mathbf{y}(s)$ and the closed-loop system $H_{\mathbf{xw}}(s)$ from $\mathbf{w}(s)$ to the position state $\mathbf{x}(s)$. The performance output $\mathbf{y}(s)$ is given by (2.15) if $r(s) = 1$ and by (2.16) if $r(s) = s$.

4.2 Block-diagonalization of the Closed-loop Dynamics

In this section, we express the dynamics given in (4.1) and (4.2) in the frequency domain using an approach based on [59]. The framework, denoted in Figure 4-1, describes identical systems $g(s)$ receiving feedback that depends on an arbitrary transfer function $f(s)$ and the weighted graph Laplacian L emitted by the network interconnection. Assuming that $\mathbf{x}(0) = \mathbf{v}(0) = 0$ (we consider perturbations to the equilibrium), the closed-loop system from the input $\mathbf{w}$ to the position state $\mathbf{x}$ is given by

$$\left[(g(s)^{-1}I + f(s)L\right]\mathbf{x}(s) = \mathbf{w}(s),$$

which leads to

$$\mathbf{x}(s) = \left[(I + g(s)f(s)L\right]^{-1} g(s)\mathbf{w}(s) =: H_{\mathbf{xw}}(s)\mathbf{w}(s), \tag{4.3}$$

where $H_{\mathbf{xw}}(s)$ denotes the transfer function from the input $\mathbf{w}$ to the position state $\mathbf{x}$.

L can be decomposed as $L = RJR^{-1}$, where $R \in \mathbb{C}^{n\times n}$ is invertible and $J \in \mathbb{C}^{n\times n}$ is in Jordan Canonical Form (JCF). This decomposition transforms (4.3) into

$$\mathbf{x}(s) = R\left[(I + g(s)f(s)J\right]^{-1} g(s)R^{-1}\mathbf{w}(s),$$

as shown by the block diagram in Figure 4-2. Defining $\tilde{\mathbf{x}} := R^{-1}\mathbf{x}$ and $\tilde{\mathbf{w}} := R^{-1}\mathbf{w}$, the transfer function from $\tilde{\mathbf{w}}$ to $\tilde{\mathbf{x}}$ is

$$H_{\tilde{\mathbf{x}}\tilde{\mathbf{w}}}(s) = \left[(I + g(s)f(s)J\right]^{-1} g(s), \tag{4.4}$$

where the following relationship holds

$$H_{\mathbf{xw}} = RH_{\tilde{\mathbf{x}}\tilde{\mathbf{w}}}R^{-1}. \tag{4.5}$$

J is composed of Jordan blocks J_k associated with the eigenvalues $\lambda_k \in \mathbb{C}$ of L for

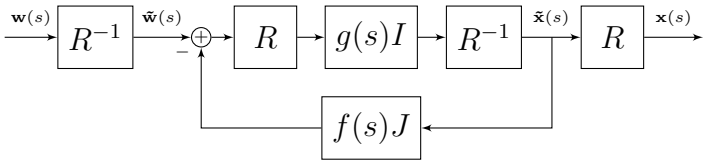

Figure 4-2. Application of a change of basis given by the Jordan decomposition $L = RJR^{-1}$ to the closed-loop system $H_{\mathbf{xw}}(s)$. The feedback loop gives the closed-loop system $H_{\tilde{\mathbf{x}}\tilde{\mathbf{w}}}(s)$.

$k = 1, \ldots, m$:

$$J = \text{blockdiag}\left(J_k\right)_{1 \leq k \leq m}, \tag{4.6}$$

where $J_k \in \mathbb{C}^{n_k \times n_k}$ and $\sum_{k=1}^{m} n_k = n$. Since L is a Laplacian matrix, $L\mathbf{1} = \mathbf{0}$ with $\mathbf{1}$ denoting the vector of all ones therefore $J_1 = \lambda_1 = 0$. Also $\text{Re}\left[\lambda_k\right] > 0$ for $k = 2, \ldots, m$ due to the fact that $\mathcal{G}$ has a globally reachable node [79, Theorem 7.4]. So (4.4) can be written as

$$H_{\tilde{\mathbf{x}}\tilde{\mathbf{w}}}(s) = \text{blockdiag}\left(H_{\tilde{\mathbf{x}}_k\tilde{\mathbf{w}}_k}(s)\right)_{1 \leq k \leq m}, \tag{4.7}$$

where

$$H_{\tilde{\mathbf{x}}_k\tilde{\mathbf{w}}_k}(s) = \left[(I + g(s)f(s)J_k\right]^{-1} g(s). \tag{4.8}$$

Here, the vectors $\tilde{\mathbf{x}}_k = [\tilde{x}_{d_k+1}, \ldots, \tilde{x}_{d_k+n_k}]^\intercal$ and $\tilde{\mathbf{w}}_k = [\tilde{w}_{d_k+1}, \ldots, \tilde{w}_{d_k+n_k}]^\intercal$ respectively denote the position state and the input to the associated subsystem, with $d_1 = 0$ and $d_k = \sum_{i=1}^{k-1} n_i$ for $k = 2, \ldots, m$. An equivalent representation of the transfer function in (4.8) is given by the block diagram in Figure 4-3. The following lemma describes the form of the transfer function in (4.8) which will be used to compute the performance metric (2.14) in what follows.

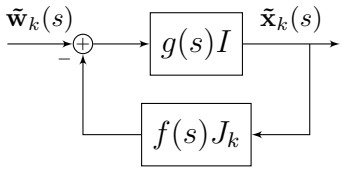

Figure 4-3. Block diagram of each subsystem $H_{\tilde{\mathbf{x}}_k\tilde{\mathbf{w}}_k}$ for $k = 1, \ldots, m$.

Lemma 4.1. *$H_{\tilde{\mathbf{x}}_k\tilde{\mathbf{w}}_k}(s)$ in (4.8) is an upper triangular Toeplitz matrix given by*

$$H_{\tilde{\mathbf{x}}_k\tilde{\mathbf{w}}_k}(s) = \frac{1}{f(s)}\begin{bmatrix} h_k(s) & \dots & (-1)^{n_k-1}h_k(s)^{n_k} \\ & \ddots & \vdots \\ & & h_k(s) \end{bmatrix},$$

where $h_k(s) = \frac{g(s)f(s)}{1+\lambda_k g(s)f(s)}$.

Proof. Using (4.8) and the definition of J_k

$$H_{\tilde{\mathbf{x}}_k\tilde{\mathbf{w}}_k}(s) = \begin{bmatrix} \frac{1+\lambda_k g(s)f(s)}{g(s)} & f(s) & & \\ & \ddots & \ddots & \\ & & \ddots & f(s) \\ & & & \frac{1+\lambda_k g(s)f(s)}{g(s)} \end{bmatrix}^{-1},$$

where factoring out $g(s)f(s)$ gives

$$H_{\tilde{\mathbf{x}}_k\tilde{\mathbf{w}}_k}(s) = \frac{1}{f(s)}\begin{bmatrix} h_k(s)^{-1} & 1 & & \\ & \ddots & \ddots & \\ & & \ddots & 1 \\ & & & h_k(s)^{-1} \end{bmatrix}^{-1}. \tag{4.9}$$

Using the inverse of the JCF in (4.9) yields the result. □

Remark 4.1. *The form of the closed-loop transfer function in Lemma 4.1 holds for arbitrary open-loop and feedback transfer functions $g(s)$ and $f(s)$, and therefore applies to a general class of networked dynamical systems.*

We next apply Lemma 4.1 to the special cases of the single and double-integrator networks.

Corollary 4.1. *Consider the single-integrator network (4.1). Then, $H_{\tilde{\mathbf{x}}_k\tilde{\mathbf{w}}_k}(s)$ in (4.8) is an upper triangular Toeplitz matrix*

$$H_{\tilde{\mathbf{x}}_k\tilde{\mathbf{w}}_k}(s) = \begin{bmatrix} h_k(s) & \dots & (-1)^{n_k-1}h_k(s)^{n_k} \\ & \ddots & \vdots \\ & & h_k(s) \end{bmatrix},$$

where $h_k(s) = \frac{1}{s+\lambda_k}$.

Proof. Taking the Laplace transform of (4.1) leads to $g(s) = \frac{1}{s}$ and $f(s) = 1$. Evaluating the result of Lemma 4.1 at these values gives the desired result. □

Corollary 4.2. *Consider the double-integrator network* (4.2)*. Then,* $H_{\tilde{\mathbf{x}}_k \tilde{\mathbf{w}}_k}(s)$ *in* (4.8) *is an upper triangular Toeplitz matrix*

$$H_{\tilde{\mathbf{x}}_k \tilde{\mathbf{w}}_k}(s) = \frac{1}{\gamma_p + s\gamma_d} \begin{bmatrix} h_k(s) & \dots & (-1)^{n_k-1} h_k(s)^{n_k} \\ & \ddots & \vdots \\ & & h_k(s) \end{bmatrix},$$

where $h_k(s) = \frac{\gamma_p + s\gamma_d}{s^2 + (k_d + \gamma_d \lambda_k)s + k_p + \gamma_p \lambda_k}$.

Proof. Taking the Laplace transform of (4.2) leads to $g(s) = \frac{1}{s^2 + k_d s + k_p}$ and $f(s) = \gamma_p + s\gamma_d$. Evaluating the result of Lemma 4.1 at these values gives the desired result. □

The transfer function from the input $\mathbf{w}$ to the velocity state $\mathbf{v}$ is given by $H_{\mathbf{vw}}(s) := sH_{\mathbf{xw}}(s)$ since $\mathbf{v}(s) = s\mathbf{x}(s) = sH_{\mathbf{xw}}(s)\mathbf{w}(s)$. Therefore, the closed-loop transfer function $T(s)$ from the input $\mathbf{w}$ to the output $\mathbf{y}$ can be written as

$$T(s) = Cr(s)H_{\mathbf{xw}}(s), \tag{4.10}$$

using the notation in Figure 4-1 and specifying $r(s)$ such that

$$T(s) = \begin{cases} CH_{\mathbf{xw}}(s), & r(s) = 1 \quad \text{(4.11a)} \\ CH_{\mathbf{vw}}(s), & r(s) = s\ . \quad \text{(4.11b)} \end{cases}$$

The cases (4.11a) and (4.11b) correspond to the outputs (2.15) and (2.16), respectively. We next provide necessary and sufficient conditions for the input-output stability of (4.11a) and (4.11b), which ensure the finiteness of the performance metric (2.14).

4.2.1 Input-Output Stability

In this subsection we state necessary and sufficient conditions for the input-output stability of (4.11a) and (4.11b). The following assumption will be imposed throughout the remainder of the thesis to eliminate the unstable consensus mode of the Laplacian from the performance output.

Assumption 4.2. *The output matrix C satisfies $C\mathbf{1} = \mathbf{0}$.*

First, we apply the change of basis in (4.5) to the closed-loop system (4.10). Since $L\mathbf{1} = \mathbf{0}$, we can apply the partitioning

$$R = \begin{bmatrix} \alpha\mathbf{1} & \tilde{R} \end{bmatrix} \text{ and } R^{-1} = \begin{bmatrix} \mathbf{q}_1 & \tilde{Q}^* \end{bmatrix}^*, \tag{4.12}$$

where $\alpha \in \mathbb{C}$, $\mathbf{q}_1^* \in \mathbb{C}^{1\times n}$ is the left eigenvector of $\lambda_1 = 0$, $\tilde{R} \in \mathbb{C}^{n\times n-1}$ and $\tilde{Q} \in \mathbb{C}^{n-1\times n}$. Substituting (4.5), (4.7) and (4.12) into (4.10) we obtain

$$\begin{aligned} T(s) &= C\left(\alpha r(s) H_{\tilde{\mathbf{x}}_1\tilde{\mathbf{w}}_1}(s)\mathbf{1}\mathbf{q}_1^* + \tilde{R}\,\tilde{H}(s)\tilde{Q}\right) \\ &= C\tilde{R}\,\tilde{H}(s)\tilde{Q}, \end{aligned} \tag{4.13}$$

where

$$\tilde{H}(s) = \text{blockdiag}\left(\tilde{H}_k(s)\right) := r(s)\,\text{blockdiag}\left(H_{\tilde{\mathbf{x}}_k\tilde{\mathbf{w}}_k}(s)\right), \tag{4.14}$$

for $k = 2, \ldots, m$ and we have used Assumption 4.2 and the fact that $H_{\tilde{\mathbf{x}}_1\tilde{\mathbf{w}}_1}(s)$ is a scalar. We can partition $\tilde{R}$ in (4.12) as

$$\tilde{R} = \begin{bmatrix} \tilde{R}_2 & \ldots & \tilde{R}_m \end{bmatrix}, \tag{4.15}$$

which is in a form that conforms to (4.6). Then the columns of $\tilde{R}_k \in \mathbb{C}^{n\times n_k}$ are the right generalized eigenvectors associated with the Jordan block J_k in (4.6) for $k = 2, \ldots, m$. This partitioning leads to the following useful definition.

Definition 4.1. *The set of observable indices $\mathcal{N}_{obsv}$ is given by*

$$\mathcal{N}_{obsv} = \left\{k \in \{2, \ldots, m\} \mid C\tilde{R}_k \neq 0\right\}. \tag{4.16}$$

We now state the stability conditions. We begin with the system T in (4.11a) for the single-integrator network (4.1).

Proposition 4.1. *Consider the single-integrator network (4.1). The system T in (4.11a) is input-output stable if and only if Assumption 4.2 holds [79, Theorem 7.4].*

As we show next for the double-integrator network (4.2), stability of the observable modes is necessary and sufficient for the input-output stability of the system T given by (4.11a) or (4.11b). For simplicity, we assume L to be diagonalizable; the result can be extended by relaxing this assumption.

Proposition 4.2. *Consider the double-integrator network* (4.2) *and suppose that* L *is diagonalizable and assumptions 4.1 and 4.2 hold. The system* T *given by* (4.11a) *or* (4.11b) *is input-output stable if and only if*

$$s^2 + (k_d + \gamma_d \lambda_k)s + k_p + \gamma_p \lambda_k = 0 \tag{4.17}$$

has solutions that satisfy $\mathrm{Re}(s) < 0$ *for all* $k \in \mathcal{N}_{obsv}$.

Proof. Using the block diagram in Figure 4-3 and the fact that $J_k = \lambda_k$ leads to the following realization for $H_{\tilde{\mathbf{x}}_k \tilde{\mathbf{w}}_k}$

$$\begin{aligned}
\begin{bmatrix} \dot{\tilde{\mathbf{x}}}_k \\ \dot{\tilde{\mathbf{v}}}_k \end{bmatrix} &= \underbrace{\begin{bmatrix} 0 & 1 \\ -k_p - \gamma_p \lambda_k & -k_d - \gamma_d \lambda_k \end{bmatrix}}_{\Lambda_k} \begin{bmatrix} \tilde{\mathbf{x}}_k \\ \tilde{\mathbf{v}}_k \end{bmatrix} + \begin{bmatrix} 0 \\ 1 \end{bmatrix} \tilde{\mathbf{w}}_k \\
\tilde{\mathbf{y}}_k &= \begin{bmatrix} 1 & 0 \end{bmatrix} \begin{bmatrix} \tilde{\mathbf{x}}_k \\ \tilde{\mathbf{v}}_k \end{bmatrix} = \tilde{\mathbf{x}}_k.
\end{aligned} \tag{4.18}$$

Since L is diagonalizable, the partitioning of $\tilde{R}$ in (4.15) becomes $\tilde{R} = \begin{bmatrix} \mathbf{r}_2 & \dots & \mathbf{r}_n \end{bmatrix}$. Using the block-diagonal form of $\tilde{H}(s)$ in (4.14) and the conformal partitioning $\tilde{Q} = \begin{bmatrix} \mathbf{q}_2 & \dots & \mathbf{q}_n \end{bmatrix}^*$, (4.13) can be expressed in time-domain as

$$T(t) = C \sum_{k=2}^{n} \mathbf{r}_k \tilde{H}_k(t) \mathbf{q}_k^* = C \sum_{k \in \mathcal{N}_{obsv}} \mathbf{r}_k \tilde{H}_k(t) \mathbf{q}_k^*.$$

For (4.11a), we can use (4.14) and the realization for $H_{\tilde{\mathbf{x}}_k \tilde{\mathbf{w}}_k}$ in (4.18) to re-write the equation above as

$$T(t) = \sum_{k \in \mathcal{N}_{obsv}} \begin{bmatrix} C\mathbf{r}_k & 0 \end{bmatrix} e^{\Lambda_k t} \begin{bmatrix} 0 \\ \mathbf{q}_k^* \end{bmatrix},$$

which has a realization

$$T(t) = \left(\begin{array}{c|c} \begin{bmatrix} \ddots & & \\ & \Lambda_k & \\ & & \ddots \end{bmatrix} & \begin{bmatrix} \vdots \\ \begin{bmatrix} 0 \\ \mathbf{q}_k^* \end{bmatrix} \\ \vdots \end{bmatrix} \\ \hline \begin{bmatrix} \dots & [C\mathbf{r}_k \ 0] & \dots \end{bmatrix} & 0 \end{array} \right), \quad k \in \mathcal{N}_{obsv}. \tag{4.19}$$

The associated observability matrix is given by

$$\mathcal{O} = \begin{bmatrix} \begin{bmatrix} \dots & C\mathbf{r}_k & 0 & \dots \end{bmatrix} \\ \begin{bmatrix} \dots & C\mathbf{r}_k & 0 \end{bmatrix}\Lambda_k \ \dots \\ \vdots \\ \begin{bmatrix} \dots & C\mathbf{r}_k & 0 \end{bmatrix}\Lambda_k^{2|\mathcal{N}_{obsv}|-1} \ \dots \end{bmatrix}, \tag{4.20}$$

where $k \in \mathcal{N}_{obsv}$ and $|\mathcal{N}_{obsv}|$ denotes the cardinality of $\mathcal{N}_{obsv}$. Due to the form of Λ_k in (4.18), we can see that $\begin{bmatrix} C\mathbf{r}_k & 0 \end{bmatrix}\Lambda_k = \begin{bmatrix} 0 & C\mathbf{r}_k \end{bmatrix}$. Then the first two block-rows of (4.20) imply that $\mathcal{O}$ is full rank if the vectors $C\mathbf{r}_k$ are linearly independent for $k \in \mathcal{N}_{obsv}$. For a proof by contradiction, assume that $C\mathbf{r}_k$ are linearly dependent, i.e. $\sum_{k\in\mathcal{N}_{obsv}} \alpha_k C\mathbf{r}_k = 0$ where α_k is non-zero for some k. This implies that $\sum_{k\in\mathcal{N}_{obsv}} \alpha_k \mathbf{r}_k \in \ker\{C\}$, which can be expressed as a linear combination of the vectors that span $\ker\{C\}$. Then

$$\sum_{k\in\mathcal{N}_{obsv}} \alpha_k \mathbf{r}_k = -\sum_{k\in\{1,\dots,n\}\setminus\mathcal{N}_{obsv}} \alpha_k \mathbf{r}_k \Rightarrow \sum_{k=1}^{n} \alpha_k \mathbf{r}_k = 0,$$

which would contradict the fact that R is invertible. Therefore, $\mathcal{O}$ in (4.20) is full rank, so the realization in (4.19) is observable. By a similar argument we can prove the controllability, hence the minimality of (4.19). Therefore, the poles of $T(s)$ in (4.11a) are given precisely by the eigenvalues of the system matrix in (4.19), which are determined by (4.17). Then $T(s)$ is input-output stable if and only if its poles are on the open left half-plane.

We now repeat the argument for (4.11b) which is given by

$$T(t) \ = \sum_{k\in\mathcal{N}_{obsv}} \begin{bmatrix} 0 & C\mathbf{r}_k \end{bmatrix} e^{\Lambda_k t} \begin{bmatrix} 0 \\ \mathbf{q}_k^* \end{bmatrix}$$

in time-domain with a realization

$$T(t) = \left(\begin{array}{c|c} \begin{bmatrix} \ddots & & \\ & \Lambda_k & \\ & & \ddots \end{bmatrix} & \begin{bmatrix} \vdots \\ \begin{bmatrix} 0 \\ \mathbf{q}_k^* \end{bmatrix} \\ \vdots \end{bmatrix} \\ \hline \begin{bmatrix} \dots & 0 & C\mathbf{r}_k & \dots \end{bmatrix} & 0 \end{array}\right), \quad k \in \mathcal{N}_{obsv}. \tag{4.21}$$

The associated observability matrix is given by

$$\mathcal{O} = \begin{bmatrix} \begin{bmatrix} \dots & [0 & C\mathbf{r}_k] & \dots \end{bmatrix} \\ \begin{bmatrix} \dots & [0 & C\mathbf{r}_k]\Lambda_k & \dots \end{bmatrix} \\ \vdots \\ \begin{bmatrix} \dots & [0 & C\mathbf{r}_k]\Lambda_k^{2|\mathcal{N}_{obsv}|-1} & \dots \end{bmatrix} \end{bmatrix}, \tag{4.22}$$

where $k \in \mathcal{N}_{obsv}$. Since

$$\begin{bmatrix} 0 & C\mathbf{r}_k \end{bmatrix} \Lambda_k = C\mathbf{r}_k \begin{bmatrix} -k_p - \gamma_p \lambda_k & -k_d - \gamma_d \lambda_k \end{bmatrix},$$

and assumption 4.1 holds, (4.22) is full rank and (4.21) is observable, hence minimal. Therefore, the poles of $T(s)$ in (4.11b) are given precisely by the eigenvalues of the system matrix in (4.21), which are determined by (4.17). Then $T(s)$ is input-output stable if and only if its poles are on the open left half-plane. □

Remark 4.2. *Assumption 4.2 can be relaxed for specific values of k_p and k_d for which the consensus modes become Hurwitz. If $k_p > 0$ and $k_d > 0$, the assumption can be relaxed for both (4.11a) and (4.11b) since $H_{\tilde{\mathbf{x}}_1\tilde{\mathbf{w}}_1}(s) = \frac{h_1(s)}{f(s)} = g(s) = \frac{1}{s^2+k_d s+k_p}$ and $H_{\tilde{\mathbf{v}}_1\tilde{\mathbf{w}}_1}(s) = sH_{\tilde{\mathbf{x}}_1\tilde{\mathbf{w}}_1}(s) = \frac{s}{s^2+k_d s+k_p}$ have stable poles by the Routh-Hurwitz criterion.*

Similarly, one can relax the assumption for (4.11b) but not for (4.11a) if $k_p = 0$ and $k_d > 0$ since $H_{\tilde{\mathbf{x}}_1\tilde{\mathbf{w}}_1}(s) = \frac{1}{s^2+k_d s}$ has a pole at $s = 0$ but $H_{\tilde{\mathbf{v}}_1\tilde{\mathbf{w}}_1}(s) = \frac{s}{s^2+k_d s} = \frac{1}{s+k_d}$ has a stable pole. However for the sake of simplicity, we only consider performance metrics such that Assumption 4.2 is satisfied for both (4.11a) and (4.11b).

The stability condition in Proposition 4.2 can be restated as follows.

Proposition 4.3. *Consider the double-integrator network (4.2) and suppose that L is diagonalizable and assumptions 4.1 and 4.2 hold. The system T given by (4.11a) or (4.11b) is input-output stable if and only if*

$$\alpha_k \phi_k^2 + \beta_k \xi_k \phi_k - \beta_k^2 > 0 \text{ and } \phi_k > 0, \quad k \in \mathcal{N}_{obsv}, \tag{4.23}$$

where $\alpha_k = k_p + \gamma_p \operatorname{Re}[\lambda_k]$, $\phi_k = k_d + \gamma_d \operatorname{Re}[\lambda_k]$, $\beta_k = \gamma_p \operatorname{Im}[\lambda_k]$ and $\xi_k = \gamma_d \operatorname{Im}[\lambda_k]$.

Proof. The result follows from applying [9, Lemma 2] to Proposition 4.2. □

Propositions 4.2 and 4.3 generalize the necessary and sufficient conditions for second order consensus ([9, Theorem 1]) to input-output stability conditions, which are required for the performance evaluation. We next introduce our framework for analyzing the performance of directed networks.

4.3 Performance over Arbitrary Digraphs

In this section, we use the block-diagonalization procedure outlined in Section 4.2 to develop an analysis framework for the performance of the single and double-integrator networks (4.1) and (4.2). This framework is applicable to systems over arbitrary directed graphs that have at least one globally reachable node. We will use this framework in the subsequent chapters to derive closed-form solutions to performance metrics of various subclasses of systems. Throughout the discussion we use both time and frequency domain representations, which simplifies the analysis.

First, we simplify (2.14) using the block-diagonal form of (4.7) and show that performance can be quantified as a linear combination of scalar integrals. These integrals can be interpreted as $\mathcal{L}_2$ scalar products of the elements of the closed-loop impulse response function matrix blocks $H_{\tilde{\mathbf{x}}_k\tilde{\mathbf{w}}_k}(t)$ and $H_{\tilde{\mathbf{v}}_k\tilde{\mathbf{w}}_k}(t)$.

Combining (2.14) and (4.13), the performance metric in (2.14) can be written as

$$P = \int_0^\infty \mathbf{w}_0^* \tilde{Q}^* \tilde{H}(t)^* \tilde{N} \tilde{H}(t) \tilde{Q} \mathbf{w}_0 dt, \tag{4.24}$$

where $\tilde{N} = \tilde{R}^* C^* C \tilde{R}$ and $\tilde{H}$ is defined as in (4.14) with

$$\tilde{H}_k(s) = \begin{bmatrix} \tilde{h}_{11}^{(k)}(s) & \dots & \tilde{h}_{1,n_k}^{(k)}(s) \\ & \ddots & \vdots \\ & & \tilde{h}_{n_k,n_k}^{(k)}(s) \end{bmatrix} \tag{4.25}$$

for $k = 2, \dots, m$. The upper triangular form of (4.25) is given in Lemma 4.1. Since

$$M := C^* C \tag{4.26}$$

is a symmetric matrix, it is unitarily diagonalizable, i.e.

$$M = \Theta W \Theta^*, \quad W = \operatorname{diag}(\mu_i)_{1\le i\le n} \in \mathbb{R}^{n\times n}, \quad \text{and} \quad \Theta\Theta^* = I,$$

therefore $\tilde{N} = \tilde{R}^*\Theta W \Theta^* \tilde{R}$. Using Assumption 4.2 and assuming without loss of generality that $\mu_1 = 0$ is associated with the eigenvector $\boldsymbol{\theta}_1 = \frac{1}{\sqrt{n}}\mathbf{1}$, we can state $\tilde{N}$ element-wise as

$$(\tilde{N})_{\eta-1,\kappa-1} = \sum_{l=2}^{n} \langle \boldsymbol{\theta}_l, \mathbf{r}_\eta\rangle\langle \mathbf{r}_\kappa, \boldsymbol{\theta}_l\rangle \mu_l =: \nu_{\eta,\kappa} \tag{4.27}$$

for $\eta, \kappa = 2, \dots, n$, where $\langle \boldsymbol{\theta}_l, \mathbf{r}_\eta\rangle = \mathbf{r}_\eta^* \boldsymbol{\theta}_l$, $\mathbf{r}_\kappa$ and $\boldsymbol{\theta}_l$ denote respectively the columns κ and l of $\tilde{R}$ and Θ.

Using this notation, (4.24) can be written in terms of the scalar products between the elements of $\tilde{H}_k(t)$, which are given by the element-wise inverse Laplace transforms of (4.25).

Lemma 4.2. *The performance metric P in (4.24) is given by*

$$P = \operatorname{tr}(\Sigma_Q \Psi), \tag{4.28}$$

where

$$\Sigma_Q = \tilde{Q}\Sigma_0\tilde{Q}^*, \ \Sigma_0 = \mathbf{w}_0\mathbf{w}_0^*, \tag{4.29}$$

and the matrix Ψ is partitioned as $\Psi = [\Psi_{kl}]_{2\le k,l\le m}$.

Furthermore, the entry (q, b) of the matrix Ψ_{kl} for $k, l = 2, \dots, m$ is given by

$$[\Psi_{kl}]_{qb} = \sum_{p=1}^{q}\sum_{a=1}^{b} \nu_{d_k+p, d_l+a} \left\langle \tilde{h}_{ab}^{(l)}(t), \tilde{h}_{pq}^{(k)}(t)\right\rangle_{\mathcal{L}_2}, \tag{4.30}$$

where

$$\left\langle \tilde{h}_{ab}^{(l)}(t), \tilde{h}_{pq}^{(k)}(t)\right\rangle_{\mathcal{L}_2} = \int_0^\infty \overline{\tilde{h}_{pq}^{(k)}(t)}\tilde{h}_{ab}^{(l)}(t)dt. \tag{4.31}$$

Here the indices $q = 1, \dots, n_k$ and $b = 1, \dots, n_l$ are determined by the Jordan block sizes n_k and n_l. Terms of the form in (4.27) appear in the summand of (4.30) and their indices take values larger than the sum of the previous Jordan block sizes, namely $d_k = \sum_{i=1}^{k-1} n_i$ and $d_l = \sum_{i=1}^{l-1} n_i$.

Remark 4.3. *For the special case in which L is diagonalizable each Jordan block is a scalar, i.e. $n_k = 1$, and (4.30) leads to*

$$\Psi_{kl} = \nu_{kl} \left\langle \tilde{h}^{(l)}(t), \tilde{h}^{(k)}(t) \right\rangle_{\mathcal{L}_2}.$$

Here we dropped the subscripts of $\tilde{h}^{(k)}_{pq}$ for simplicity. The case with diagonalizable L was studied in [59, 60] and Lemma 4.2 provides a generalization to the case of arbitrary Jordan block size n_k for $k = 2, \ldots, m$.

Proof of Lemma 4.2. Taking the trace of both sides of (4.24) and using the permutation property of the trace, we have $P = \operatorname{tr}\left(\tilde{Q}\mathbf{w}_0\mathbf{w}_0^*\tilde{Q}^*\Psi\right)$, where $\Psi(t) = \int_0^\infty \tilde{H}(t)^*\tilde{N}\tilde{H}(t)dt$. Partitioning $\tilde{N}$ conformally so that its (k,l) block is given by $\tilde{N}_{kl}$, one can write

$$\Psi_{kl} = \int_0^\infty \tilde{H}_k(t)^*\tilde{N}_{kl}\tilde{H}_l(t)dt, \tag{4.32}$$

for $k, l = 2, \ldots, m$. Direct multiplication of the matrices in the integral argument and interchanging the order of integration with the summation gives the desired result. □

Remark 4.4. *Since $\tilde{N} = \tilde{N}^*$, i.e. $\tilde{N}_{kl} = \tilde{N}^*_{lk}$, (4.32) leads to $\Psi_{kl} = \Psi^*_{lk}$, therefore Ψ is Hermitian. The fact that Σ_Q in (4.29) is also Hermitian leads to $\operatorname{tr}(\Sigma_Q\Psi) = \operatorname{tr}[(\Sigma_Q\Psi)^*] = \overline{\operatorname{tr}(\Sigma_Q\Psi)}$, which verifies that P in (4.28) is real as expected.*

As Lemma 4.2 indicates, (4.28) can be expressed in closed-form if the integral in (4.31) can be evaluated. This provides a general framework for the computation of the performance metrics, which we utilize by first deriving time-domain realizations for the transfer functions $\tilde{h}^{(k)}_{pq}(s)$ in (4.25) for systems defined over various families of graphs, and then using these realizations in order to evaluate the integral in (4.31). By using our closed-form solutions in the upcoming chapters, we analyze system properties pertaining to the directionality of the underlying network interconnection.

We next use our framework in order to derive the closed-form solutions for the general quadratic performance metrics of single and double-integrator networks over

arbitrary directed graphs that have at least one globally reachable node.

4.3.1 Performance of Single-Integrator Networks

We first present the result pertaining to the single-integrator network (4.1). The following theorem provides a closed-form solution for the performance metric P in (2.12).

Theorem 4.1. *Consider the single-integrator network* (4.1)*. The performance metric* P *in* (2.12) *for the system* T *given by* (4.11a) *is* $P = \operatorname{tr}(\Sigma_Q \Psi)$*. The elements of* Ψ *are defined in* (4.30) *and the scalar product in* (4.31) *is given by*

$$\left\langle \tilde{h}_{ab}^{(l)}(t), \tilde{h}_{pq}^{(k)}(t) \right\rangle_{\mathcal{L}_2} = \frac{(-1)^{b-a+q-p}\Phi}{\left(\overline{\lambda_k} + \lambda_l\right)^{b-a+q-p+1}}, \tag{4.33}$$

where $\Phi = \frac{(b-a+q-p)!}{(b-a)!(q-p)!}$.

Proof. Using the result of Corollary 4.1 and the notation in (4.25)

$$\tilde{h}_{pq}^{(k)}(s) = (-1)^{q-p} \frac{1}{(s+\lambda_k)^{q-p+1}}.$$

Here, $\frac{1}{(s+\lambda_k)^{q-p+1}}$ has the following realization $(\mathcal{A}_{k,\delta}, \mathcal{B}_{k,\delta}, \mathcal{C}_{k,\delta})$ in JCF

$$\mathcal{A}_{k,\delta} = \mathcal{J}(-\lambda_k, \delta), \tag{4.34}$$

$$\mathcal{B}_{k,\delta} = \Big[\underbrace{0 \quad \dots \quad 1}_{1\times\delta}\Big]^{\intercal}, \mathcal{C}_{k,\delta} = \Big[\underbrace{1 \quad \dots \quad 0}_{1\times\delta}\Big],$$

where $\mathcal{J}(-\lambda_k, \delta)$ denotes the size-δ Jordan block with the eigenvalue $-\lambda_k$ and $\delta = q - p + 1$. Then, $\tilde{h}_{pq}^{(k)}(t)$ is given by

$$\tilde{h}_{pq}^{(k)}(t) = (-1)^{q-p} C_{k,\delta} e^{A_{k,\delta} t} B_{k,\delta}. \tag{4.35}$$

where

$$e^{A_{k,\delta}t} = e^{\mathcal{J}(-\lambda_k,\delta)t} = e^{-\lambda_k t} \begin{bmatrix} 1 & t & \dots & \frac{t^{(\delta-1)}}{(\delta-1)!} \\ & \ddots & \ddots & \vdots \\ & & & t \\ & & & 1 \end{bmatrix}. \tag{4.36}$$

Combining (4.34) and (4.35) leads to

$$\tilde{h}_{pq}^{(k)}(t) = (-1)^{q-p} e^{-\lambda_k t} \frac{t^{q-p}}{(q-p)!}.$$

The proof is completed by evaluating the integral in (4.31) using the fact that $\int_0^\infty t^n e^{-\lambda t} dt = \frac{n!}{\lambda^{n+1}}$ for $\lambda \in \mathbb{C}$, $\mathrm{Re}[\lambda] > 0$. □

The denominator of the right-hand side of (4.33) is given by a power of the sum of the graph Laplacian eigenvalues that are associated with possibly distinct Jordan blocks k and l. The power of this term depends on the Jordan block sizes n_k and n_l through the indices q and b and it increases as the Jordan block size increases. This indicates that performance is affected not only by the network size, but also by the graph Laplacian spectrum and the size of the individual Jordan blocks.

We next present the analogous result for the double-integrator network (4.2).

4.3.2 Performance of Double-Integrator Networks

We now provide the closed-form solution for the performance metric P in (2.12) for the double-integrator network (4.2). A similar approach to the one in Theorem 4.1 is taken but the computation of the impulse response functions $\tilde{h}_{pq}^{(k)}(t)$ is more involved. We compute these functions through Lemmas 4.3 and 4.4 in the Appendix. Then by evaluating the integral in (4.31), the result of this subsection is stated as follows.

Theorem 4.2. *Consider the double-integrator network (4.2). Let $\rho_1^{(k)}$ and $\rho_2^{(k)}$ denote the roots of*

$$s^2 + (k_d + \gamma_d \lambda_k)s + k_p + \gamma_p \lambda_k = 0. \tag{4.37}$$

The performance metric P in (2.12) for the system T given by (4.11a) or (4.11b) is $P = \mathrm{tr}\,(\Sigma_Q \Psi)$, where Ψ is given element-wise by (4.30) and the scalar product in (4.31) is as follows:

If $\rho_1^{(k)} \neq \rho_2^{(k)}$ *and* $\rho_1^{(l)} \neq \rho_2^{(l)}$

$$\begin{aligned}\left\langle \tilde{h}_{ab}^{(l)}(t), \tilde{h}_{pq}^{(k)}(t) \right\rangle_{\mathcal{L}_2} &= \sum_{\zeta=1}^{\sigma} \sum_{r=1}^{\upsilon} \frac{\Phi_{\zeta r}(\sigma,\upsilon)\overline{c_\zeta^{(k)}} c_r^{(l)}}{\left(\overline{\rho_1^{(k)}} + \rho_1^{(l)}\right)^{\sigma+\upsilon-\zeta-r+1}} \\ &+ \frac{\Phi_{\zeta r}(\sigma,\upsilon)\overline{c_\zeta^{(k)}} c_{r+\upsilon}^{(l)}}{\left(\overline{\rho_1^{(k)}} + \rho_2^{(l)}\right)^{\sigma+\upsilon-\zeta-r+1}} + \frac{\Phi_{\zeta r}(\sigma,\upsilon)\overline{c_{\zeta+\sigma}^{(k)}} c_r^{(l)}}{\left(\overline{\rho_2^{(k)}} + \rho_1^{(l)}\right)^{\sigma+\upsilon-\zeta-r+1}} \\ &+ \frac{\Phi_{\zeta r}(\sigma,\upsilon)\overline{c_{\zeta+\sigma}^{(k)}} c_{r+\upsilon}^{(l)}}{\left(\overline{\rho_2^{(k)}} + \rho_2^{(l)}\right)^{\sigma+\upsilon-\zeta-r+1}},\end{aligned} \tag{4.38}$$

If $\rho_1^{(k)} \neq \rho_2^{(k)}$ *and* $\rho_1^{(l)} = \rho_2^{(l)} = \rho^{(l)}$

$$\begin{aligned}\left\langle \tilde{h}_{ab}^{(l)}(t), \tilde{h}_{pq}^{(k)}(t) \right\rangle_{\mathcal{L}_2} &= \sum_{\zeta=1}^{\sigma} \sum_{r=1}^{2\upsilon} \frac{(-1)^{\upsilon}\Phi_{\zeta r}(\sigma,2\upsilon)\overline{c_\zeta^{(k)}} c_r^{(l)}}{\left(\overline{\rho_1^{(k)}} + \rho^{(l)}\right)^{\sigma+2\upsilon-\zeta-r+1}} \\ &+ \frac{(-1)^{\upsilon}\Phi_{\zeta r}(\sigma,2\upsilon)\overline{c_{\zeta+\sigma}^{(k)}} c_r^{(l)}}{\left(\overline{\rho_2^{(k)}} + \rho^{(l)}\right)^{\sigma+2\upsilon-\zeta-r+1}},\end{aligned} \tag{4.39}$$

If $\rho_1^{(k)} = \rho_2^{(k)} = \rho^{(k)}$ *and* $\rho_1^{(l)} = \rho_2^{(l)} = \rho^{(l)}$

$$\left\langle \tilde{h}_{ab}^{(l)}(t), \tilde{h}_{pq}^{(k)}(t) \right\rangle_{\mathcal{L}_2} = \sum_{\zeta=1}^{2\sigma} \sum_{r=1}^{2\upsilon} \frac{(-1)^{\sigma+\upsilon}\Phi_{\zeta r}(2\sigma,2\upsilon)\overline{c_\zeta^{(k)}} c_r^{(l)}}{\left(\overline{\rho^{(k)}} + \rho^{(l)}\right)^{2\sigma+2\upsilon-\zeta-r+1}}, \tag{4.40}$$

where $\sigma = q - p + 1$, $\upsilon = b - a + 1$ *and* $\Phi_{\zeta r}(\sigma,\upsilon) = (-1)^{1-\zeta-r}\frac{(\sigma+\upsilon-\zeta-r)!}{(\sigma-\zeta)!(\upsilon-r)!}$.

The coefficients $c_\zeta^{(k)}$ *are given in the Appendix by Lemma 4.3 if* $\rho_1^{(k)} \neq \rho_2^{(k)}$ *and by Lemma 4.4 if* $\rho_1^{(k)} = \rho_2^{(k)}$.

Remark 4.5. *For double-integrator networks, the scalar products in* (4.38) - (4.40) *depend on both the control gains and the eigenvalues of* L*, via the roots of* (4.37) *and the coefficients* $c_\zeta^{(k)}$*. In contrast, for single-integrator networks, eigenvalues of* L *appear explicitly in the analogous expression in* (4.33).

Proof of Theorem 4.2. Using the result of Corollary 4.2, the notation in (4.25) and (4.42), $\tilde{h}_{pq}^{(k)}(t)$ is given by

$$\tilde{h}_{pq}^{(k)}(t) = (-1)^{\sigma-1}\Omega_{k,\sigma}(t). \tag{4.41}$$

If $\rho_1^{(k)} \neq \rho_2^{(k)}$, the realization in (4.43) can be used to calculate

$$\Omega_{k,\sigma}(t) = C_{k,\sigma} e^{A_{k,\sigma} t} B_{k,\sigma},$$

where $e^{A_{k,\sigma}t} = \text{blockdiag}\left(e^{\mathcal{J}(\rho_i^{(k)},\sigma)t}\right)_{i=1,2}$ and $e^{\mathcal{J}(\rho_i^{(k)},\sigma)t}$ can be expanded as in (4.36). Then, using (4.41) and the definitions of $C_{k,\sigma}$ and $B_{k,\sigma}$ in (4.43)

$$\tilde{h}_{pq}^{(k)}(t) = (-1)^{\sigma-1} \sum_{\zeta=1}^{\sigma} \left(c_\zeta^{(k)} e^{\rho_1^{(k)} t} + c_{\zeta+\sigma}^{(k)} e^{\rho_2^{(k)} t} \right) \frac{t^{\sigma-\zeta}}{(\sigma-\zeta)!}.$$

If $\rho_1^{(k)} = \rho_2^{(k)} = \rho^{(k)}$, a similar argument combined with (4.52) leads to

$$\tilde{h}_{pq}^{(k)}(t) = (-1)^{\sigma-1} \sum_{\zeta=1}^{2\sigma} c_\zeta^{(k)} e^{\rho^{(k)} t} \frac{t^{2\sigma-\zeta}}{(2\sigma-\zeta)!}.$$

The proof is completed by evaluating the integral in (4.31) using the fact that $\int_0^\infty t^n e^{\lambda t} dt = (-1)^{n+1} \frac{n!}{\lambda^{n+1}}$ for $\lambda \in \mathbb{C}$, $\text{Re}[\lambda] < 0$. □

Theorems 4.1 and 4.2 provide closed-form solutions for the performance metric (2.12) which consist of terms that: (a) are geometric, i.e. terms that depend on the input direction, the eigenvalues and the eigenvectors of M in (4.26) and the eigenvectors of L as in (4.27) and (4.29); and (b) terms that depend on the closed-loop dynamics of the system, as in (4.31). Overall, performance is given by a linear combination of the entries of the matrix Ψ in (4.30), weighted by the entries of the matrix Σ_Q in (4.29). Therefore, in the most general case, it is not straightforward to deduce the individual effect of properties such as network size, graph topology and the spectrum of the output matrix for an arbitrary system.

4.4 Summarizing Remarks

We developed a novel analysis framework to evaluate the performance of directed networks. Using this framework, we derived the closed-form solutions for the general quadratic performance metrics of single and double-integrator networks over arbitrary directed graphs that have at least one globally reachable node. In the following chapters,

we focus on systems defined over a special class of graphs that emit diagonalizable weighted Laplacian matrices. We derive the closed-form solutions for the performance metrics of these systems, which we then use to analyze system properties pertaining to the directionality of the underlying network interconnection.

4.5 APPENDIX

4.5.1 Lemmas from Subsection 4.3.2

Lemma 4.3. *Consider the transfer function*

$$\Omega_{k,\delta}(s) = \frac{r(s)(\gamma_p + s\gamma_d)^{\delta-1}}{\left[s^2 + (k_d + \gamma_d\lambda_k)s + k_p + \gamma_p\lambda_k\right]^{\delta}} \tag{4.42}$$

for some $\delta \in \mathbb{Z}_+$. Suppose that $s^2 + (k_d + \gamma_d\lambda_k)s + k_p + \gamma_p\lambda_k = 0$ has distinct roots $\rho_1^{(k)}$ and $\rho_2^{(k)}$, i.e. $\rho_1^{(k)} \neq \rho_2^{(k)}$. Then, $\Omega_{k,\delta}(s)$ has a realization $(\mathcal{A}_{k,\delta}, \mathcal{B}_{k,\delta}, \mathcal{C}_{k,\delta})$ in Jordan canonical form given by

$$\mathcal{A}_{k,\delta} = \text{blockdiag}\left(\mathcal{J}(\rho_i^{(k)}, \delta)\right)_{i=1,2}, \tag{4.43}$$

$\mathcal{B}_{k,\delta} = \Big[\underbrace{0 \ \ldots \ 1}_{1\times\delta} \underbrace{0 \ \ldots \ 1}_{1\times\delta}\Big]^{\mathsf{T}}$, $\mathcal{C}_{k,\delta} = \begin{bmatrix} c_1^{(k)} & \ldots & c_{2\delta}^{(k)} \end{bmatrix}$, *where $\mathcal{J}(\rho_1^{(k)}, \delta)$ denotes the size-δ Jordan block with the eigenvalue $\rho_1^{(k)}$.*

If $r(s) = 1$, i.e. we consider system T given by (4.11a), the elements of $\mathcal{C}_{k,\delta}$ are given by

$$c_l^{(k)} = \sum_{\zeta=0}^{l-1} \tau(\zeta, l)\gamma_d{}^{\zeta} \frac{\left(\gamma_p + \rho_1^{(k)}\gamma_d\right)^{\delta-\zeta-1}}{\left(\rho_1^{(k)} - \rho_2^{(k)}\right)^{\delta+l-\zeta-1}},$$
$$c_{l+\delta}^{(k)} = \sum_{\zeta=0}^{l-1} \tau(\zeta, l)\gamma_d{}^{\zeta} \frac{\left(\gamma_p + \rho_2^{(k)}\gamma_d\right)^{\delta-\zeta-1}}{\left(\rho_2^{(k)} - \rho_1^{(k)}\right)^{\delta+l-\zeta-1}},$$

if $r(s) = s$, i.e. we consider system T given by (4.11b), the elements of $\mathcal{C}_{k,\delta}$ are given

by

$$c_l^{(k)} = \sum_{\zeta=0}^{l-1} \tau(\zeta,l)\gamma_d{}^{\zeta-1}\left(\frac{\zeta\gamma_p+\delta\rho_1^{(k)}\gamma_d}{\delta-\zeta}\right)\frac{\left(\gamma_p+\rho_1^{(k)}\gamma_d\right)^{\delta-\zeta-1}}{\left(\rho_1^{(k)}-\rho_2^{(k)}\right)^{\delta+l-\zeta-1}},$$
$$c_{l+\delta}^{(k)} = \sum_{\zeta=0}^{l-1} \tau(\zeta,l)\gamma_d{}^{\zeta-1}\left(\frac{\zeta\gamma_p+\delta\rho_2^{(k)}\gamma_d}{\delta-\zeta}\right)\frac{\left(\gamma_p+\rho_2^{(k)}\gamma_d\right)^{\delta-\zeta-1}}{\left(\rho_2^{(k)}-\rho_1^{(k)}\right)^{\delta+l-\zeta-1}},$$

for $l=1,\ldots,\delta$, *where* $\tau(\zeta,l)=(-1)^{l-\zeta-1}\binom{l-1}{\zeta}\binom{\delta+l-\zeta-2}{l-1}$.

Proof. Using the fact that the denominator of $\Omega_{k,\delta}(s)$ has distinct roots

$$\Omega_{k,\delta}(s)=\frac{\Gamma(s)}{\left(s-\rho_1^{(k)}\right)^{\delta}\left(s-\rho_2^{(k)}\right)^{\delta}},$$

where $\Gamma(s)=r(s)(\gamma_p+s\gamma_d)^{\delta-1}$. Applying partial fractions, we have

$$\Omega_{k,\delta}(s)=\sum_{l=1}^{\delta}\frac{c_l^{(k)}}{\left(s-\rho_1^{(k)}\right)^{\delta-l+1}}+\frac{c_{l+\delta}^{(k)}}{\left(s-\rho_2^{(k)}\right)^{\delta-l+1}}, \tag{4.44}$$

which can be represented by the Jordan canonical realization (4.43). Here the coefficients $c_l^{(k)}$ and $c_{l+\delta}^{(k)}$ are given by

$$c_l^{(k)}=\frac{1}{(l-1)!}\lim_{s\to\rho_1^{(k)}}\frac{d^{l-1}}{ds^{l-1}}\left[\left(s-\rho_1^{(k)}\right)^{\delta}\Omega_{k,\delta}(s)\right], \tag{4.45}$$
$$c_{l+\delta}^{(k)}=\frac{1}{(l-1)!}\lim_{s\to\rho_2^{(k)}}\frac{d^{l-1}}{ds^{l-1}}\left[\left(s-\rho_2^{(k)}\right)^{\delta}\Omega_{k,\delta}(s)\right]. \tag{4.46}$$

The general Leibniz rule for the derivative of product yields

$$c_l^{(k)}=\lim_{s\to\rho_1^{(k)}}\sum_{\zeta=0}^{l-1}\frac{\binom{l-1}{\zeta}}{(l-1)!}\frac{d^{\zeta}\Gamma(s)}{ds^{\zeta}}\frac{d^{l-1-\zeta}}{ds^{l-1-\zeta}}\left[\left(s-\rho_2^{(k)}\right)^{-\delta}\right], \tag{4.47}$$
$$c_{l+\delta}^{(k)}=\lim_{s\to\rho_2^{(k)}}\sum_{\zeta=0}^{l-1}\frac{\binom{l-1}{\zeta}}{(l-1)!}\frac{d^{\zeta}}{ds^{\zeta}}\Gamma(s)\frac{d^{l-1-\zeta}}{ds^{l-1-\zeta}}\left[\left(s-\rho_1^{(k)}\right)^{-\delta}\right], \tag{4.48}$$

For the cases of $r(s)=1$ or $r(s)=s$, a direct calculation shows that

$$\frac{d^{\zeta}}{ds^{\zeta}}\left[(\gamma_p+s\gamma_d)^{\delta-1}\right]=\gamma_d{}^{\zeta}\frac{(\delta-1)!}{(\delta-\zeta-1)!}(\gamma_p+s\gamma_d)^{\delta-\zeta-1}, \tag{4.49}$$

$$\begin{aligned}\frac{d^{\zeta}}{ds^{\zeta}}\left[s(\gamma_p+s\gamma_d)^{\delta-1}\right]=&s\gamma_d{}^{\zeta}\frac{(\delta-1)!}{(\delta-\zeta-1)!}(\gamma_p+s\gamma_d)^{\delta-\zeta-1}\\&+\gamma_d{}^{\zeta-1}\zeta\frac{(\delta-1)!}{(\delta-\zeta)!}(\gamma_p+s\gamma_d)^{\delta-\zeta},\end{aligned} \tag{4.50}$$

$$\frac{d^{l-1-\zeta}}{ds^{l-1-\zeta}}\left[(s-\rho_2^{(k)})^{-\delta}\right]=(-1)^{l-1-\zeta}\frac{(\delta+l-\zeta-2)!}{(\delta-1)!}(s-\rho_2^{(k)})^{-\delta-l+\zeta+1}. \tag{4.51}$$

Substituting (4.49), (4.50) and (4.51) into (4.47) and taking the limit gives the desired result. A similar procedure can be followed to evaluate the expression in (4.48). □

Lemma 4.4. *Consider the transfer function $\Omega_{k,\delta}(s)$ in (4.42) for some $\delta \in \mathbb{Z}_+$. Suppose that $s^2+(k_d+\gamma_d\lambda_k)s+k_p+\gamma_p\lambda_k=0$ has repeated roots $\rho_1^{(k)}$ and $\rho_2^{(k)}$, i.e. $\rho_1^{(k)}=\rho_2^{(k)}=\rho^{(k)}$. Then, $\Omega_{k,\delta}(s)$ has a realization $(\mathcal{A}_{k,\delta},\mathcal{B}_{k,\delta},\mathcal{C}_{k,\delta})$ in Jordan canonical form given by*

$$\mathcal{A}_{k,\delta}=\mathcal{J}(\rho^{(k)},2\delta), \tag{4.52}$$

$$\mathcal{B}_{k,\delta}=\Big[\underbrace{0\quad\dots\quad 1}_{1\times 2\delta}\Big]^{\intercal},\mathcal{C}_{k,\delta}=\begin{bmatrix}c_1^{(k)} & \dots & c_{2\delta}^{(k)}\end{bmatrix}.$$

If $r(s)=1$, i.e. we consider system T given by (4.11a), the elements of $\mathcal{C}_{k,\delta}$ are given by

$$c_l^{(k)}=\begin{cases}{\gamma_d}^{l-1}\binom{\delta-1}{l-1}(\gamma_p+\rho^{(k)}\gamma_d)^{\delta-l}, & 1\le l\le\delta\\ 0, & \delta+1\le l\le 2\delta\end{cases},$$

if $r(s)=s$, i.e. we consider system T given by (4.11b), the elements of $\mathcal{C}_{k,\delta}$ are given by

$$c_l^{(k)}=\begin{cases}\left[\frac{(l-1)\gamma_p+\delta\rho^{(k)}\gamma_d}{\delta-l+1}\right]{\gamma_d}^{l-2}\binom{\delta-1}{l-1}(\gamma_p+\rho^{(k)}\gamma_d)^{\delta-l}, & 1\le l\le\delta\\ {\gamma_d}^{\delta-1}, & l=\delta+1\\ 0, & \delta+2\le l\le 2\delta\end{cases}.$$

Proof. Using the fact that $\Omega_{k,\delta}(s)$ has repeated roots leads to

$$\Omega_{k,\delta}(s)=\frac{r(s)(\gamma_p+s\gamma_d)^{\delta-1}}{(s-\rho^{(k)})^{2\delta}}.$$

Applying partial fractions, we have

$$\Omega_{k,\delta}(s)=\sum_{l=1}^{2\delta}\frac{c_l^{(k)}}{(s-\rho^{(k)})^{2\delta-l+1}},$$

which can be represented by the Jordan canonical realization (4.52). Here the coefficients $c_l^{(k)}$ are given by

$$c_l^{(k)}=\frac{1}{(l-1)!}\lim_{s\to\rho^{(k)}}\frac{d^{l-1}}{ds^{l-1}}\left[r(s)(\gamma_p+s\gamma_d)^{\delta-1}\right]. \tag{4.53}$$

For the cases of $r(s) = 1$ or $r(s) = s$, using respectively (4.49) and (4.50) and taking the limit in (4.53) gives the desired result. □

Chapter 5

Effect of Communication Directionality on Performance

In this chapter, we investigate the role of the directionality associated with the underlying network interconnection. We use systems with normal Laplacian matrices as an example, since their spectral structures exhibit properties (unitary eigenbasis, the relationship between directed edges and complex eigenvalues) that enable a comprehensive analysis of directionality. We present a comparative analysis between directed graphs and their undirected counterparts represented by the Hermitian part of the graph Laplacian. For the family of graphs that emit normal Laplacian matrices, the Hermitian part of the Laplacian represents a "symmetrized" version of the original directed graph, preserving the weighted out-degree of nodes.

In this setting, we show that directed graphs and their undirected counterparts provide identical performance for single integrator networks. In the case of double-integrator networks, we demonstrate that the presence of observable Laplacian eigenvalues with nonzero imaginary part (i.e. the observability of modes associated with directed paths) can significantly degrade both position and velocity based performance compared to the undirected topology. Nevertheless, this degradation can be eliminated for velocity-based metrics using absolute position feedback. On the other hand, for the case of position-based metrics a proper combination of relative position and

velocity feedback can, not only mitigate this degradation, but also lead to improved performance over systems with the undirected topology.

5.1 Closed-form Solutions with Normal Laplacians

In this section, we first provide the closed-form solutions for the performance metrics of the class of systems whose interconnection topologies emit normal weighted Laplacian matrices, using our general framework from Chapter 4. We then investigate the role of communication directionality in performance using these closed-form solutions.

First recall Definition 4.1, which introduced the set of observable indices $\mathcal{N}_{obsv}$ in (4.16). If L is normal therefore diagonalizable, we can re-state this set as

$$\mathcal{N}_{obsv} = \{k \in \{2, \dots, n\} \mid C\mathbf{r}_k \neq 0\},$$

recalling that $\mathbf{r}_k$ denote the right eigenvectors of L as defined in (4.12). We now present two lemmas that will be useful in proving the upcoming results.

Lemma 5.1. *For $k \in \{2, \dots, n\}$, the eigenvalue-eigenvector pair $(\mu_k, \boldsymbol{\theta}_k)$ of M in (4.26) satisfies $\mu_k = 0$ if and only if $C\boldsymbol{\theta}_k = 0$.*

Proof. Assume for any $k \in \{2, \dots, n\}$ that $\mu_k = 0$. Then $0 = M\boldsymbol{\theta}_k = C^T C\boldsymbol{\theta}_k$. This implies that the vector $C\boldsymbol{\theta}_k$ is in the left nullspace of C, therefore is orthogonal to the column space of C. But $C\boldsymbol{\theta}_k$ also has to be in the column space of C therefore $C\boldsymbol{\theta}_k = 0$.

Conversely, if $C\boldsymbol{\theta}_k = 0$ for any $k \in \{2, \dots, n\}$, then $0 = M\boldsymbol{\theta}_k = \mu_k\boldsymbol{\theta}_k$ which gives $\mu_k = 0$ since $\boldsymbol{\theta}_k \neq 0$. □

Lemma 5.2. *Suppose that L is normal. For $k \in \{2, \dots, n\}$, ν_{kk} in (4.27) satisfies*

1. *$\nu_{kk} = 0$ if and only if $k \notin \mathcal{N}_{obsv}$.*

2. *$\nu_{kk} > 0$ if and only if $k \in \mathcal{N}_{obsv}$.*

Proof. Normality of L means that it is unitarily diagonalizable, therefore $R^{-1} = R^*$. We also recall that M in (4.26) is symmetric, therefore unitarily diagonalizable. Therefore $\mathbf{r}_1 = \boldsymbol{\theta}_1 = \frac{1}{\sqrt{n}}\mathbf{1}$ and it holds that $\mathbf{r}_k, \boldsymbol{\theta}_l \in \text{span}\{\mathbf{1}\}^\perp \subset \mathbb{C}^n$ for $k, l \in \{2, \dots, n\}$. So, we have $\mathbf{r}_k = \sum_{i=2}^n \chi_i^k \boldsymbol{\theta}_i$ with constants $\chi_i^k \in \mathbb{C}$ for $k \in \{2, \dots, n\}$.

Given any $k \in \{2, \dots, n\}$, it follows from (4.27) and Lemma 5.1 that $\nu_{kk} = 0$ if and only if $\langle \boldsymbol{\theta}_l, \mathbf{r}_k \rangle = 0$ for all $l \in \{2, \dots, n\}$ such that $C\boldsymbol{\theta}_l \neq 0$. Combining the preceding arguments leads to

$$\nu_{kk} = 0 \;\Leftrightarrow\; \left(\sum_{i=2}^n \overline{\chi_i^k} \boldsymbol{\theta}_i^* \right) \boldsymbol{\theta}_l = 0, \;\forall l \in \{2, \dots, n\}, \; C\boldsymbol{\theta}_l \neq 0,$$

which is equivalent to having $\chi_l^k = 0$ for all such l, due to the orthonormality of $\boldsymbol{\theta}_l$. In other words, $\nu_{kk} = 0 \;\Leftrightarrow\; \mathbf{r}_k = \sum_{C\boldsymbol{\theta}_i = 0,\; i \in \{2,\dots,n\}} \chi_i^k \boldsymbol{\theta}_i \;\Leftrightarrow\; C\mathbf{r}_k = 0$, which proves the first result. Since M in (4.26) is postive semi-definite, ν_{kk} for $k \in \{2, \dots, n\}$ is given by a summation in (4.27) with each summand being non-negative. So, $\nu_{kk} \geq 0$ and the first result implies the second result. □

5.1.1 Single-Integrator Networks

We now provide the closed-form solution for the performance of the class of single-integrator systems that emit normal weighted Laplacian matrices.

Lemma 5.3 (Single-Integrator, Normal Laplacian)**.** *Consider the single-integrator network* (4.1)*. Suppose that L is normal and the input $\mathbf{w}_0$ has unit covariance, i.e. $E[\Sigma_0] = I$. Then, the expectation of the metric P in* (2.12) *for the system T given by* (4.11a) *is*

$$E[P] = \|T\|_{\mathcal{H}_2}^2 = \sum_{k \in \mathcal{N}_{obsv}} \nu_{kk} \frac{1}{2\,\text{Re}[\lambda_k]}. \tag{5.1}$$

Proof. The fact that L is normal implies that it is diagonalizable, which leads to $m = n$, i.e. all Jordan blocks are scalars. Then using (4.30) from Lemma 4.2, we have $\Psi_{kl} = \nu_{kl} \left\langle \tilde{h}_{11}^{(l)}(t), \tilde{h}_{11}^{(k)}(t) \right\rangle_{\mathcal{L}_2}$. In addition, orthonormality of the eigenvectors $\mathbf{r}_j$ for

$j = 1, \ldots, n$ yields $E[\Sigma_Q] = I$ due to (4.29) and leads to $E[P] = \sum_{k=2}^{n} \Psi_{kk}$ due to (4.28) from Lemma 4.2. Using the result of Corollary 4.1, the notation in (4.25) and the fact that L is diagonalizable gives $\tilde{h}_{11}^{(k)}(s) = \frac{1}{s+\lambda_k}$. This transfer function can be used to evaluate Ψ_{kk} and the resulting expression leads to (5.1) by using Proposition 2.1 and Lemma 5.2. □

Lemma 5.3 generalizes [36, Proposition 1] to performance metrics with arbitrary output matrices.

5.1.2 Double-Integrator Networks

We now repeat our argument for the double-integrator networks, providing the closed-form solutions to their performance metrics.

Lemma 5.4 (Double-Integrator, Normal Laplacian)**.** *Consider the double-integrator network (4.2). Suppose that L is normal and the input $\mathbf{w}_0$ has unit covariance, i.e. $E[\Sigma_0] = I$. Then, the expectation of the performance metric P in (2.12) is*

$$E[P] = \|T\|_{\mathcal{H}_2}^2 = \sum_{k \in \mathcal{N}_{obsv}} \nu_{kk} \frac{\phi_k}{2(\alpha_k \phi_k^2 + \beta_k \xi_k \phi_k - \beta_k^2)}, \tag{5.2}$$

for the position-based output, i.e. system T given by (4.11a) and

$$E[P] = \|T\|_{\mathcal{H}_2}^2 = \sum_{k \in \mathcal{N}_{obsv}} \nu_{kk} \frac{\xi_k \beta_k + \phi_k \alpha_k}{2(\alpha_k \phi_k^2 + \beta_k \xi_k \phi_k - \beta_k^2)}, \tag{5.3}$$

for the velocity-based output, i.e. system T given by (4.11b); where $\alpha_k = k_p + \gamma_p \operatorname{Re}[\lambda_k]$, $\phi_k = k_d + \gamma_d \operatorname{Re}[\lambda_k]$, $\beta_k = \gamma_p \operatorname{Im}[\lambda_k]$ and $\xi_k = \gamma_d \operatorname{Im}[\lambda_k]$.

Proof. By the same argument used in the proof of Lemma 5.3, we have $\Psi_{kl} = \nu_{kl} \left\langle \tilde{h}_{11}^{(l)}(t), \tilde{h}_{11}^{(k)}(t) \right\rangle_{\mathcal{L}_2}$ and $E[P] = \sum_{k=2}^{n} \Psi_{kk}$. First consider the position-based performance metric, i.e. the system T given by (4.11a). Using the result of Corollary 4.2, the notation in (4.25) and the fact that L is diagonalizable gives $\tilde{h}_{11}^{(k)}(s) = \frac{1}{s^2 + (k_d + \gamma_d \lambda_k)s + k_p + \gamma_p \lambda_k}$, which has the realization $(\mathcal{A}_k, \mathcal{B}_k, \mathcal{C}_k)$ in controllable canonical

form given by $\mathcal{A}_k = \begin{bmatrix} 0 & 1 \\ -k_p - \gamma_p \lambda_k & -k_d - \gamma_d \lambda_k \end{bmatrix}$, $\mathcal{B}_k = \begin{bmatrix} 0 & 1 \end{bmatrix}^\mathsf{T}$ and $\mathcal{C}_k = \begin{bmatrix} 1 & 0 \end{bmatrix}$. Since the case of $k = l$ is sufficient, performing a standard computation results in $\left\langle \tilde{h}_{11}^{(k)}(t), \tilde{h}_{11}^{(k)}(t) \right\rangle_{\mathcal{L}_2} = \mathcal{B}_k^\mathsf{T} \mathcal{X}_k \mathcal{B}_k$, where $\mathcal{X}_k$ satisfies the Lyapunov equation $\mathcal{A}_k^* \mathcal{X}_k + \mathcal{X}_k \mathcal{A}_k = -\mathcal{C}_k^* \mathcal{C}_k$. Then we get

$$\left\langle \tilde{h}_{11}^{(k)}(t), \tilde{h}_{11}^{(k)}(t) \right\rangle_{\mathcal{L}_2} = \frac{\phi_k}{2(\alpha_k \phi_k^2 + \beta_k \xi_k \phi_k - \beta_k^2)}.$$

We now consider the velocity-based performance metric, i.e. the system T given by (4.11b). Using the result of Corollary 4.2, the notation in (4.25) and the fact that L is diagonalizable, we have $\tilde{h}_{11}^{(k)}(s) = \frac{s}{s^2 + (k_d + \gamma_d \lambda_k) s + k_p + \gamma_p \lambda_k}$, so that $\mathcal{A}_k$ and $\mathcal{B}_k$ are the same but $\mathcal{C}_k = \begin{bmatrix} 0 & 1 \end{bmatrix}$. Since $k = l$, solving the Lyapunov equation leads to

$$\left\langle \tilde{h}_{11}^{(k)}(t), \tilde{h}_{11}^{(k)}(t) \right\rangle_{\mathcal{L}_2} = \frac{\xi_k \beta_k + \phi_k \alpha_k}{2(\alpha_k \phi_k^2 + \beta_k \xi_k \phi_k - \beta_k^2)}.$$

This expression leads to the desired result by using Proposition 2.1 and Lemma 5.2. □

Note that per Lemma 5.2 all ν_{kk} in (5.2) and (5.3) are positive. In addition, stability guarantees that the numerators and the denominators in (5.2) and (5.3) are positive due to Proposition 4.3. Therefore the performance metrics are guaranteed to be positive quantities as expected. This result generalizes the result given in [47, Corollary 2] to position and velocity based performance metrics with arbitrary output matrices.

In the next section, we study the effect of communication directionality on performance.

5.2 The Role of Communication Directionality

In this section, we use the closed-form solutions from the previous section in order to investigate the effect of directed feedback. The class of graphs that emit normal weighted Laplacian matrices can for example arise in spatially invariant systems [1, 43]. Given any normal weighted Laplacian matrix L, we extract its Hermitian part as

$$L' := \frac{L + L^*}{2}. \tag{5.4}$$

Since L is weight-balanced [36, Lemma 4], (5.4) gives the Laplacian matrix of an undirected graph $\mathcal{G}' = \{\mathcal{N}, \mathcal{E}', \mathcal{W}'\}$, where $\mathcal{E}' = \mathcal{E} \cup \{(j,i) \mid (i,j) \in \mathcal{E}\}$ and $\mathcal{W}' = \{\frac{b_{ij}+b_{ji}}{2} \mid b_{ij} \in \mathcal{W}\}$. Put another way, $\mathcal{G}'$ is the *undirected counterpart* of $\mathcal{G}$ resulting from creating reverse edges in $\mathcal{G}$ and re-defining edge weights such that both graphs have the same nodal out-degree.

Normality of L and (5.4) imply that the spectrum of L',

$$\text{spec}(L') = \{\text{Re}[\lambda_i] | \lambda_i \in \text{spec}(L), i = 1, \ldots, n\}. \tag{5.5}$$

In addition, since L is normal, it has eigenvalues with non-zero imaginary parts if and only if its graph $\mathcal{G}$ is directed. For disturbance inputs that are uniform and uncorrelated across the network, we observe that both the position and velocity based performance metrics (5.2) and (5.3) depend on both the real and imaginary parts of the Laplacian eigenvalues. Therefore, comparison of directed graphs $\mathcal{G}$ and their undirected counterparts $\mathcal{G}'$ can reveal the interplay between the imaginary parts, i.e. edge directionality and control strategy (judicious selection of control gains) that determines overall performance.

5.2.1 Position based Performance

5.2.1.1 Single-Integrator Networks

The following theorem provides a comparison of the single-integrator systems with respective Laplacians L and L' in terms of the performance metric given in (5.1).

Theorem 5.1 (Equal Performance with Directed Networks and Undirected Counterparts)**.** *Consider the single-integrator network* (4.1) *and the performance metric* P *in* (2.12)*. Let* T *and* T' *be two systems given by* (4.11a) *with weighted Laplacian matrices* L *and* L'*. Suppose* L *is normal and* L' *is given by* (5.4)*. Then* $\|T\|_{\mathcal{H}_2}^2 = \|T'\|_{\mathcal{H}_2}^2$.

Proof. The result follows from (5.1) and (5.5). □

As Theorem 5.1 indicates, directed and associated undirected single-integrator systems perform identically for any output matrix C satisfying Assumption 4.2. This implies that the same level of performance can be achieved either using directed paths in the commmunication graph or using the corresponding undirected graph per (5.4). The directed system might be preferable in certain cases due to reduced communication requirements (e.g. uni-directional vs. bi-directional paths).

Theorem 5.1 also provides a generalization of previous results obtained for this class of directed and undirected single-integrator systems. For example, performance of directed systems can be bounded by functions of the spectrums of output performance matrices and associated undirected system Laplacians (see e.g. [71, Theorem 5]). Here, we provide exact solutions in Lemma 5.3 by additionally accounting for the eigenvectors of these matrices, which lead to the equivalence between directed and associated undirected systems as shown by Theorem 5.1.

5.2.1.2 Double-Integrator Networks

We now provide a comparison of the double-integrator systems with respective Laplacians L and L' for the performance metric given in (5.2).

Remark 5.1. *The performance metric in* (5.2) *simplifies to an expression that does not explicitly depend on* $\mathrm{Im}[\lambda_k]$ *if* $\beta_k\xi_k\phi_k - \beta_k^2 = 0$ *for* $k \in \mathcal{N}_{obsv}$. *This holds if* $\mathrm{Im}[\lambda_k] = 0$ *for* $k \in \mathcal{N}_{obsv}$ *or* L *is symmetric or* $\gamma_p = 0$. *If* $\beta_k\xi_k\phi_k - \beta_k^2 = 0$ *for* $k \in \mathcal{N}_{obsv}$, (5.2) *reduces to*

$$\|T\|_{\mathcal{H}_2}^2 = \sum_{k\in\mathcal{N}_{obsv}} \nu_{kk} \frac{1}{2(k_p + \gamma_p \,\mathrm{Re}[\lambda_k])(k_d + \gamma_d \,\mathrm{Re}[\lambda_k])}, \tag{5.6}$$

when the stability condition (4.23) *from Proposition 4.3 holds.*

Depending on the values of k_p, k_d, γ_p and γ_d in (5.6), the denominator in (5.2) can be quadratic in $\mathrm{Re}[\lambda_k]$, which could indicate a smaller $\mathcal{H}_2$ norm for sufficiently

large $\mathrm{Re}[\lambda_k]$, hence better performance compared to the performance of the first order system given by (5.1).

The following Lemma shows the effect of the imaginary parts of the weighted Laplacian eigenvalues on the position based performance (5.2) of the double-integrator network (4.2).

Lemma 5.5 (Characterization of Position based Performance via the Observable Eigenvalues)**.** *Consider the double-integrator network* (4.2) *and the performance metric* P *in* (2.12)*. Let* T *and* T' *be two systems given by* (4.11a) *with weighted Laplacian matrices* L *and* L'*. Suppose* L *is normal and* L' *is given by* (5.4)*. Then the following hold:*

1. $\|T\|_{\mathcal{H}_2}^2 = \|T'\|_{\mathcal{H}_2}^2$ *if* $\mathrm{Im}[\lambda_k] = 0\ \forall k \in \mathcal{N}_{obsv}$.

2. $\|T\|_{\mathcal{H}_2}^2 \leq \|T'\|_{\mathcal{H}_2}^2$ *if*

$$\gamma_d(k_d + \gamma_d \,\mathrm{Re}[\lambda_k]) - \gamma_p \geq 0, \quad \forall k \in \mathcal{N}_{obsv}. \tag{5.7}$$

Furthermore, $\|T\|_{\mathcal{H}_2}^2 < \|T'\|_{\mathcal{H}_2}^2$ *if in addition at least one of the inequalities in* (5.7) *strictly holds for some* $k \in \mathcal{N}_{obsv}$ *such that* $\mathrm{Im}[\lambda_k] \neq 0$ *and relative position feedback is present, i.e.* $\gamma_p > 0$.

Similarly, $\|T\|_{\mathcal{H}_2}^2 \geq \|T'\|_{\mathcal{H}_2}^2$ *if*

$$\gamma_d(k_d + \gamma_d \,\mathrm{Re}[\lambda_k]) - \gamma_p \leq 0, \quad \forall k \in \mathcal{N}_{obsv}. \tag{5.8}$$

Furthermore $\|T\|_{\mathcal{H}_2}^2 > \|T'\|_{\mathcal{H}_2}^2$ *if in addition at least one of the inequalities in* (5.8) *strictly holds for some* $k \in \mathcal{N}_{obsv}$ *such that* $\mathrm{Im}[\lambda_k] \neq 0$ *and relative position feedback is present, i.e.* $\gamma_p > 0$.

Proof. Invoking Remark 5.1 and using (5.5), both $\|T\|_{\mathcal{H}_2}^2$ and $\|T'\|_{\mathcal{H}_2}^2$ are given by (5.6) which leads to Item *1)*. Condition (5.7) implies that $\beta_k \xi_k \phi_k - \beta_k^2 \geq 0$ for $k \in \mathcal{N}_{obsv}$

therefore

$$\frac{\phi_k}{2(\alpha_k\phi_k^2+\beta_k\xi_k\phi_k-\beta_k^2)} \leq \frac{1}{2\alpha_k\phi_k}, \quad k\in\mathcal{N}_{obsv}. \tag{5.9}$$

Since $\nu_{kk}>0$ for $k\in\mathcal{N}_{obsv}$ due to Lemma 5.2, multiplication of both sides of (5.9) by ν_{kk} and summation of the inequalities gives $\|T\|_{\mathcal{H}_2}^2 \leq \|T'\|_{\mathcal{H}_2}^2$. If in addition to (5.7) at least one of these inequalities strictly holds for some $k\in\mathcal{N}_{obsv}$ such that $\mathrm{Im}[\lambda_k]\neq 0$ and $\gamma_p>0$, then $\|T\|_{\mathcal{H}_2}^2 < \|T'\|_{\mathcal{H}_2}^2$. The reverse inequalities follow from (5.8) using a similar argument. □

Note that the results in Lemma 5.5 hold for any output matrix C satisfying Assumption 4.2. It is necessary that at least one observable eigenvalue does not lie on the real line for the performance of the directed and undirected systems to differ, and the gains need to be tuned based on these eigenvalues to improve performance. We next use this result to characterize the position-based performance of directed and undirected double-integrator systems in terms of relative feedback.

Theorem 5.2 (Characterization of Position based Performance via Relative Feedback)**.** *Consider the double-integrator network* (4.2) *and the performance metric* P *in* (2.12)*. Let* T *and* T' *be two systems given by* (4.11a) *with weighted Laplacian matrices* L *and* L'*. Suppose that* L *is normal and* L' *is given by* (5.4)*. Then the following hold:*

1. *If relative position feedback is absent, i.e.* $\gamma_p=0$*, then* $\|T\|_{\mathcal{H}_2}^2 = \|T'\|_{\mathcal{H}_2}^2$.

2. *If relative position feedback is present and relative velocity feedback is absent, i.e.* $\gamma_p>0$ *and* $\gamma_d=0$*, and* $\mathrm{Im}[\lambda_k]\neq 0$ *for some* $k\in\mathcal{N}_{obsv}$*, then* $\|T\|_{\mathcal{H}_2}^2 > \|T'\|_{\mathcal{H}_2}^2$.

3. *If both relative position and velocity feedback are present, i.e.* $\gamma_p>0$ *and* $\gamma_d>0$*, and* $\mathrm{Im}[\lambda_k]\neq 0$ *for some* $k\in\mathcal{N}_{obsv}$*, then there exists* $\underline{\gamma}_p$ *and* $\overline{\gamma}_p$ *that satisfy*

$$\min_{\substack{k\in\mathcal{N}_{obsv},\\ \mathrm{Im}[\lambda_k]\neq 0}} \mathrm{Re}[\lambda_k] \;\leq\; \frac{\underline{\gamma}_p}{\gamma_d^2}-\frac{k_d}{\gamma_d} \;\leq\; \frac{\overline{\gamma}_p}{\gamma_d^2}-\frac{k_d}{\gamma_d} \;\leq\; \max_{\substack{k\in\mathcal{N}_{obsv},\\ \mathrm{Im}[\lambda_k]\neq 0}} \mathrm{Re}[\lambda_k],$$

such that $\|T\|_{\mathcal{H}_2}^2 < \|T'\|_{\mathcal{H}_2}^2$ *if* $\gamma_p<\underline{\gamma}_p$ *and* $\|T\|_{\mathcal{H}_2}^2 > \|T'\|_{\mathcal{H}_2}^2$ *if* $\gamma_p>\overline{\gamma}_p$.

Proof. Invoking Remark 5.1 and using (5.5) leads to Item *1)*. Item *2)* follows from Lemma 5.5 by setting $\gamma_p > 0$ and $\gamma_d = 0$ in (5.8). To prove Item *3)* we observe from Lemma 5.5 that

$$\gamma_p > \max_{\substack{k\in\mathcal{N}_{obsv},\\ \mathrm{Im}[\lambda_k]\neq 0}} \gamma_d(k_d + \gamma_d \,\mathrm{Re}[\lambda_k]) =: \gamma_u \Rightarrow \|T\|_{\mathcal{H}_2}^2 > \|T'\|_{\mathcal{H}_2}^2,$$
$$\gamma_p < \min_{\substack{k\in\mathcal{N}_{obsv},\\ \mathrm{Im}[\lambda_k]\neq 0}} \gamma_d(k_d + \gamma_d \,\mathrm{Re}[\lambda_k]) =: \gamma_l \Rightarrow \|T\|_{\mathcal{H}_2}^2 < \|T'\|_{\mathcal{H}_2}^2.$$

So $\|T\|_{\mathcal{H}_2}^2 = \|T'\|_{\mathcal{H}_2}^2$ if $\gamma_p = \underline{\gamma}_p$ and $\|T\|_{\mathcal{H}_2}^2 < \|T'\|_{\mathcal{H}_2}^2$ if $\gamma_p < \underline{\gamma}_p$ for some $\underline{\gamma}_p \in [\gamma_l, \gamma_u]$, since $\|T\|_{\mathcal{H}_2}^2$ and $\|T'\|_{\mathcal{H}_2}^2$ are continuous in γ_p. Similarly, $\|T\|_{\mathcal{H}_2}^2 = \|T'\|_{\mathcal{H}_2}^2$ if $\gamma_p = \overline{\gamma}_p$ and $\|T\|_{\mathcal{H}_2}^2 > \|T'\|_{\mathcal{H}_2}^2$ if $\gamma_p > \overline{\gamma}_p$ for some $\overline{\gamma}_p \in [\gamma_l, \gamma_u]$. Finally we note that $\underline{\gamma}_p \leq \overline{\gamma}_p$, because otherwise $\gamma_p = \underline{\gamma}_p > \overline{\gamma}_p$ would imply that $\|T\|_{\mathcal{H}_2}^2 = \|T'\|_{\mathcal{H}_2}^2$ and $\|T\|_{\mathcal{H}_2}^2 > \|T'\|_{\mathcal{H}_2}^2$ must simultaneously hold, which is a contradiction. □

Directed communication degrades performance for metrics that capture some of the modes resulting from the directed paths (i.e. $\mathrm{Im}[\lambda_k] \neq 0$ for some $k \in \mathcal{N}_{obsv}$) if relative position feedback is used without relative velocity feedback. For such metrics, this issue can be addressed in several ways depending on the available feedback. For example, omitting relative position feedback (which requires absolute position feedback due to Assumption 4.1) can mitigate this degradation. In this case, the directionality of relative velocity feedback does not affect performance since directed and undirected systems perform identically.

It is when both types of relative feedback are used that tuning their respective gains properly can, not only mitigate the performance degradation, but also lead to the directed system outperforming its undirected counterpart. Therefore, it is critical to have relative velocity feedback in addition to relative position feedback. Namely, the directed system performs better than its undirected counterpart for sufficiently small relative position gain (the converse is true for sufficiently large relative position gain). This sufficient magnitude is determined by the velocity gains as well as the

magnitude of the real parts of the observable eigenvalues that have non-zero imaginary parts. As a consequence, a judicious control strategy depends on the topological characteristics of the network.

5.2.2 Velocity based Performance

This subsection provides a comparison of the double integrator systems with respective Laplacians L and L' in terms of the performance metric given in (5.3).

Remark 5.2. *The performance metric in* (5.3) *simplifies to an expression that does not explicitly depend on* $\mathrm{Im}[\lambda_k]$ *if* $\beta_k = 0$ *for* $k \in \mathcal{N}_{obsv}$. *This holds if* $\mathrm{Im}[\lambda_k] = 0$ *for* $k \in \mathcal{N}_{obsv}$ *or* L *is symmetric or* $\gamma_p = 0$. *If* $\beta_k = 0$ *for* $k \in \mathcal{N}_{obsv}$, (5.3) *reduces to*

$$\|T\|_{\mathcal{H}_2}^2 = \sum_{k \in \mathcal{N}_{obsv}} \nu_{kk} \frac{1}{2(k_d + \gamma_d \,\mathrm{Re}[\lambda_k])}, \tag{5.10}$$

when the stability condition (4.23) *from Proposition 4.3 holds.*

In contrast to the position based performance metric in (5.6), the velocity based performance in (5.10) depends only on absolute or relative velocity feedback and its denominator is affine in $\mathrm{Re}[\lambda_k]$. So, absolute or relative position feedback does not affect velocity based performance if $\mathcal{G}$ is undirected.

The following theorem demonstrates that if the velocity based performance of the system given by (4.11b) is considered and its directed graph emits a normal weighted Laplacian, its $\mathcal{H}_2$ norm is lower bounded by the $\mathcal{H}_2$ norm of the corresponding undirected system whose interconnection is defined by (5.4). This result highlights the inability of standard feedback schemes to mitigate velocity-based performance degradation.

Theorem 5.3 (Characterization of Velocity based Performance)**.** *Consider the double-integrator network* (4.2) *and the performance metric* P *in* (2.12). *Let* T *and* T' *be two systems given by* (4.11b) *with weighted Laplacian matrices* L *and* L'. *Suppose that* L *is normal and* L' *is given by* (5.4). *Then the following hold:*

1. $\|T\|_{\mathcal{H}_2}^2 \geq \|T'\|_{\mathcal{H}_2}^2$.

2. $\|T\|_{\mathcal{H}_2}^2 > \|T'\|_{\mathcal{H}_2}^2$ *if and only if* $\mathrm{Im}[\lambda_k] \neq 0$ *for some* $k \in \mathcal{N}_{obsv}$ *and relative position feedback is present, i.e.* $\gamma_p > 0$.

3. $\|T\|_{\mathcal{H}_2}^2 = \|T'\|_{\mathcal{H}_2}^2$ *if and only if* $\mathrm{Im}[\lambda_k] = 0 \ \forall k \in \mathcal{N}_{obsv}$ *or relative position feedback is absent, i.e.* $\gamma_p = 0$.

Proof. Since $-\beta_k^2 = -\gamma_p^2 \,\mathrm{Im}[\lambda_k]^2 \leq 0$, it holds that

$$\alpha_k \phi_k^2 + \beta_k \xi_k \phi_k - \beta_k^2 \leq \alpha_k \phi_k^2 + \beta_k \xi_k \phi_k, \quad k \in \mathcal{N}_{obsv}. \tag{5.11}$$

Stability condition (4.23) from Proposition 4.3 states that

$$\alpha_k \phi_k^2 + \beta_k \xi_k \phi_k - \beta_k^2 > 0 \text{ and } \phi_k > 0, \quad k \in \mathcal{N}_{obsv}. \tag{5.12}$$

Therefore, (5.11) can be re-arranged as

$$\frac{\xi_k \beta_k + \phi_k \alpha_k}{\alpha_k \phi_k^2 + \beta_k \xi_k \phi_k - \beta_k^2} \geq \frac{1}{\phi_k}, \quad k \in \mathcal{N}_{obsv}. \tag{5.13}$$

Since $\nu_{kk} > 0$ for $k \in \mathcal{N}_{obsv}$ as shown in Lemma 5.2,

$$\nu_{kk} \frac{\xi_k \beta_k + \phi_k \alpha_k}{2(\alpha_k \phi_k^2 + \beta_k \xi_k \phi_k - \beta_k^2)} \geq \nu_{kk} \frac{1}{2\phi_k}, \quad k \in \mathcal{N}_{obsv}. \tag{5.14}$$

Summation of the inequalities given in (5.14) and using (5.3) and (5.10) leads to Item *1)*.

To prove the necessity part of Item *2)*, we observe that $-\beta_k^2 = -\gamma_p^2 \,\mathrm{Im}[\lambda_k]^2 < 0$ for some $k \in \mathcal{N}_{obsv}$ therefore (5.11) strictly holds for such k. Then by a similar argument to the one used above, (5.14) strictly holds for such k as well, which leads to $\|T\|_{\mathcal{H}_2}^2 > \|T'\|_{\mathcal{H}_2}^2$. To prove sufficiency suppose that $\|T\|_{\mathcal{H}_2}^2 > \|T'\|_{\mathcal{H}_2}^2$. Using (5.3) and (5.10), this implies that (5.14) strictly holds for some $k \in \mathcal{N}_{obsv}$ (otherwise $\|T\|_{\mathcal{H}_2}^2 = \|T'\|_{\mathcal{H}_2}^2$). Since $\nu_{kk} > 0$ for $k \in \mathcal{N}_{obsv}$, (5.13) strictly holds for some $k \in \mathcal{N}_{obsv}$ as well. Using (5.12) and re-arranging terms leads to $\beta_k^2 = \gamma_p^2 \,\mathrm{Im}[\lambda_k]^2 > 0$ for some $k \in \mathcal{N}_{obsv}$ implying that $\mathrm{Im}[\lambda_k] \neq 0$ for some $k \in \mathcal{N}_{obsv}$ and $\gamma_p > 0$. Finally we note that items *1)* and *2)* imply Item *3)*. □

Unlike position based performance, there does not exist a choice of control gains for the directed system that can result in better velocity based performance compared to its undirected counterpart for any output matrix C satisfying Assumption 4.2. Furthermore, when relative position feedback is used, the directed system performs strictly worse compared to its undirected counterpart for metrics capturing the effect of the directed interconnection. They perform identically without relative position feedback or if metrics do not capture the edge directionality.

When the overall system performance is considered in terms of both position and velocity based metrics, a trade-off emerges. For systems with observable directed paths, it is possible to have equal performance to that of their undirected counterparts in the case of both position and velocity based metrics by omitting relative position feedback. But this is true only if absolute position feedback is used, as it is required for stability (Assumption 4.1). Therefore, unless absolute position measurements are available, the directed system requires well-tuned gains to prevent degradation of the position-based performance (or to possibly improve it) while it will always have worse velocity-based performance compared to the undirected system. For directed systems with absolute position feedback, improving position-based performance comes at the expense of the velocity-based performance.

Remark 5.3. *For the particular metric defined as the variance of the full-state, the $\mathcal{H}_2$ norm of a linear system can be upper bounded by the $\mathcal{H}_2$ norm of a system whose dynamics emit the Hermitian part of the original state matrix [71, Theorem 2]. In the case of double-integrator networks, this comparison does not explicitly account for the Laplacian eigenvalues, i.e. communication directionality. In contrast, we have studied communication directionality for general quadratic metrics by comparing directed graphs and their undirected counterparts represented by the Hermitian part of the Laplacian (5.4). Our results characterize performance as an aggregate outcome of judicious control strategy and network topology.*

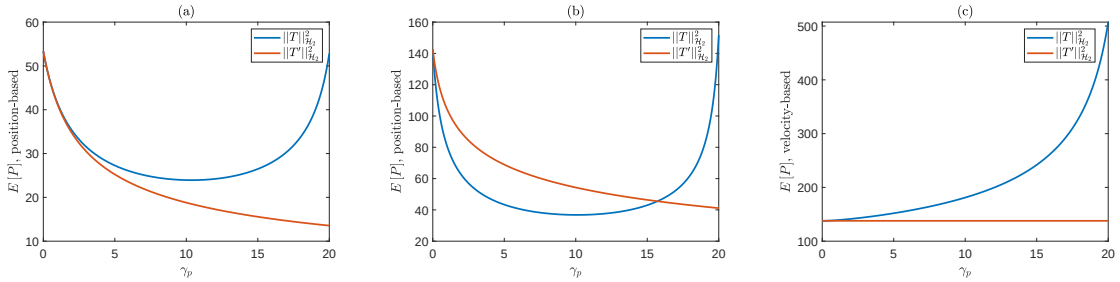

Figure 5-1. The expectation of the position-based performance of the double-integrator system (4.2) given by (4.11a), for $E[\Sigma_0] = I$ and the gains **(a)** $k_p = 3, k_d = 5, \gamma_d = 0$, **(b)** $k_p = 1, k_d = 2, \gamma_d = 6.5$. **(c)** The expectation of the velocity-based performance of the double-integrator system (4.2) given by (4.11b), for $E[\Sigma_0] = I$ and the gains $k_p = 1, k_d = 2, \gamma_d = 7$.

5.2.3 Example: Position and Velocity based Performance with Uni-directional vs. Bi-directional Feedback

We now consider a cyclic digraph in which each node has uniform out-degree d and the uniformly weighted edges that start at each node reach ω succeeding nodes. This results in 'look-ahead' type state measurements through ω communication hops. The respective weighted Laplacian is given by

$$L^{cyc}(d,\omega) = d \times \mathrm{circ}\left(\begin{bmatrix} 1 & -\frac{1}{\omega} & \dots & -\frac{1}{\omega} & 0 & \dots & 0 \end{bmatrix}\right), \tag{5.15}$$

where $d \in \mathbb{R}^+$, $\omega \in \mathbb{Z}^+$, $\omega \leq n-1$ and $\mathrm{circ}(\cdot)$ denotes the circulant matrix generated by permuting the row vector in the argument. The Jordan decomposition of $L = L^{cyc}$ gives [82]

$$J_k = \lambda_k = d\left(1 - \frac{1}{\omega}\sum_{i=1}^{\omega} e^{-\mathbf{j}\frac{2\pi}{n}i(k-1)}\right), \tag{5.16}$$

for $k = 1, \dots, n$. Choosing $\alpha = \frac{1}{\sqrt{n}}$ in (4.12), the columns of $\tilde{R}$ are given by

$$\mathbf{r}_l = \frac{1}{\sqrt{n}}\begin{bmatrix} 1 & e^{\mathbf{j}\frac{2\pi}{n}(l-1)} & \dots & e^{\mathbf{j}\frac{2\pi}{n}(l-1)(n-1)} \end{bmatrix}^*, \tag{5.17}$$

for $l = 2, \dots, n$. For the special case of uni-directional feedback, we set $d = 1$ and $\omega = 1$ in (5.15) therefore

$$L = L^{cyc}(1,1) \quad \text{and} \quad L' = \frac{L^{cyc}(1,1) + L^{cyc}(1,1)^*}{2},$$

where we have used (5.4) to also define the corresponding bi-directional feedback. We consider the respective systems T and T' with an arbitrary output matrix $C \in \mathbb{R}^{n\times n}$ that satisfies Assumption 4.2, for $n = 50$.

For the double-integrator network (4.2) given by (4.11a) (position based performance), Figure 5-1a shows that, as suggested by Item *2)* of Theorem 5.2, using relative position feedback without relative velocity feedback ($\gamma_p > 0$ and $\gamma_d = 0$) leads to worse performance with directed interconnection. It is when both relative position and velocity measurements are used ($\gamma_p > 0$ and $\gamma_d > 0$) that the directed cycles can be utilized for better performance by tuning the gains. Per Item *3)* of Theorem 5.2, sufficiently small γ_p (i.e. sufficiently large velocity gains k_d and γ_d) improves the performance of the directed interconnection relative to its undirected counterpart; but the performance degrades for sufficiently large γ_p, as shown in Figure 5-1b. Directed cycles require less communication thus can be preferable, provided the gains are carefully selected.

For the double-integrator network (4.2) given by (4.11b) (velocity based performance), Figure 5-1c shows that relative position feedback degrades performance if the cycles are directed. But the performance becomes comparable to that of the undirected system for sufficiently small γ_p, equaling it at $\gamma_p = 0$. This supports the findings of Theorem 5.3.

In the next chapter, we focus on a more general class of directed graphs, which emit diagonalizable weighted Laplacian matrices. This class of graphs will be used to investigate the relationship between graph connectivity and network performance.

Chapter 6

Effect of Connectivity on the Performance of Directed Networks

In this chapter, we investigate the role of the degree of connectivity in system performance. We will study examples of directed graphs that arise in common applications such as vehicular networks and social influence networks.

We first focus on the class of systems that we term ω-nearest neighbor networks, which have a cyclic and directed communication structure. Each agent in the network admits uniformly weighted uni-directional state measurements from ω consecutive neighbors, resulting in a spatially invariant formation. For the special case of the metric quantifying the aggregate state deviation from the average, we show that performance does not monotonically improve by increasing ω. We also investigate a special case of leader-follower networks that we term all-to-one (imploding star) networks. Here uni-directional state measurements are uniformly weighted and relative to a single designated "leader" that does not receive any relative feedback. We show an equivalence between directed all-to-one and all-to-all (represented by a complete graph) networks for the same performance metric.

We begin by providing the closed-form solutions for the performance metrics.

6.1 Closed-form Solutions with Diagonalizable Laplacians

In this section we use our general analysis framework from Chapter 4 to derive the closed-form solutions for the performance metrics of directed networks that emit diagonalizable weighted Laplacian matrices. This class of graphs encapsulates the interconnection topologies we are interested in, in order to examine the effect of connectivity on the performance of directed networks.

6.1.1 Single-Integrator Networks

The following result provides the closed-form solution for the performance of single-integrator networks (4.1).

Lemma 6.1 (Single-Integrator, Diagonalizable Laplacian)**.** *Consider the single-integrator network* (4.1) *and suppose that* L *is diagonalizable. Then, the metric* P *in* (2.12) *for the system* T *given by* (4.11a) *is* $P = \operatorname{tr}(\Sigma_Q \Psi)$*, where* $\mathbf{j}^2 = -1$ *and*

$$\Psi_{kl} = \nu_{kl} \frac{\operatorname{Re}[\lambda_k] + \operatorname{Re}[\lambda_l] + \mathbf{j}(\operatorname{Im}[\lambda_k] - \operatorname{Im}[\lambda_l])}{(\operatorname{Re}[\lambda_k] + \operatorname{Re}[\lambda_l])^2 + (\operatorname{Im}[\lambda_k] - \operatorname{Im}[\lambda_l])^2}. \tag{6.1}$$

Proof. The fact that L is diagonalizable leads to $m = n$, i.e. all Jordan blocks are scalars. Then using (4.30) from Lemma 4.2, we have $\Psi_{kl} = \nu_{kl} \left\langle \tilde{h}_{11}^{(l)}(t), \tilde{h}_{11}^{(k)}(t) \right\rangle_{\mathcal{L}_2}$. Using the result of Corollary 4.1, the notation in (4.25) and the fact that L is diagonalizable gives $\tilde{h}_{11}^{(k)}(s) = \frac{1}{s+\lambda_k}$. Using this transfer function leads to $\left\langle \tilde{h}_{11}^{(l)}(t), \tilde{h}_{11}^{(k)}(t) \right\rangle_{\mathcal{L}_2} = \frac{1}{\overline{\lambda_k}+\lambda_l}$. Combining these facts and re-arranging terms yields the result. □

Note that the diagonal terms Ψ_{kk} are real and the cross-terms Ψ_{kl} for $k \neq l$ are possibly imaginary in (6.1). However, P is guaranteed to be real due to Remark 4.4.

6.1.2 Double-Integrator Networks

Next we present the closed-form solution for the double-integrator network (4.2).

Lemma 6.2 (Double-Integrator, Diagonalizable Laplacian)**.** *Consider the double-integrator network* (4.2)*. Suppose that L is diagonalizable. The performance metric P in* (2.12) *is $P = \operatorname{tr}(\Sigma_Q \Psi)$, where*

$$\Psi_{kk} = \nu_{kk} \frac{\phi_k}{2(\alpha_k \phi_k^2 + \beta_k \xi_k \phi_k - \beta_k^2)} \tag{6.2}$$

for the position-based output, i.e. system T given by (4.11a) *and*

$$\Psi_{kk} = \nu_{kk} \frac{\xi_k \beta_k + \phi_k \alpha_k}{2(\alpha_k \phi_k^2 + \beta_k \xi_k \phi_k - \beta_k^2)} \tag{6.3}$$

for the velocity-based output, i.e. system T given by (4.11b)*; where $\alpha_k = k_p + \gamma_p \operatorname{Re}[\lambda_k]$, $\phi_k = k_d + \gamma_d \operatorname{Re}[\lambda_k]$, $\beta_k = \gamma_p \operatorname{Im}[\lambda_k]$ and $\xi_k = \gamma_d \operatorname{Im}[\lambda_k]$.*

Remark 6.1. *Here, the cross-terms Ψ_{kl} for $k \neq l$ are not given explicitly for brevity. A Gramian computation as in [59, 60] would give Ψ_{kl} in closed-form for $k \neq l$, which is not tractable due to the number of terms involved. To gain some insight from the computation, we focus on the diagonal terms which are the only required ones when Σ_Q in* (4.29) *is diagonal.*

Proof of Lemma 6.2. The fact that L is diagonalizable leads to $m = n$, i.e. all Jordan blocks are scalars. Then, using (4.30) from Lemma 4.2 we have $\Psi_{kl} = \nu_{kl} \left\langle \tilde{h}_{11}^{(l)}(t), \tilde{h}_{11}^{(k)}(t) \right\rangle_{\mathcal{L}_2}$. First consider the position-based performance metric, i.e. the system T given by (4.11a). Using the result of Corollary 4.2, the notation in (4.25) and the fact that L is diagonalizable gives $\tilde{h}_{11}^{(k)}(s) = \frac{1}{s^2 + (k_d + \gamma_d \lambda_k)s + k_p + \gamma_p \lambda_k}$, which has the realization $(\mathcal{A}_k, \mathcal{B}_k, \mathcal{C}_k)$ in controllable canonical form given by $\mathcal{A}_k = \begin{bmatrix} 0 & 1 \\ -k_p - \gamma_p \lambda_k & -k_d - \gamma_d \lambda_k \end{bmatrix}$, $\mathcal{B}_k = \begin{bmatrix} 0 & 1 \end{bmatrix}^\intercal$ and $\mathcal{C}_k = \begin{bmatrix} 1 & 0 \end{bmatrix}$. If $k = l$, performing a standard computation, $\left\langle \tilde{h}_{11}^{(k)}(t), \tilde{h}_{11}^{(k)}(t) \right\rangle_{\mathcal{L}_2} = \mathcal{B}_k^\intercal \mathcal{X}_k \mathcal{B}_k$, where $\mathcal{X}_k$ satisfies the Lyapunov equation $\mathcal{A}_k^* \mathcal{X}_k + \mathcal{X}_k \mathcal{A}_k = -\mathcal{C}_k^* \mathcal{C}_k$. Then we get

$$\left\langle \tilde{h}_{11}^{(k)}(t), \tilde{h}_{11}^{(k)}(t) \right\rangle_{\mathcal{L}_2} = \frac{\phi_k}{2(\alpha_k \phi_k^2 + \beta_k \xi_k \phi_k - \beta_k^2)}.$$

We now consider the velocity-based performance metric, i.e. the system T given by (4.11b). Using the result of Corollary 4.2, the notation in (4.25) and the fact that L

is diagonalizable, we have $\tilde{h}_{11}^{(k)}(s) = \frac{s}{s^2+(k_d+\gamma_d\lambda_k)s+k_p+\gamma_p\lambda_k}$, so that $\mathcal{A}_k$ and $\mathcal{B}_k$ are the same but $\mathcal{C}_k = \begin{bmatrix}0 & 1\end{bmatrix}$. If $k = l$, solving the Lyapunov equation leads to

$$\left\langle \tilde{h}_{11}^{(k)}(t), \tilde{h}_{11}^{(k)}(t) \right\rangle_{\mathcal{L}_2} = \frac{\xi_k\beta_k + \phi_k\alpha_k}{2(\alpha_k\phi_k^2 + \beta_k\xi_k\phi_k - \beta_k^2)}. \qquad \square$$

If we further assume real eigenvalues, we obtain a result similar to the one in [59,60] for diagonalizable Laplacians.

Lemma 6.3 (Double-Integrator, Diagonalizable Laplacian with Real Eigenvalues)**.** *Consider the double-integrator network (4.2). Suppose that L is diagonalizable and has real eigenvalues. Then*

$$\Psi_{kl} = \nu_{kl}\frac{2k_d + \gamma_d(\lambda_k + \lambda_l)}{\Psi_{kl}^{denom}}, \tag{6.4}$$

for the position-based output, i.e. system T given by (4.11a) and

$$\Psi_{kl} = \nu_{kl}\frac{(k_p + \gamma_p\lambda_l)(k_d + \gamma_d\lambda_k) + (k_p + \gamma_p\lambda_k)(k_d + \gamma_d\lambda_l)}{\Psi_{kl}^{denom}} \tag{6.5}$$

for the velocity-based output, i.e. system T given by (4.11b), where

$$\begin{aligned}\Psi_{kl}^{denom} \;=\; & (k_d + \gamma_d\lambda_k)(k_d + \gamma_d\lambda_l)(2k_p + \gamma_p(\lambda_k + \lambda_l)) + \\ & \gamma_p^2(\lambda_k - \lambda_l)^2 + (k_p + \gamma_p\lambda_k)(k_d + \gamma_d\lambda_l)^2 + (k_p + \gamma_p\lambda_l)(k_d + \gamma_d\lambda_k)^2.\end{aligned}$$

Proof. The argument from the proof of Lemma 6.2 gives $\Psi_{kl} = \nu_{kl}\left\langle \tilde{h}_{11}^{(l)}(t), \tilde{h}_{11}^{(k)}(t) \right\rangle_{\mathcal{L}_2}$ and $\left\langle \tilde{h}_{11}^{(l)}(t), \tilde{h}_{11}^{(k)}(t) \right\rangle_{\mathcal{L}_2} = \mathcal{B}_k^\intercal\mathcal{X}_{kl}\mathcal{B}_l$, where $\mathcal{X}_{kl}$ satisfies the Sylvester equation $\mathcal{A}_k^*\mathcal{X}_{kl} + \mathcal{X}_{kl}\mathcal{A}_l = -\mathcal{C}_k^*\mathcal{C}_l$ [59,60]. Considering (4.11a) and (4.11b) individually and solving for $\mathcal{X}_{kl}$ in each case leads to respectively (6.4) and (6.5). $\square$

The real and imaginary parts of the Laplacian eigenvalues, and the control gains appear explicitly in the solutions for the performance metrics in Lemma 6.2 and Lemma 6.3. However, these solutions are still given by a weighted linear combination of Ψ_{kl}. In the next section, we use these closed-form solutions for specific graph structures to investigate the effect of the degree of connectivity on performance.

6.2 All-to-One vs. ω-Nearest Neighbor Networks

In this section, we compare two different relative feedback schemes. The first one is called an all-to-one network, which designates a 'leader' node that receives no relative feedback, where the remaining nodes have access to uniformly weighted uni-directional state measurements relative to the leader only. The second one is referred to as an ω-nearest neighbor network, which is based on uniformly weighted uni-directional state measurements of each node relative to ω succeeding nodes. We consider performance metrics that have circulant output matrices C, which arise in many applications such as quantifying lack of coherence in a system in terms of global or local disorder [1, 43, 70].

6.2.1 Imploding Star Graph: All-to-One Networks

All-to-one networks can be modeled as the imploding star graph whose edge weights are normalized such that the out-degree of each node is $\frac{n}{n-1}$. The corresponding weighted Laplacian is given by

$$L = \frac{n}{n-1}\begin{bmatrix} I_{n-1} & -\mathbf{1} \\ \mathbf{0}^{\mathsf{T}} & 0 \end{bmatrix}, \tag{6.6}$$

with total out-degree n. The Jordan decomposition gives

$$J = \frac{n}{n-1}\begin{bmatrix} 0 & \mathbf{0}^{\mathsf{T}} \\ \mathbf{0} & I_{n-1} \end{bmatrix}. \tag{6.7}$$

Choosing $\alpha = 1$ in (4.12), the matrices $\tilde{R}$ and $\tilde{Q}$ are given by

$$\tilde{R} = \begin{bmatrix} I_{n-1} \\ \mathbf{0}^{\mathsf{T}} \end{bmatrix} \text{ and } \tilde{Q} = \begin{bmatrix} I_{n-1} & -\mathbf{1} \end{bmatrix}. \tag{6.8}$$

6.2.1.1 Single-Integrator Networks

The next theorem provides the solution for (2.12) for the single-integrator network (4.1) using Lemma 6.1 and the decomposition given by (6.7) and (6.8).

Theorem 6.1. *Consider the single-integrator network (4.1). Suppose that $\mathcal{G}$ is an imploding star graph with the weighted Laplacian (6.6), C is circulant and the disturbance has unit covariance, i.e. $E[\Sigma_0] = I$. Then the expectation of the performance metric (2.12) for the system T given by (4.11a) is*

$$E[P] = \|T\|_{\mathcal{H}_2}^2 = \frac{n-1}{n^2}\sum_{i=2}^{n}\mu_i\left(n-1 \quad + \sum_{\substack{l>k,\\ k,l\in\{2,\dots,n\}}}\cos\left(\frac{2\pi}{n}(i-1)(l-k)\right)\right). \tag{6.9}$$

Proof. Using the fact that $E[\Sigma_0] = I$, we have $E[P] = \mathrm{tr}(\tilde{Q}\tilde{Q}^*\Psi)$. (6.8) leads to $\tilde{Q}\tilde{Q}^* = I_{n-1} + \mathbf{1}\mathbf{1}^\intercal$ which gives

$$E[P] = \sum_{k=2}^{n}\Psi_{kk} + \sum_{k=2}^{n}\sum_{l=2}^{n}\Psi_{kl}. \tag{6.10}$$

The matrix M in (4.26) has the eigenvectors

$$\boldsymbol{\theta}_l = \frac{1}{\sqrt{n}}\begin{bmatrix}1 & e^{\mathbf{j}\frac{2\pi}{n}(l-1)} & \dots & e^{\mathbf{j}\frac{2\pi}{n}(l-1)(n-1)}\end{bmatrix}^* \tag{6.11}$$

for $l = 2,\dots,n$. Using (6.11) and the columns of $\tilde{R}$ given in (6.8), the scalar products in (4.27) are obtained as

$$\langle\boldsymbol{\theta}_i, \mathbf{r}_k\rangle = \frac{1}{\sqrt{n}}e^{-\mathbf{j}\frac{2\pi}{n}(i-1)(k-2)}, \quad k = 2,\dots,n. \tag{6.12}$$

By (6.1) and the fact that $\lambda_i = \frac{n}{n-1}$ for $i = 2,\dots,n$ we have $\Psi_{kl} = \frac{n-1}{2n}\nu_{kl}$, therefore using (4.27) and (6.12) results in

$$E[P] = \frac{n-1}{2n^2}\left(\sum_{k=2}^{n}\sum_{i=2}^{n}\mu_i + \sum_{k=2}^{n}\sum_{l=2}^{n}\sum_{i=2}^{n}e^{\mathbf{j}\frac{2\pi}{n}(i-1)(l-k)}\mu_i\right). \tag{6.13}$$

Rearranging the terms in (6.13) and using Proposition 2.1 gives the result. □

We now consider a special case of circulant output matrices C, which leads to a global measure of disorder that quantifies the aggregate state deviation from the average through

$$C = I - \frac{1}{n}\mathbf{1}\mathbf{1}^\intercal = L^{cyc}\left(\frac{n-1}{n}, n-1\right). \tag{6.14}$$

This metric will be denoted by P_{dav}.

Relationship to Previous Results

For P_{dav}, the following proposition shows that the result in [36] can be reproduced as a special case of Theorem 6.1.

Proposition 6.1. *Consider the single-integrator network (4.1) and the output matrix (6.14), i.e. the performance metric P_{dav}. Suppose that $\mathcal{G}$ is an imploding star graph with the weighted Laplacian (6.6), and the disturbance has unit covariance, i.e. $E[\Sigma_0] = I$. Then the expectation of the performance metric (2.12) for the system T given by (4.11a) is*

$$E\left[P_{dav}\right] = \|T\|_{\mathcal{H}_2}^2 = \frac{(n-1)^2}{2n}. \tag{6.15}$$

Proof. The fact that $\mu_i = 1\ \forall i$ and (6.13) gives

$$E\left[P_{dav}\right] = \frac{n-1}{2n^2}\left(2(n-1)^2 + \sum_{k\neq l}\sum_{i=2}^{n} e^{\mathbf{j}\frac{2\pi}{n}(i-1)(l-k)}\right).$$

Since $\sum_{i=1}^{n} e^{\mathbf{j}\frac{2\pi}{n}(i-1)(l-k)} = 0$ for $l-k = \pm 1, \ldots, \pm(n-2)$,

$$E\left[P_{dav}\right] = \frac{n-1}{2n^2}\left(2(n-1)^2 - \underbrace{\sum_{k\neq l} e^{\mathbf{j}\frac{2\pi}{n}0(l-k)}}_{=(n-1)(n-2)}\right). \qquad \square$$

6.2.1.2 Double-Integrator Networks

Using Lemma 6.3, the following theorem characterizes performance metric (2.12) for all-to-one networks with double-integrator dynamics (4.2).

Theorem 6.2. *Consider the double-integrator network (4.2). Suppose that $\mathcal{G}$ is an imploding star graph with the weighted Laplacian (6.6), the output matrix C is circulant and the disturbance has unit covariance, i.e. $E[\Sigma_0] = I$. Then the expectation of the performance metric (2.12) is*

$$E\left[P\right] = \|T\|_{\mathcal{H}_2}^2 = P_0 \frac{1}{2(k_p + \gamma_p \frac{n}{n-1})(k_d + \gamma_d \frac{n}{n-1})} \tag{6.16}$$

for the system T given by (4.11a) and

$$E[P] = \|T\|_{\mathcal{H}_2}^2 = P_0 \frac{1}{2(k_d + \gamma_d \frac{n}{n-1})} \tag{6.17}$$

for the system T given by (4.11b), where

$$P_0 = \frac{1}{n}\left(\sum_{k=2}^{n}\sum_{i=2}^{n}\mu_i + \sum_{k=2}^{n}\sum_{l=2}^{n}\sum_{i=2}^{n} e^{\mathbf{j}\frac{2\pi}{n}(i-1)(l-k)}\mu_i\right).$$

Furthermore, if the output matrix is given by (6.14), then

$$E[P_{dav}] = \|T\|_{\mathcal{H}_2}^2 = \frac{n-1}{2(k_p + \gamma_p \frac{n}{n-1})(k_d + \gamma_d \frac{n}{n-1})} \tag{6.18}$$

for the system T given by (4.11a) and

$$E[P_{dav}] = \|T\|_{\mathcal{H}_2}^2 = \frac{n-1}{2(k_d + \gamma_d \frac{n}{n-1})} \tag{6.19}$$

for the system T given by (4.11b).

Proof. Substitution of $\lambda_k = \frac{n}{n-1}$ for $k = 2, \ldots, n$ into (6.4) and (6.5) gives $\Psi_{kl} = \nu_{kl} \frac{1}{2(k_p+\gamma_p \frac{n}{n-1})(k_d+\gamma_d \frac{n}{n-1})}$ for the system T given by (4.11a) and $\Psi_{kl} = \nu_{kl} \frac{1}{2(k_d+\gamma_d \frac{n}{n-1})}$ for the system T given by (4.11b). By the argument given in the proof of Theorem 6.1, using the expressions above and (6.10) leads to (6.16) and (6.17). The argument given in the proof of Proposition 6.1 combined with (6.16) and (6.17) yields (6.18) and (6.19). □

When P_{dav} is considered, Proposition 6.1 and Theorem 6.2 show that the performance metric grows unboundedly with the network size. Next we study ω-nearest neighbor networks.

6.2.2 Cyclic Digraphs: ω-Nearest Neighbor Networks

The cyclic digraph defined by the weighted Laplacian (5.15) can be used to model ω-nearest neighbor networks. In order to normalize the edge weights of the digraphs

with different number of communication hops we choose the out-degree of each node as $d = 1$ in (5.15), which leads to

$$L = L^{cyc}(1, \omega) \tag{6.20}$$

so that the total out-degree in the graph is n. Since we consider circulant output matrices C, the eigenvectors of M in (4.26) are given by (6.11). Combining this with (5.17), the scalar products in (4.27) are obtained as

$$\langle \boldsymbol{\theta}_l, \mathbf{r}_k \rangle = \begin{cases} 1 & k = l \\ 0 & k \neq l \end{cases}, \ k = 2, \ldots, n, \tag{6.21}$$

therefore (4.27) leads to

$$\nu_{kk} = \mu_k. \tag{6.22}$$

This means that the dependence of (5.1), (5.2) and (5.3) on the output matrix C is only through the eigenvalues μ_k of M.

Then performance is given by (5.1) for the single-integrator system, and by (5.2) or (5.3) for the double-integrator system, where due to (5.16) the eigenvalues of L satisfy

$$\lambda_k = 1 - \frac{1}{\omega} \sum_{i=1}^{\omega} e^{-\mathbf{j}\frac{2\pi}{n} i(k-1)}, \ k = 1, \ldots, n. \tag{6.23}$$

Next we present two examples to demonstrate the effect of the number of communication hops ω on the performance of ω-nearest neighbor networks and to investigate the relationship between all-to-one and all-to-all communication structures.

6.2.3 Example: Number of Communication Hops

In the following we investigate how performance changes with respect to ω. We first show that performance does not necessarily improve by increasing ω, i.e. through communication with a larger number of nearest neighbors.

For convenience suppose that n is odd. Consider the case where $\omega = \frac{n-1}{2}$ such

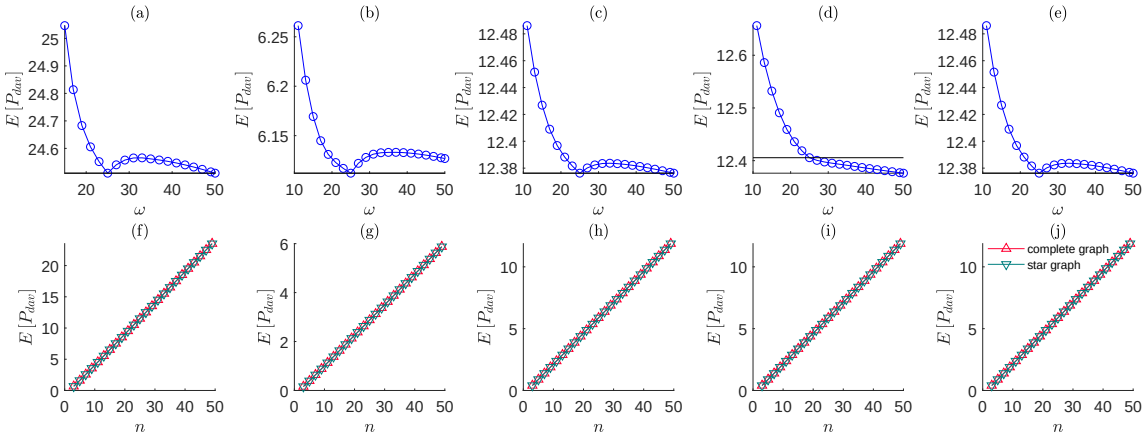

Figure 6-1. (Top) The expectation of P_{dav} defined by (6.14) versus the number of communication hops ω of the ω-nearest neighbor networks given by (6.20) where the network size is $n = 51$. **(Bottom)** The expectation of P_{dav} versus the network size n for the imploding star graph and the complete graph given by (6.6) and (6.24). The disturbance has unit covariance, i.e. $E[\Sigma_0] = I$. Plots respectively illustrate the cases of: **(a, f)** single-integrator (4.1) given by (4.11a), **(b, g)** double-integrator (4.2) given by (4.11a) (position-based performance), $k_p = k_d = \gamma_p = \gamma_d = 1$, **(c, h)** double-integrator (4.2) given by (4.11a) (position-based performance), $k_p = k_d = \gamma_d = 1, \gamma_p = 0$, **(d, i)** double-integrator (4.2) given by (4.11b) (velocity-based performance), $k_p = k_d = \gamma_p = \gamma_d = 1$, **(e, j)** double-integrator (4.2) given by (4.11b) (velocity-based performance), $k_p = k_d = \gamma_d = 1, \gamma_p = 0$.

that $L = L^{cyc}(1, \frac{n-1}{2})$. Using the definition given by (5.4)

$$L' = \frac{L^{cyc}(1, \frac{n-1}{2}) + L^{cyc}(1, \frac{n-1}{2})^*}{2} = L^{cyc}(1, n-1), \tag{6.24}$$

i.e. L' is the weighted Laplacian associated with the complete graph with uniform edge weights $\frac{1}{n-1}$. Then the associated systems T and T' have the following properties for any performance metric satisfying Assumption 4.2:

- $\|T\|^2_{\mathcal{H}_2} = \|T'\|^2_{\mathcal{H}_2}$ for the single-integrator network (4.1) defined by (4.11a) due to Theorem 5.1,

- It is possible due to Theorem 5.2 that $\|T\|^2_{\mathcal{H}_2} < \|T'\|^2_{\mathcal{H}_2}$, $\|T\|^2_{\mathcal{H}_2} = \|T'\|^2_{\mathcal{H}_2}$ or $\|T\|^2_{\mathcal{H}_2} > \|T'\|^2_{\mathcal{H}_2}$ for the position based performance of the double-integrator network (4.2) defined by system (4.11a),

- It can only hold that $\|T\|^2_{\mathcal{H}_2} = \|T'\|^2_{\mathcal{H}_2}$ or $\|T\|^2_{\mathcal{H}_2} > \|T'\|^2_{\mathcal{H}_2}$ for the velocity based performance of the double-integrator network (4.2) defined by system (4.11b) due

to Theorem 5.3.

As this example suggests, using half the number of communication hops as compared to the complete graph, i.e. the case in which ω is maximal, provides identical performance for the single integrator network (4.1). It is possible to achieve better performance using half the number of hops compared to the complete graph in the case of the position based metrics of the double integrator network (4.2); but this is not the case for the velocity based metrics.

The dependence of $E\left[P_{dav}\right]$ on ω is illustrated in figures 6-1a - 6-1e for a case in which $n = 51$ and the disturbance has unit covariance, i.e. $E[\Sigma_0] = I$. For the single integrator network (4.1) we observe in Figure 6-1a that $\|T\|^2_{\mathcal{H}_2} = \|T'\|^2_{\mathcal{H}_2}$. This is also true for the position and velocity based performance of the double-integrator network (4.2) if relative position feedback is absent ($k_p = k_d = \gamma_d = 1$ and $\gamma_p = 0$) as shown in figures 6-1c (due to Item 1 in Theorem 5.2) and 6-1e (due to Item 3 in Theorem 5.3). Conversely, using relative position feedback ($k_p = k_d = \gamma_p = \gamma_d = 1$) leads to $\|T\|^2_{\mathcal{H}_2} < \|T'\|^2_{\mathcal{H}_2}$ as shown in Figure 6-1b (due to Item 3 in Theorem 5.2) for the position based performance and to $\|T\|^2_{\mathcal{H}_2} > \|T'\|^2_{\mathcal{H}_2}$ as shown in Figure 6-1d (due to Item 2 in Theorem 5.3) for the velocity based performance. For all cases, increasing ω up to $\omega = 25$ monotonically improves performance. Compared to $\omega = 25$, choosing $25 < \omega < 50$ degrades performance, excluding the velocity based performance with relative position feedback ($\gamma_p > 0$, Figure 6-1d) which improves monotonically as ω is increased. Therefore at least for $n = 51$ and the cases in figures 6-1a-6-1c and 6-1e, $\omega = \frac{n-1}{2}$ provides the optimal performance.

The next example provides a comparison between all-to-one and all-to-all networks.

6.2.4 Example: All-to-One versus All-to-All Networks

For the special case of P_{dav} which is determined by (6.14), (6.22) holds and we have $\mu_k = 1$ for $k = 2, \ldots, n$. If all-to-all networks are considered, i.e. L is given by (6.24),

(6.23) reduces to $\lambda_k = \frac{n}{n-1}$ for $k = 2, \ldots, n$. Then P_{dav} is given by

- (6.15) for the single-integrator network (4.1) given by (4.11a),
- (6.18) for the double-integrator network (4.2) given by (4.11a),
- (6.19) for the double-integrator network (4.2) given by (4.11b),

where we respectively used (5.1), (5.6) and (5.10). Therefore, ω-nearest neighbor networks with $\omega = n - 1$ (all-to-all) and all-to-one networks perform *identically* if P_{dav} is considered, which is illustrated in figures 6-1f - 6-1j for up to $n = 49$. In conclusion, given that the total out-degree is normalized to be n for each graph, the same P_{dav} is achieved by using $n - 1$ directed edges that follow a common leader as that of using $n(n - 1)$ directed edges such that each node follows every other node. The latter feedback scheme can be interpreted as every node being a common leader in the sense of the former feedback scheme. In other words, the all-to-all network can be interpreted as the superposition of n all-to-one networks with edge weights scaled by $\frac{1}{n}$. Thus the same level of deviation from the average state (position or velocity) is achieved by following a single common leader instead of using all-to-all communication, provided the edge weights are sufficiently large. As n grows, the number of edges grow linearly and each edge weight $\frac{n}{n-1}$ remains bounded in all-to-one networks. In contrast, the number of edges grow quadratically and each edge weight $\frac{1}{n-1}$ decays to zero in all-to-all networks. We note for double-integrator networks (4.2) given by (4.11a) that compared to both all-to-one and all-to-all communication, it is possible to achieve better position-based P_{dav} with $\omega = \frac{n-1}{2}$ nearest neighbor interactions (odd n), if both relative position and velocity feedback are employed and the relative position feedback gain γ_p is sufficiently small (e.g. Figure 6-1b).

6.3 Summarizing Remarks

In chapters 5 and 6, we analyzed subclasses of directed interconnection topologies using our general framework from Chapter 4. We have demonstrated the role of communication directionality and degree of connectivity in overall network performance for systems defined over such topologies. Our results revealed previously undiscovered properties of these systems.

The results presented until this point pertain to finite-size networks. In the next chapter, we examine large-scale networks with directed interconnection topologies and discuss performance trade-offs that emerge as a result of communication directionality and growing network size.

Chapter 7

Disorder in Large-scale Networks with Uni-directional Feedback

Performance metrics evaluating network disorder have been investigated as a function of network size and the number of spatial dimensions of feedback interconnections (e.g. in vehicle formations). For networks of double integrators with undirected and static feedback interconnections (undirected second order consensus networks), both long and short range disorder can grow unboundedly with network size with only relative measurements of both the position and velocity states [1]. Scaling of metrics of disorder with network size has been investigated in directed first order consensus networks controlled by static feedback [38–41, 46]. as well as in directed 1-dimensional double-integrator networks [45, 46].

Improved scaling of these metrics were demonstrated in 1-dimensional vehicle strings with directed nearest-neighbor interactions [46]. However, as in the undirected case, coherence cannot be achieved in these systems without absolute state measurements, using directed nearest neighbor feedback [44]. When undirected second order consensus networks are additionally equipped with dynamic feedback with undirected interconnections, at least one type of absolute state measurement can uniformly bound the state deviation from the average with respect to network size [43, 48]. However, the scaling properties of standard second order consensus networks with directed

interconnections in multiple spatial dimensions remain to be investigated.

We have shown in Chapter 5 that double-integrator networks with more general directed feedback interconnections (emitting normal weighted Laplacian matrices) can attain improved performance. In this chapter, we take a step toward determining whether or not a directed feedback structure can improve how performance scales with respect to network size by considering uni-directional feedback in networks with arbitrary but finite spatial dimension. More precisely, we compare the performance of a network of agents with double-integrator dynamics and directed uni-directional local state measurements defined over a multi-dimensional torus to that of the network with symmetric bi-directional local state measurements studied in [1]. These models represent, for example, spatially invariant vehicle networks where comparible performance in systems with directed uni-directional feedback structures would be desirable due to the reduced sensing/communication requirements. Performance of the network is evaluated in terms of both a local metric quantifying the variance of an agent's position error with respect to its nearest predecessor and a global metric describing the variance of each agent's position deviation from the network average (dispersion of consensus error). We compute these metrics using an $\mathcal{H}_2$ norm of the system subjected to distributed stochastic disturbances for system outputs defined to yield the desired metrics. We then extend the scaling laws in [1] to the case of directed uni-directional feedback.

We exploit the spatial invariance of the interconnection structure to define the feedback laws and the performance outputs in terms of circular convolution operators based on the machinary used in [1]. After establishing the necessary and sufficient condition for input-output stability, we provide the closed-form solution for the $\mathcal{H}_2$ norm of the system for general feedback laws and performance outputs. Then we focus on the special case of directed uni-directional feedback which employs 'look-ahead' state measurements. For networks with absolute measurements of velocity, we provide

a sufficient condition under which the $\mathcal{H}_2$ norm (performance metric) for a system with uni-directional feedback lower bounds the $\mathcal{H}_2$ norm of systems with symmetric bi-directional ('look-ahead / look-behind') feedback for any finite network size and spatial dimension. This bound provides a special case of Theorem 5.2 from Chapter 5. We then show that local and global metrics of disorder scale identically in systems with uni-directional and symmetric bi-directional feedback if at least one type of absolute state (position or velocity) feedback is employed. Conversely, in the absence of absolute velocity measurements we prove that it is impossible to maintain the input-output stability with uni-directional relative position and velocity feedback as the network size increases for arbitrary spatial dimension, which is consistent with the observations for 1-dimensional cyclic networks [84–87]. We note that a similar result more recently appeared in [88]. This condition represents an important difference between the uni-directional and the symmetric bi-directional feedback structures, as the latter maintains the stability for arbitrarily large spatially invariant networks [1].

Our results highlight a trade-off between performance and stability in large-scale networks with uni-directional feedback; while achieving comparable performance with reduced communication can be favorable, it comes at the cost of degradation of stability for certain feedback interconnection structures. Numerical examples confirm the theoretical results regarding performance scaling with respect to network size and the loss of stability for arbitrarily large networks without absolute velocity feedback.

The remainder of this chapter is organized as follows. Section 7.1.1 defines the notation and provides the mathematical background used throughout. Section 7.1.2 presents the system models and Section 7.1.3 presents the feedback policies. Section 7.1.4 describes the performance metrics. Sections 7.2 provides the conditions for the input-output stability of the system, the closed-form solution for the $\mathcal{H}_2$ norm as well as a description of how performance scales with respect to network size and dimension. Section 7.3 presents numerical examples supporting the theoretical results. Section

7.4 concludes the chapter.

7.1 Problem Formulation

7.1.1 Preliminaries and Notation

We consider systems connected over the d-dimensional torus $\mathbb{Z}_N^d = \mathbb{Z}_N \times \cdots \times \mathbb{Z}_N$ defined as the d-fold cartesian product of the 1-dimensional torus $\mathbb{Z}_N = \{0, 1, \ldots, N-1\}$. An array A is defined as the mapping $A : \mathbb{Z}_N^d \mapsto \mathbb{C}^{p \times q}$ where p and q are scalars and A_k denotes each of the array elements corresponding to the spatial multi-index $k = (k_1, \ldots, k_d) \in \mathbb{Z}_N^d$. We denote vector-valued arrays ($q = 1$) with a lower-case letter. For example, the position state $x(t)$ is an array whose elements $x_k(t) \in \mathbb{R}^d$ represent the position of the k^{th} system in d spatial dimensions. Addition is performed modulo N for indices $k, l \in \mathbb{Z}_N^d$, i.e. $m = k + l$ with $m_i = (k_i + l_i)_N$ for $i = 1, \ldots, d$.

The multi-dimensional circular convolution of the arrays A and h yields an array z with elements given by

$$z_k = \sum_{l \in \mathbb{Z}_N^d} A_{k-l} h_l. \tag{7.1}$$

We equivalently write (7.1) as $z = \mathcal{A}h$, where $\mathcal{A}$ denotes the circular convolution operator associated with array A acting on array h. The multi-dimensional Discrete Fourier Transform (DFT) of A is defined by

$$\hat{A}_n := \sum_{k \in \mathbb{Z}_N^d} A_k e^{-j \frac{2\pi}{N} n \cdot k}, \tag{7.2}$$

where $(\cdot)$ denotes the scalar product, $n \in \mathbb{Z}_N^d$ is the wavenumber and $\hat{A}_n$ is the Fourier symbol of $\mathcal{A}$. It is a well-known fact that the DFT diagonalizes a circular convolution operator [1], so

$$\hat{z}_n = \hat{A}_n \hat{h}_n \quad \forall n \in \mathbb{Z}_N^d.$$

If $\hat{A}_n$ is a square matrix, then the eigenvalues of the circular convolution operator $\mathcal{A}$ are the union of the eigenvalues of all $\hat{A}_n$, i.e. $\sigma(\mathcal{A}) = \cup_{n \in \mathbb{Z}_N^d} \sigma(\hat{A}_n)$, where $\sigma(\cdot)$

denotes the spectrum of its argument.

The adjoint (conjugate transpose) of an operator (matrix) Q is denoted by Q^*. $E\{\cdot\}$ denotes the expected value of a random variable and $\|\cdot\|_{\mathcal{H}_2}$ denotes the $\mathcal{H}_2$ norm of a linear system. The zero and identity operators (matrices) are denoted by $\mathcal{O}$ (0) and $\mathcal{I}$ (I), respectively. T denotes an array with identical non-zero elements, i.e. $T_k = T_l \neq 0$ for all k, $l \in \mathbb{Z}_N^d$, and $\mathbf{1}$ denotes the array with elements $\mathbf{1}_k = I$ for all $k \in \mathbb{Z}_N^d$. The arrows $\nearrow$ and $\searrow$ repsectively denote the left and right limits to a real number. $O(\cdot)$ denotes the approximation order.

7.1.2 Double-Integrator Systems over the d-Dimensional Torus

We consider $M := N^d$ identical systems defined over $\mathbb{Z}_N^d$ each having double-integrator dynamics given by

$$\begin{aligned} \dot{v}_k &= u_k + w_k, \\ v_k &= \dot{x}_k \quad \forall k \in \mathbb{Z}_N^d, \end{aligned} \tag{7.3}$$

where $x_k \in \mathbb{R}^d$, $v_k \in \mathbb{R}^d$, $u_k \in \mathbb{R}^d$ and $w_k \in \mathbb{R}^d$ respectively denote the position, velocity, control input and an exogenous local disturbance. The control input is of the form

$$u_k = -g_o x_k - f_o v_k - \sum_{l \in \mathbb{Z}_N^d} G_{k-l} x_l - \sum_{l \in \mathbb{Z}_N^d} F_{k-l} v_l, \tag{7.4}$$

where $g_o, f_o \geq 0$ are the feedback gains associated with the measurements of states with respect to an absolute reference frame (absolute feedback). The circular convolutions of the states with the feedback arrays $G : \mathbb{Z}_N^d \mapsto \mathbb{R}^{d \times d}$ and $F : \mathbb{Z}_N^d \mapsto \mathbb{R}^{d \times d}$ define feedback laws based on relative state measurements (relative feedback).

Combining (7.3) and (7.4) yields

$$\begin{bmatrix} \dot{x} \\ \dot{v} \end{bmatrix} = \begin{bmatrix} \mathcal{O} & \mathcal{I} \\ -\mathcal{A} & -\mathcal{B} \end{bmatrix} \begin{bmatrix} x \\ v \end{bmatrix} + \begin{bmatrix} \mathcal{O} \\ \mathcal{I} \end{bmatrix} w, \tag{7.5}$$

where $\mathcal{A} = g_o\mathcal{I} + \mathcal{G}$ and $\mathcal{B} = f_o\mathcal{I} + \mathcal{F}$. Here, $\mathcal{G}$ and $\mathcal{F}$ are the circular convolution operators associated with the arrays G and F, respectively.

Remark 7.1. *Since the feedback laws in* (7.5) *are determined by circulant operators, the feedback laws are invariant to the specific location* $k \in \mathbb{Z}_N^d$*, i.e.* (7.5) *describes a spatially invariant system [1, 89].*

Assumptions

The following standard assumptions [1] will be imposed on $\mathcal{G}$ and $\mathcal{F}$ throughout the chapter. Note that for clarity of exposition we state them only in terms of $\mathcal{G}$.

(A1) The feedback laws satisfy the property

$$\sum_{k \in \mathbb{Z}_N^d} G_k = 0,$$

which implies that $T \in \ker(\mathcal{G})$.

(A2) If $d \geq 2$, the feedback laws are decoupled in spatial coordinates, i.e. the interactions in the i^{th} spatial coordinate only depend on the state measurements in that spatial coordinate, for $i = 1, \ldots, d$. This results in diagonal array elements G_k. In addition setting the non-zero entries of G_k to be equal leads to

$$G_k = g_k I, \quad g_k \in \mathbb{R}.$$

This condition also implies that the Fourier symbol of $\mathcal{G}$ is a scalar matrix

$$\hat{G}_n = \hat{g}_n I.$$

Therefore, by a slight abuse of notation we will refer to $\hat{g}_n$ as the Fourier symbol of $\mathcal{G}$.

(A3) If (A2) holds, the diagonal entries of each array element $G_k = g_k I$ satisfy the property

$$g_k \begin{cases} > 0, & k_1 = \cdots = k_d = 0 \\ \leq 0, & \text{otherwise.} \end{cases}$$

For spatially invariant systems, (A1) - (A3) generalize the properties of a circulant weighted graph Laplacian matrix to systems with arbitrary spatial dimension.

Under these assumptions, $\mathcal{G}$ and $\mathcal{F}$ can be specified to define feedback laws based on relative state measurements. In this setting, if $g_o > 0$ ($f_o > 0$), then the system is said to have absolute position (velocity) feedback. If $g_o = 0$ ($f_o = 0$), then we assume the system has relative position (velocity) feedback. If no relative position (velocity) feedback is used, then we assume $g_o > 0$ ($f_o > 0$).

7.1.3 Feedback Policies

We are interested in examining the effect of directed communication on the performance of large-scale networks by comparing systems with uni-directional and symmetric bi-directional feedback. In particular, we will investigate how the performance scales with network size. We next define the two feedback policies and then specify the peformance metrics of interest in the subsequent subsection.

Bi-directional Feedback

In this communication structure, each agent employs a look-ahead / look-behind policy, in which the information flow in either direction is equally weighted. For example, if $d = 1$, this feedback interconnection is attained through the control input

$$u_k = -g_o x_k - f_o v_k - \frac{1}{2}[\gamma_g(x_k - x_{k+1}) + \gamma_g(x_k - x_{k-1}) + \gamma_f(v_k - v_{k+1}) + \gamma_f(v_k - v_{k-1})],$$

where $\gamma_g, \gamma_f \geq 0$ are control gains and the factor of $\frac{1}{2}$ provides a normalization of weights with respect to the uni-directional feedback described in the following subsection. For $d \geq 1$, the array associated with the corresponding local symmetric

bi-directional feedback operator $\mathcal{Q}$ is given by

$$Q_k = \begin{cases} dI, & k_1 = \cdots = k_d = 0 \\ -\frac{1}{2}I, & k_i = \pm 1,\ k_j = 0 \text{ for } j \neq i \\ 0, & \text{otherwise,} \end{cases} \tag{7.6}$$

such that the operators $\mathcal{G}$ and $\mathcal{F}$ in (7.5) are given by

$$\mathcal{G} = \gamma_g \mathcal{Q}, \quad \mathcal{F} = \gamma_f \mathcal{Q}. \tag{7.7}$$

This feedback law was studied extensively in [1, 43].

Uni-directional Feedback

For directed communication, we consider uni-directional (look-ahead) feedback. For $d = 1$, the associated control input is given by

$$u_k = -g_o x_k - f_o v_k - \gamma_g(x_k - x_{k+1}) - \gamma_f(v_k - v_{k+1}).$$

For $d \geq 1$, the array associated with the corresponding local uni-directional feedback operator $\mathcal{R}$ is given by

$$R_k = \begin{cases} dI, & k_1 = \cdots = k_d = 0 \\ -I, & k_i = -1,\ k_j = 0 \text{ for } j \neq i \\ 0, & \text{otherwise.} \end{cases} \tag{7.8}$$

In this case, the operators $\mathcal{G}$ and $\mathcal{F}$ in (7.5) are given by

$$\mathcal{G} = \gamma_g \mathcal{R}, \quad \mathcal{F} = \gamma_f \mathcal{R}. \tag{7.9}$$

The following proposition about the Fourier symbols of $\mathcal{Q}$ and $\mathcal{R}$ will be used in the subsequent results.

Proposition 7.1. *The respective Fourier symbols $\hat{q}_n$ and $\hat{r}_n$ of the circular convolution operators $\mathcal{Q}$ and $\mathcal{R}$ defined by (7.6) and (7.8) are given by*

$$\hat{r}_n = \sum_{i=1}^{d} \left(1 - e^{j\frac{2\pi}{N}n_i}\right), \quad \hat{q}_n = \sum_{i=1}^{d} \left(1 - \cos\left(\frac{2\pi}{N}n_i\right)\right). \tag{7.10}$$

Proof. Since $\mathcal{Q}$ can be decomposed as $\mathcal{Q} = \frac{\mathcal{R}+\mathcal{R}^*}{2}$, it holds that $\hat{q}_n = \mathrm{Re}\,(\hat{r}_n)$ for $n \in \mathbb{Z}_N^d$. Using the definition of the DFT given in (7.2) leads to $\hat{R}_n = \left(d - \sum_{i=1}^{d} e^{j\frac{2\pi}{N}n_i}\right) I$. The result is then obtained by invoking (A2), i.e. $\hat{R}_n = \hat{r}_n I$. □

7.1.4 Performance Metrics

We now define system outputs that allow us to quantify local and global metrics of system disorder through the input-output $\mathcal{H}_2$ norm of a system of the form (7.5) for the two feedback interconnection structures (7.7) and (7.9). These metrics were detailed in [1] for systems with the feedback interconnection structure (7.7) but we repeat their definitions here for completeness.

Since we focus on spatially invariant systems, it is convenient to define a nodal performance metric of the form

$$P_k := \lim_{t\to\infty} E\{y_k^*(t)y_k(t)\}, \tag{7.11}$$

where y_k is the performance output given by the circular convolution

$$y_k = \sum_{l\in\mathbb{Z}_N^d} C_{k-l}x_l \quad \forall k \in \mathbb{Z}_N^d. \tag{7.12}$$

Here, we assume that C_k satisfies assumptions (A1) and (A2). Due to (A1), the consensus modes of (7.5) will be unobservable from the system output

$$y = \begin{bmatrix}\mathcal{C} & \mathcal{O}\end{bmatrix}\begin{bmatrix}x\\ v\end{bmatrix}, \tag{7.13}$$

where $\mathcal{C}$ represents the respective circular convolution operator associated with the operation in (7.12). We denote the input-output system defined by (7.5) and (7.13) by H. In this chapter we limit the analysis to performance metrics based solely on the position, which is common for coordination [1, 43] and phase synchronization [49, 50] applications.

For white noise disturbance inputs w with unit covariance, the squared $\mathcal{H}_2$ norm of H quantifies the steady-state variance of the output [49]

$$\|H\|_{\mathcal{H}_2}^2 = \lim_{t\to\infty} E\{y^*(t)y(t)\}, \tag{7.14}$$

whenever H is input-output stable. Since the performance output of each system y_k is also spatially invariant, it is sufficient to divide (7.14) by the network size to recover

each system's metric P_k, i.e.

$$P_k = \frac{1}{M}\|H\|^2_{\mathcal{H}_2},$$

where we recall that $M = N^d$.

7.1.4.1 Local Error

This metric quantifies the steady-state variance of the deviation of each agent's position from that of its predecessor. For $d = 1$, the corresponding output for each system is

$$y_k = x_k - x_{k+1}.$$

The system output (7.13) for $d \geq 1$ can be obtained using the right shift operator along dimension i, namely $\mathcal{D}^i$ such that

$$(\mathcal{D}^i x)_{(k_1,\ldots,k_i,\ldots,k_d)} := x_{(k_1,\ldots,k_i+1,\ldots,k_d)},$$

and specifying

$$\mathcal{C} = \begin{bmatrix} \mathcal{I} - \mathcal{D}^1 \\ \vdots \\ \mathcal{I} - \mathcal{D}^d \end{bmatrix} \Rightarrow \begin{array}{r} (y_k)_i = x_{(k_1,\ldots,k_i,\ldots,k_d)} \\ - \; x_{(k_1,\ldots,k_i+1,\ldots,k_d)}, \\ i = 1,\ldots,d. \end{array} \tag{7.15}$$

The local metric of disorder for each system at location k is then given by

$$P_{loc} = \lim_{t\to\infty} E\left\{\sum_{i=1}^{d} (y_k)_i^* (y_k)_i\right\}. \tag{7.16}$$

7.1.4.2 Deviation from the Average

This metric quantifies the steady-state variance of the deviation of each system's position from the average position of all of the systems. Therefore each system's output gives the consensus error

$$y_k = x_k - \frac{1}{M}\sum_{l\in\mathbb{Z}_N^d} x_l. \tag{7.17}$$

In this case, the output operator $\mathcal{C}$ becomes

$$\mathcal{C} = \mathcal{I} - \frac{1}{M}\mathcal{J}, \tag{7.18}$$

where $\mathcal{J}$ denotes the circular convolution operator associated with the array $\mathbf{1}$. The corresponding performance metric of the form (7.11) quantifies the global degree of disorder in the network and will be denoted by P_{dav} for each system.

7.2 Disorder in Large-scale Uni-directional Networks

In this section, we first provide conditions for the input-output stability of H. We then derive the closed-form solution of its $\mathcal{H}_2$ norm, for the case in which the directed feedback operators $\mathcal{A}$ and $\mathcal{B}$ (satisfying (A1)-(A3)) in (7.5) and the directed output operator $\mathcal{C}$ (satisfying (A1) and (A2)) in (7.13) are circular convolution operators. These results for directed networks can be used to recover those in [1], which deal with the special case of undirected feedback.

Then we focus on the uni-directional feedback structure described in (7.9) and the specific performance metrics P_{loc} and P_{dav} defined through the outputs in (7.15) and (7.17). We investigate these metrics under various combinations of absolute and relative feedback and establish upper bounds on the $\mathcal{H}_2$ norm of H as a function of network size and spatial dimension. In particular, we provide sufficient conditions under which the uni-directional and the symmetric bi-directional feedback provide the same performance scaling.

Furthermore, for certain cases lacking absolute velocity feedback we show that uni-directional local measurements cannot maintain stability with finite control gains in any number of spatial dimensions if the network size is arbitrarily large.

7.2.1 Input-Output Stability

In this subsection, we derive conditions for the input-output stability of H. We first provide a condition for the case of any circulant output operator $\mathcal{C}$ satisfying assumptions (A1) and (A2), and then restate this condition for the specific cases of

P_{loc} and P_{dav}.

We begin by stating a result from [9], which provides a generalization of the Routh-Hurwitz stability criterion to a second order polynomial with complex coefficients.

Proposition 7.2 (Lemma 2, [9])**.** *The roots of a complex-coefficient polynomial* $p(s) = s^2 + \beta s + \alpha$*, where* $\alpha, \beta \in \mathbb{C}$*, satisfy* $\mathrm{Re}(s) < 0$ *if and only if the inequalities*

$$\mathrm{Re}(\beta) > 0 \quad \textit{and}$$
$$\mathrm{Re}\,(\alpha)\,\mathrm{Re}\,(\beta)^2 + \mathrm{Im}\,(\alpha)\,\mathrm{Im}\,(\beta)\,\mathrm{Re}\,(\beta) - \mathrm{Im}\,(\alpha)^2 > 0$$

simultaneously hold.

The following proposition provides the necessary and sufficient condition for the input-output stability of H. The proof builds upon (Corollary 3, [89]).

Proposition 7.3. *System* H *defined by* (7.5) *and* (7.13) *is input-output stable if and only if the inequalities*

$$\mathrm{Re}\,(\hat{b}_n) > 0 \quad \textit{and} \tag{7.19a}$$
$$\Theta_n := \mathrm{Re}\,(\hat{a}_n)\,\mathrm{Re}\,(\hat{b}_n)^2 \tag{7.19b}$$
$$+ \mathrm{Im}\,(\hat{a}_n)\,\mathrm{Im}\,(\hat{b}_n)\,\mathrm{Re}\,(\hat{b}_n) - \mathrm{Im}\,(\hat{a}_n)^2 > 0$$

simultaneously hold for all non-zero wavenumbers $n \neq 0,\ n \in \mathbb{Z}_N^d$ *such that* $\hat{c}_n \neq 0$*.*

Proof. Taking the DFT of the arrays on both sides of (7.5) and (7.13), one can obtain n subsystems of the form

$$\begin{bmatrix} \dot{\hat{x}}_n \\ \dot{\hat{v}}_n \end{bmatrix} = \begin{bmatrix} 0 & I \\ -\hat{A}_n & -\hat{B}_n \end{bmatrix} \begin{bmatrix} \hat{x}_n \\ \hat{v}_n \end{bmatrix} + \begin{bmatrix} 0 \\ I \end{bmatrix} \hat{w}_n,$$
$$\hat{y}_n = \begin{bmatrix} \hat{C}_n & 0 \end{bmatrix} \begin{bmatrix} \hat{x}_n \\ \hat{v}_n \end{bmatrix}, \quad n \in \mathbb{Z}_N^d. \tag{7.20}$$

Due to Assumption (A2), each subsystem can be decomposed into i identical subsys-

tems

$$\begin{bmatrix}(\dot{\hat{x}}_n)_i\\(\dot{\hat{v}}_n)_i\end{bmatrix} = \begin{bmatrix}0 & 1\\-\hat{a}_n & -\hat{b}_n\end{bmatrix}\begin{bmatrix}(\hat{x}_n)_i\\(\hat{v}_n)_i\end{bmatrix} + \begin{bmatrix}0\\1\end{bmatrix}(\hat{w}_n)_i,$$
$$(\hat{y}_n)_i = \begin{bmatrix}\hat{c}_n & 0\end{bmatrix}\begin{bmatrix}(\hat{x}_n)_i\\(\hat{v}_n)_i\end{bmatrix}, \quad i = 1, \ldots, d. \tag{7.21}$$

Denoting the transfer function of the realization in (7.20) by $\hat{H}_n(s)$ and that of the realization in (7.21) by $\hat{h}_n(s)$ leads to

$$\hat{H}_n(s) = \hat{h}_n(s)I \quad \text{and} \quad \hat{h}_n(s) = \frac{\hat{c}_n}{s^2 + \hat{b}_n s + \hat{a}_n}, \tag{7.22}$$

where we used the fact that (7.21) is in controllable canonical form. Since all of the modes associated with (7.20) are controllable, the poles of $H(s)$ are precisely given by the union of the poles of $\hat{H}_n(s)$ for all wavenumbers $n \in \mathbb{Z}_N^d$ such that $\hat{c}_n \neq 0$, i.e. they are determined by the observable modes. Since C_k satisfies Assumption (A1), we can use the definition of the DFT in (7.2) to obtain

$$\hat{C}_0 = \sum_{k \in \mathbb{Z}_N^d} C_k = 0,$$

which implies that $\hat{c}_0 = 0$ due to Assumption (A2), i.e. the output operator $\mathcal{C}$ has a zero Fourier symbol at $n = 0$. Therefore it is sufficient to consider only $n \neq 0$.

Then disregarding the multiplicities, the poles of $H(s)$ are precisely given by the poles of $\hat{h}_n(s)$ for all non-zero wavenumbers $n \neq 0,\ n \in \mathbb{Z}_N^d$ such that $\hat{c}_n \neq 0$. Invoking Proposition 7.2, the poles satisfy $\mathrm{Re}(s) < 0$ if and only if the inequalities in (7.19) simultaneously hold. □

The interpretation of Proposition 7.3 is as follows. Since the output operator $\mathcal{C}$ satisfies (A1), the consensus modes of (7.5) associated with the wavenumber $n = 0$ (which are unstable in the absence of absolute feedback [46]) are unobservable from the output. Therefore, the input-output stability of H is equivalent to the stability of the observable modes associated with the non-zero wavenumbers. The next Lemma specializes this result to the cases of P_{loc} and P_{dav}.

Table 7-I. In systems with uni-directional feedback, asymptotic scalings of upper bounds on performance metrics with respect to network size M in finite spatial dimension d. Quantities are up to a multiplicative factor that is independent of M,γ_g or γ_f.

	P_{loc}	P_{dav}
abs. pos. & **abs. vel.** $\left(f_o \geq \frac{\gamma_g}{\gamma_f}, \gamma_f > 0\right)$	$\frac{1}{\max\{\gamma_g, \gamma_f\}}$	1
rel. pos. & **abs. vel.** $\left(f_o \geq \frac{\gamma_g}{\gamma_f}, \gamma_f > 0\right)$	$1/\gamma_g$	$\frac{1}{\gamma_g}\begin{cases} M & d=1 \\ \ln(M) & d=2 \\ 1 & d\geq 3 \end{cases}$
abs. pos. & **rel. vel.** $(\gamma_g = 0)$	$1/\gamma_f$	$\frac{1}{\gamma_f}\begin{cases} M & d=1 \\ \ln(M) & d=2 \\ 1 & d\geq 3 \end{cases}$
abs. pos. & **rel. vel.** $(\gamma_g > 0)$	$+\infty$	$+\infty$
rel. pos. & **rel. vel.**	$+\infty$	$+\infty$

Lemma 7.1. *Consider the output matrices* (7.15) *and* (7.18) *associated with the performance metrics P_{loc} and P_{dav}. System H defined by* (7.5) *and* (7.13) *is input-output stable if and only if the inequalities in* (7.19) *simultaneously hold for all $n \neq 0, n \in \mathbb{Z}_N^d$.*

Proof. We first consider P_{loc}. Using (7.15) we get $\mathcal{Q} = \frac{1}{2}\mathcal{C}^*\mathcal{C}$ [1] therefore $|\hat{c}_n|^2 = 2\hat{q}_n$. Then for any n such that $n \neq 0$, we observe from (7.10) that $\hat{q}_n > 0$, which implies $\hat{c}_n \neq 0$. For P_{dav}, $\hat{c}_n = 1$ for any $n \neq 0$ [1]. In both cases $\hat{c}_n \neq 0$ for all $n \neq 0$, so Proposition 7.3 yields the result. □

7.2.2 Performance Scaling with Respect to Network Size

In this subsection we present the closed-form solution for the $\mathcal{H}_2$ norm of H. We then derive corresponding scaling bounds for the case of uni-directional feedback, in analogy with those reported in [1] for symmetric bi-directional feedback.

We first discuss the general setting with circulant directed feedback operators $\mathcal{A}$ and $\mathcal{B}$ (satisfying (A1)-(A3)) and a circulant directed output operator $\mathcal{C}$ (satisfying

(A1) and (A2)).

Lemma 7.2. *Suppose that system H defined by (7.5) and (7.13) is input-output stable. Then its $\mathcal{H}_2$ norm is given by*

$$\|H\|_{\mathcal{H}_2}^2 = \frac{d}{2} \sum_{\substack{\hat{c}_n \neq 0, \\ n \neq 0, n \in \mathbb{Z}_N^d}} |\hat{c}_n|^2 \frac{\mathrm{Re}\,(\hat{b}_n)}{\Theta_n}, \tag{7.23}$$

where Θ_n is given by

$$\Theta_n = \mathrm{Re}\,(\hat{a}_n)\,\mathrm{Re}\,(\hat{b}_n)^2 + \mathrm{Im}\,(\hat{a}_n)\,\mathrm{Im}\,(\hat{b}_n)\,\mathrm{Re}\,(\hat{b}_n) - \mathrm{Im}\,(\hat{a}_n)^2.$$

Proof. Since the $\mathcal{H}_2$ norm of H is invariant to the change of basis that yields (7.20) [1], it is given by

$$\|H\|_{\mathcal{H}_2}^2 = \sum_{\substack{\hat{c}_n \neq 0, \\ n \neq 0, n \in \mathbb{Z}_N^d}} \|\hat{H}_n\|_{\mathcal{H}_2}^2 = d \sum_{\substack{\hat{c}_n \neq 0, \\ n \neq 0, n \in \mathbb{Z}_N^d}} \|\hat{h}_n\|_{\mathcal{H}_2}^2,$$

where we used (7.22) and the fact that unobservable modes have no contribution. Based on the realization of $\hat{h}_n$ given in (7.21), one can solve the associated Lyapunov equation

$$\begin{bmatrix} 0 & 1 \\ -\hat{a}_n & -\hat{b}_n \end{bmatrix}^* \begin{bmatrix} \hat{\phi}_{11} & \hat{\phi}_{12} \\ \hat{\phi}_{12}^* & \hat{\phi}_{22} \end{bmatrix} + \begin{bmatrix} \hat{\phi}_{11} & \hat{\phi}_{12} \\ \hat{\phi}_{12}^* & \hat{\phi}_{22} \end{bmatrix} \begin{bmatrix} 0 & 1 \\ -\hat{a}_n & -\hat{b}_n \end{bmatrix} = \begin{bmatrix} -\hat{c}_n^* \hat{c}_n & 0 \\ 0 & 0 \end{bmatrix}$$

and use the fact that $\|\hat{h}_n\|_{\mathcal{H}_2}^2 = \hat{\phi}_{22}^{(n)}$. Solving the Lyapunov equation leads to $\hat{\phi}_{22}^{(n)} = |\hat{c}_n|^2 \frac{\mathrm{Re}\,(\hat{b}_n)}{2\Theta_n}$ and summing over all of the observable modes yields the result. □

Lemma 7.2 indicates that the $\mathcal{H}_2$ norm depends on both the real and the imaginary parts of the Fourier symbols of $\mathcal{A}$ and $\mathcal{B}$. This is in contrast to the case in which the feedback structure is undirected, where the terms with the imaginary parts do not exist.

Remark 7.2. *If the feedback operators $\mathcal{A}$ and $\mathcal{B}$ have even symmetry, i.e. if $A_k = A_{-k}$ and $B_k = B_{-k}$ for all the non-zero entries of the arrays A and B, then the feedback is undirected and Fourier symbols $\hat{a}_n$ and $\hat{b}_n$ are real. Then (7.23) reduces to the result*

in [1]

$$\|H\|_{\mathcal{H}_2}^2 = \frac{d}{2} \sum_{\substack{\hat{c}_n \neq 0, \\ n \neq 0, n \in \mathbb{Z}_N^d}} \frac{|\hat{c}_n|^2}{\hat{a}_n \hat{b}_n}. \tag{7.24}$$

The following lemma provides two sufficient conditions under which the $\mathcal{H}_2$ norm of the system with uni-directional feedback described by (7.9) respectively lower bounds or equals the $\mathcal{H}_2$ norm of the system with symmetric bi-directional feedback described by (7.7). At least one of these conditions can be satisfied for any finite network size in arbitrary spatial dimension given absolute measurements of at least one state variable (position or velocity).

Lemma 7.3. *Consider the system H defined by (7.5) and (7.13). Let $H_{\mathcal{Q}}$ and $H_{\mathcal{R}}$ respectively denote the systems that have the feedback laws defined by (7.7) and (7.9). Then*

1. $\|H_{\mathcal{R}}\|_{\mathcal{H}_2}^2 \leq \|H_{\mathcal{Q}}\|_{\mathcal{H}_2}^2$ *if the following inequality holds*

$$\gamma_f \left[f_o + \gamma_f \sum_{i=1}^{d} \left(1 - \cos\left(\frac{2\pi}{N} n_i \right) \right) \right] - \gamma_g \geq 0, \tag{7.25}$$

for all non-zero wavenumbers $n \neq 0,\ n \in \mathbb{Z}_N^d$ such that $\hat{c}_n \neq 0$.

2. $\|H_{\mathcal{R}}\|_{\mathcal{H}_2}^2 = \|H_{\mathcal{Q}}\|_{\mathcal{H}_2}^2$ *if $\gamma_g = 0$.*

Proof. We first consider the stability of $H_{\mathcal{R}}$, which has

$$\hat{a}_n = g_o + \gamma_g \hat{r}_n \quad \text{and} \quad \hat{b}_n = f_o + \gamma_f \hat{r}_n.$$

It holds that $\mathrm{Re}(\hat{r}_n) = \hat{q}_n = \sum_{i=1}^{d} \left(1 - \cos\left(\frac{2\pi}{N} n_i \right) \right)$ due to (7.10) in Proposition 7.1 and we see by inspection that $\hat{q}_n > 0$ for all $n \neq 0, n \in \mathbb{Z}_N^d$. Recalling that

$$\begin{aligned} \Theta_n = (g_o + \gamma_g \hat{q}_n)(f_o + \gamma_f \hat{q}_n)^2 \\ + \gamma_g \,\mathrm{Im}\,(\hat{r}_n)^2 \left[\gamma_f (f_o + \gamma_f \hat{q}_n) - \gamma_g \right], \end{aligned} \tag{7.26}$$

we observe that $\Theta_n > 0$ for all $n \neq 0, n \in \mathbb{Z}_N^d$ such that $\hat{c}_n \neq 0$ in either case of (7.25) or $\gamma_g = 0$ (since absolute or relative feedback is used for each state variable). Combining this with the fact that $\mathrm{Re}(\hat{b}_n) > 0$ for $n \neq 0$, we observe that (7.19) is satisfied for all $n \neq 0, n \in \mathbb{Z}_N^d$ such that $\hat{c}_n \neq 0$, hence $H_{\mathcal{R}}$ is input-output stable by Proposition 7.3. Setting $\mathrm{Im}\,(\hat{a}_n) = \mathrm{Im}\,(\hat{b}_n) = 0$ in (7.19) directly leads to the input-output stability of $H_{\mathcal{Q}}$, which has real $\hat{a}_n$ and $\hat{b}_n$.

Then one can rewrite (7.23) as

$$\|H_{\mathcal{R}}\|_{\mathcal{H}_2}^2 = \frac{d}{2} \sum_{\substack{\hat{c}_n \neq 0, \\ n \neq 0, n \in \mathbb{Z}_N^d}} \frac{|\hat{c}_n|^2 (f_o + \gamma_f \hat{q}_n)}{\Theta_n}.$$

Similarly, (7.24) reduces to

$$\|H_{\mathcal{Q}}\|_{\mathcal{H}_2}^2 = \frac{d}{2} \sum_{\substack{\hat{c}_n \neq 0, \\ n \neq 0, n \in \mathbb{Z}_N^d}} \frac{|\hat{c}_n|^2}{(g_o + \gamma_g \hat{q}_n)(f_o + \gamma_f \hat{q}_n)}.$$

Finally the inequality in (7.25) leads to

$$\frac{|\hat{c}_n|^2 (f_o + \gamma_f \hat{q}_n)}{\Theta_n} \leq \frac{|\hat{c}_n|^2}{(g_o + \gamma_g \hat{q}_n)(f_o + \gamma_f \hat{q}_n)}, \tag{7.27}$$

for all $n \neq 0, n \in \mathbb{Z}_N^d$ such that $\hat{c}_n \neq 0$. Summation over such n yields the first result. If $\gamma_g = 0$, equality holds in (7.27) due to (7.26). This leads to the second result. □

Lemma 7.3 provides a sufficient condition under which uni-directional feedback performs at least as well as symmetric bi-directional feedback in finite spatial dimension, for any circulant output operator $\mathcal{C}$ (satisfying (A1) and (A2)). Although achieving equal or better performance with a smaller number of relative state measurements is counterintuitive, this is possible through well tuned gains, for example using those that satisfy the inequality (7.25) in Lemma 7.3. However, in certain instances uni-directional feedback cannot perform better than symmetric bi-directional feedback, e.g. if the sign of this inequality is reversed. It must be emphasized that with appropriate gain selection, uni-directional feedback can be preferable due to only requiring single directional sensing.

We next employ this result to establish upper bounds on P_{loc} and P_{dav}, which we then invoke to specify how the performance scales with the network size M. The asymptotic scalings of the performance metrics for the systems with uni-directional feedback are summarized in Table 7-I.

Theorem 7.1. *Consider the system with uni-directional feedback, namely $H_{\mathcal{R}}$. Then, the upper bounds on the performance metrics have the following asymptotic scalings in finite spatial dimension d as $N \to \infty$.*

1. Suppose that absolute velocity feedback is present, i.e. $f_o > 0$. Then for $\gamma_f > 0$ and $f_o \geq \frac{\gamma_g}{\gamma_f}$,

(a) Absolute Position and Absolute Velocity Feedback

$$\begin{aligned} P_{loc} &\sim \frac{1}{\max\{\gamma_g, \gamma_f\}}, \\ P_{dav} &\sim 1, \end{aligned}$$

(b) Relative Position and Absolute Velocity Feedback

$$\begin{aligned} P_{loc} &\sim 1/\gamma_g, \\ P_{dav} &\sim \frac{1}{\gamma_g} \begin{cases} M & d = 1 \\ \ln(M) & d = 2 \\ 1 & d \geq 3 \end{cases}. \end{aligned}$$

2. Absolute (but no relative) Position ($g_o > 0$ and $\gamma_g = 0$) and Relative Velocity Feedback

$$\begin{aligned} P_{loc} &\sim 1/\gamma_f, \\ P_{dav} &\sim \frac{1}{\gamma_f} \begin{cases} M & d = 1 \\ \ln(M) & d = 2 \\ 1 & d \geq 3 \end{cases}. \end{aligned}$$

Here the quantities are given up to a multiplicative factor that is independent of M, γ_g or γ_f.

Proof. It is shown in [1] that the upper bounds given above hold for $H_{\mathcal{Q}}$, i.e. the system with symmetric bi-directional feedback given by (7.7). We start by proving the first result. Recall from the proof of Lemma 7.1 that $\hat{c}_n \neq 0$ for all $n \neq 0$ in the case of P_{loc} and P_{dav}. Therefore, we invoke the first result of Lemma 7.3 for all $n \neq 0$. By assumption $f_o \geq \frac{\gamma_g}{\gamma_f}$, which implies that (7.25) is satisfied for all $n \neq 0, n \in \mathbb{Z}_N^d$ because the sum term is positive for such n. This yields $\|H_{\mathcal{R}}\|_{\mathcal{H}_2}^2 \leq \|H_{\mathcal{Q}}\|_{\mathcal{H}_2}^2$, so the upper bounds on P_{loc} and P_{dav} also hold for $H_{\mathcal{R}}$. The second result follows from a similar argument and the second result of Lemma 7.3, since $\|H_{\mathcal{R}}\|_{\mathcal{H}_2}^2 = \|H_{\mathcal{Q}}\|_{\mathcal{H}_2}^2$ if $\gamma_g = 0$. □

Remark 7.3. *In the absence of absolute velocity feedback, i.e. if $f_o = 0$, satisfying (7.25) for given $\gamma_g > 0$ and large wavenumbers n requires that $\gamma_f \to \infty$ as $N \to \infty$. In this case, the scaling laws of Theorem 7.1 do not necessarily hold.*

As we demonstrate next for the system with uni-directional feedback, lack of absolute velocity measurements in systems with relative position and velocity feedback leads to instability (i.e. infinite $\mathcal{H}_2$ norm) in an arbitrarily large network connected over a multi-dimensional torus.

Theorem 7.2. *Consider the system with uni-directional feedback, namely $H_{\mathcal{R}}$ and the performance metrics P_{loc} and P_{dav}. Suppose that $f_o = 0$ and $\gamma_g > 0$, i.e. the system either has*

1. *Absolute (with relative) Position and Relative Velocity Feedback, or*

2. *Relative Position and Relative Velocity Feedback.*

In finite spatial dimension d, if g_o, γ_g and γ_f are finite, then there exists a finite $\bar{N} > 0$ such that for all $N > \bar{N}$, $H_{\mathcal{R}}$ is unstable, i.e. does not have a finite $\mathcal{H}_2$ norm.

Proof. For absolute (with relative) position and relative velocity feedback, using (7.10)

one can write (7.26) as

$$\Theta_n = g_o\gamma_f^2\left(\sum_{i=1}^{d} 1-\cos\frac{2\pi}{N}n_i\right)^2+\gamma_g\gamma_f^2\left(\sum_{i=1}^{d} 1-\cos\frac{2\pi}{N}n_i\right)^3$$
$$+\gamma_g\left(\sum_{i=1}^{d}\sin\frac{2\pi}{N}n_i\right)^2\left[\gamma_f^2\left(\sum_{i=1}^{d} 1-\cos\frac{2\pi}{N}n_i\right)-\gamma_g\right]. \tag{7.28}$$

Consider the wavenumber $n = (N-1,\ldots,N-1)$. Then $\frac{2\pi}{N}n_i \nearrow 2\pi$ as $N\to\infty$. Therefore, if we approximate $\cos(\cdot)$ and $\sin(\cdot)$ around 2π using the first three terms in the Taylor series expansion, we obtain

$$\cos(2\pi-\delta)\approx 1-\frac{\delta^2}{2} \quad \text{and} \quad \sin(2\pi-\delta)\approx -\delta, \quad \delta>0.$$

Using these expressions one can re-write $\Theta_{(N-1,\ldots,N-1)}$ as

$$\Theta_{(N-1,\ldots,N-1)}\approx\frac{\gamma_g\gamma_f^2 d^3}{8}\delta^6+\gamma_f^2 d^2(\frac{g_o}{4}+\frac{\gamma_g d}{2})\delta^4-\gamma_g^2 d^2\delta^2.$$

As $N\to\infty$, $\delta\searrow 0$ which leads to

$$\Theta_{(N-1,\ldots,N-1)}\approx -O(\delta^2).$$

Thus for any finite g_o, γ_g and γ_f, there exists a finite $\bar{N}>0$ such that for all $N>\bar{N}$, it holds that $\Theta_{(N-1,\ldots,N-1)}<0$, i.e. the second inequality in (7.19) is violated for $n=(N-1,\ldots,N-1)$. Then by Lemma 7.1 $H_{\mathcal{R}}$ is unstable, i.e. does not have a finite $\mathcal{H}_2$ norm. For relative position and velocity feedback, we have $g_o=0$ and the same argument holds. □

Remark 7.4. *Due to Proposition 7.3, we note that the proof of Theorem 7.2 holds for any output of the form (7.13) such that $\hat{c}_{(N-1,\ldots,N-1)}\neq 0$, i.e. the modes which become unstable as the network size grows are observable from the output.*

Systems with double-integrator [84] or more general linear dynamics [85–87], which have directed relative feedback defined over the 1-dimensional torus, have been shown to exhibit similar instability behavior. While our result provides a generalization to

the case of uni-directional feedback over a multi-dimensional torus, a similar result appeared for directed bi-directional multi-neighbor interactions over the same lattice structure [88].

Theorem 7.2 highlights the limitation of uni-directional relative feedback. If relative position feedback is used, it is not possible to find a set of finite control gains that stabilizes arbitrarily large networks in any finite number of spatial dimension unless the agents have access to their absolute velocity. However, networks with uni-directional relative feedback can not only be stabilized but also provide the same performance scaling as that of the symmetric bi-directional feedback using at least one type (position or velocity) of absolute state information, as stated in Theorem 7.1. Namely, either by adding absolute velocity feedback to the cases with relative position feedback, or by eliminating relative position feedback given that absolute position measurements are available. While uni-directional feedback can lead to instability in arbitrarily large networks without absolute state information, access to it in position or velocity combined with well-tuned gains can lead to a favorable scheme, since the same performance scaling can be achieved with reduced sensing/communication requirements.

The next section provides numerical examples that illustrate the results in theorems 7.1 and 7.2.

7.3 Numerical Examples

In this section, we provide two numerical examples that confirm the theory presented in the previous section. The first one shows the performance scalings in the case of relative position and absolute velocity feedback. The second one demonstrates that stability is lost for finite network size if uni-directional relative position feedback is used in the absence of absolute velocity feedback.

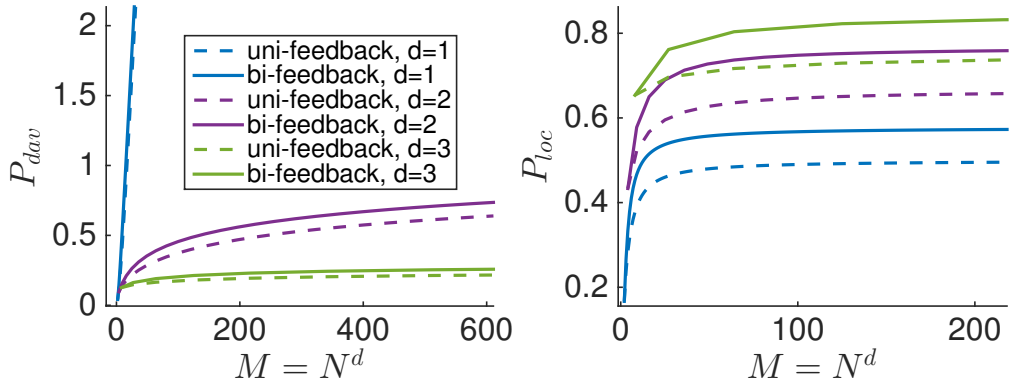

Figure 7-1. P_{dav} and P_{loc} as a function of the network size M for relative position and absolute velocity feedback ($g_o = 0$, $f_o = 1$, $\gamma_g = 1$ and $\gamma_f = 1$). Performance scales as the laws given in Theorem 7.1.

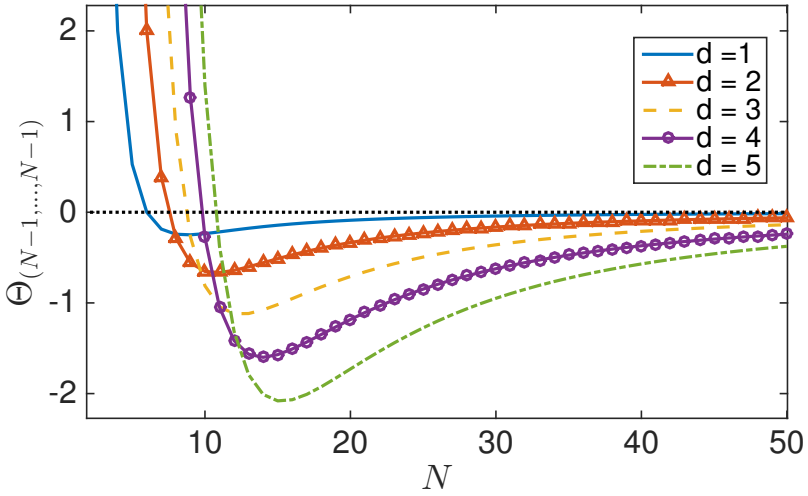

Figure 7-2. With uni-directional relative position and velocity, but no absolute velocity feedback ($g_o = 1$, $f_o = 0$, $\gamma_g = 1$ and $\gamma_f = 1$), Θ_n in (7.28) cannot remain positive for $n = (N-1, \ldots, N-1)$ and finite N, which leads to instability due to Proposition 7.3.

In Figure 7-1, performance metrics P_{loc} and P_{dav} are plotted as a function of the network size M. For relative position and absolute velocity feedback with the gains $f_o = 1$ and $\gamma_g = \gamma_f = 1$, the performance scaling obeys the laws presented in Theorem 7.1. It is also observed that the uni-directional feedback provides better performance compared to that of the symmetric bi-directional feedback, which is expected based on the result of Lemma 7.3, i.e. since the control gains strictly satisfy the inequality in (7.25).

We also confirm the result of Theorem 7.2 by plotting Θ_n in (7.28) for $n = (N-1, \ldots, N-1)$ as a function of N with uni-directional relative feedback and no absolute velocity information (i.e. $f_o = 0$) in Figure 7-2. Specifically, for absolute (with relative) position and relative velocity feedback with the gains $g_o = 1$ and $\gamma_g = \gamma_f = 1$ and spatial dimensions $d = 1, \ldots, 5$, $\Theta_{(N-1,\ldots,N-1)}$ cannot remain positive as N is increased. This leads to instability for finite N due to Proposition 7.3. As expected, $\Theta_{(N-1,\ldots,N-1)}$ goes to zero as $N \to \infty$.

7.4 Summarizing Remarks

We have studied the asymptotic scaling of local and global metrics of disorder in a large-scale directed network defined over a multi-dimensional torus. We have considered absolute as well as relative uni-directional state measurements. Our main results show that absolute state information plays a critical role in the performance and the stability of large-scale networks if the relative state measurements are uni-directional. Additionally a well-tuned uni-directional feedback structure can provide the same performance scaling with network size as the symmetric bi-directional feedback, with the advantage of requiring less sensing/communication. As a direction of future work, we will consider the performance scaling of bi-directional interactions with non-equal weights (a directed feedback structure), which has been shown to improve the transient behavior [90] but degrade string stability [87] in vehicle platoons.

Chapter 8

Conclusion and Directions for Future Work

In this chapter, we provide our concluding remarks and directions for future work.

Our results on inverter-based power systems evaluate the role of heterogeneous inverter ratings in system performance in terms of the frequency and voltage variances and the transient resistive power losses that result from maintaining the system equilibrium in the face of disturbances. This system heterogeneity, which can arise due to a non-uniform power demand from the inverters, may lead to performance limitations (in terms of the transient resistive power losses).

We have developed a novel analysis framework in order to evaluate the performance of directed networks. Using this framework, we have investigated the role of the interconnection directionality and the degree of connectivity in network performance. We have also derived the asymptotic behavior of performance metrics that quantify network disorder for large-scale spatially invariant systems with uni-directional feedback.

For the class of systems that emit normal weighted Laplacian matrices, which include spatially invariant systems, our results demonstrate the interplay between the interconnection directionality and control strategy that determines the network performance. In this setting, interconnection graphs of single-integrator networks

can be designed to be directed or undirected (symmetrized version of the directed graph) without any change in performance. However, this is in contrast to the performance of double-integrator networks, which can significantly degrade due to interconnection directionality (compared to the symmetrized topology). In certain cases, this directionality can be utilized to mitigate this degradation or exceed the performance of the symmetrized network, depending on the type of state feedback (e.g. absolute and/or relative measurements of position and/or velocity) used and tuning of control gains. The trade-off between communication cost and scalability in spatially invariant double-integrator networks, which arises due to uni-directional feedback, also indicates the importance of judicious feedback design in directed networks.

We have also demonstrated the non-monotonic relationship between the degree of connectivity in directed and cyclic ω-nearest neighbor networks (a spatially invariant topology) and their performance quantified in terms of the aggregate state deviation from the network average. For a common communication cost (total weighted out-degree of nodes is equal to the network size), increasing the number of uni-directional edges does not necessarily improve performance. In addition, we have shown that all-to-one (imploding star graph) and all-to-all (complete graph) networks with a common communication cost provide identical performance for the same metric. These results suggest that performance is determined by not only the degree of connectivity, but also the underlying communication topology.

Prior to concluding this thesis, we discuss extensions of our results and provide directions for future work.

8.1 Heterogeneity in Microgrids with Coupled Frequency and Voltage

In order to understand the performance trade-offs associated with physical constraints that lead to system heterogeneity (such as a non-uniform power sharing requirement

among the inverters), we relaxed the common assumption of homogeneous droop control gains. In this setting, we assumed a decoupling between frequency and voltage dynamics (equivalently, a small resistance-to-reactance ratio of lines), which reduces the complexity of the analysis. This leads to a 'zeroth order' approximation of the computed performance metrics, which provides insights on the role of heterogeneity. As a direction for future work, our analysis can be extended to the case of coupled frequency and voltage dynamics. In the case of homogeneous inverter ratings, a perturbation analysis shows the dependence of the approximation error in transient resistive losses on the resistance-to-reactance ratio [51]. Similar analysis can be used to extend our results that evaluate system heterogeneity in microgrids.

8.2 Extension of the Results on the Performance of Directed Networks

Our closed-form solutions, which are obtained for networks defined over arbitrary directed graphs with at least one globally reachable node, can be used to further analyze the effect of network topological characteristics on performance. A direction for future work is to investigate interconnection topologies that emit non-diagonalizable weighted graph Laplacian matrices. For a class of weighted directed graphs that are composed of a collection of paths and cycles, the algebraic structure of the adjacency matrix such as the Jordan canonical form and its associated generalized eigenvectors can be derived in closed-form [91]. For this class of graphs, evaluating the relationship between network structure (characterized in terms of the number and size of Laplacian Jordan blocks) and performance remains as an open question to be addressed using our closed-form solutions.

8.3 Generalization of the Scaling Bounds from Chapter 7

We now revisit systems with double-integrator dynamics that are interconnected over the d-dimensional torus $\mathbb{Z}_N^d$ and discuss possible generalizations of the asymptotic scaling of bounds on the performance metrics that are presented in Chapter 7. As given by (7.5), relative position and velocity feedback laws are respectively defined by the circular convolution operators $\mathcal{G}$ and $\mathcal{F}$. The uni-directional feedback policy which is given by (7.8) and (7.9) can be generalized to a policy that permits each agent to have access to relative state measurements with respect to a bounded number of neighbors. In other words, the feedback operators $\mathcal{G}$ and $\mathcal{F}$ satisfy the locality property [43]

$$G_k = 0 \quad \text{for} \quad |k_i| > q, \quad i \in \{1, \dots, d\}. \tag{8.1}$$

In this setting, the feedback interconnections of both the position and the velocity states can have directionality.

Similar to Chapter 7, we consider performance metrics that quantify network disorder. We use the same metric P_{dav}, which quantifies the state deviation from the network average and is given by the output operator (7.18), in order to capture the global degree of disorder. However, in order to evaluate the local degree of disorder, we can consider a class of metrics that generalizes the metric that quantifies the state deviation of each agent with respect to its predecessor, which is given by the output operator (7.15). Imposing the locality property in (8.1) on the output operator $\mathcal{C}$ leads to a performance output that is defined by a weighted sum of states of each agent and a bounded number of its neighbors

$$y_k = \sum_{\substack{l \in \mathbb{Z}_N^d, \\ |l_i| \leq q, \ i \in \{1, \dots, d\}}} c_{k-l} x_l. \tag{8.2}$$

The metric of local disorder for each agent at location k is then given by

$$P_{loc} = \lim_{t\to\infty} E\left\{\sum_{i=1}^{d} (y_k)_i^*(y_k)_i\right\}. \tag{8.3}$$

In addition to metrics in (7.13) which are position-based, we can also consider velocity-based metrics

$$y = \begin{bmatrix}\mathcal{O} & \mathcal{C}\end{bmatrix}\begin{bmatrix}x\\ v\end{bmatrix}. \tag{8.4}$$

We now present conjectures on how performance metrics P_{dav} and P_{loc} scale asymptotically, for respective position and velocity-based outputs (7.13) and (8.4).

Conjecture 8.1. *Consider the position-based performance output (7.13). Suppose that directed feedback operators $\mathcal{G}$ and $\mathcal{F}$ satisfy the locality property in (8.1). Then as $N \to \infty$, the upper and lower bounds on performance scale asymptotically as*

1. Suppose that absolute velocity feedback is present, i.e. $f_o > 0$.

(a) Absolute Position and Absolute Velocity Feedback

$$P_{loc} \sim 1,$$

$$P_{dav} \sim 1,$$

(b) Relative Position and Absolute Velocity Feedback

$$P_{loc} \sim 1,$$

$$P_{dav} \sim \begin{cases} M & d = 1 \\ \ln(M) & d = 2 \\ 1 & d \geq 3 \end{cases}.$$

2. Absolute (but no relative) Position ($g_o > 0$ and $\gamma_g = 0$) and Relative Velocity Feedback

$$P_{loc} \sim 1,$$

$$P_{dav} \sim \begin{cases} M & d = 1 \\ \ln(M) & d = 2 \\ 1 & d \geq 3 \end{cases}.$$

Here the quantities are given up to a multiplicative factor that is independent of M.

We now present the conjecture on the asymptotic scaling of velocity-based performance metrics.

Conjecture 8.2. *Consider the velocity-based performance output (8.4). Suppose that directed feedback operators $\mathcal{G}$ and $\mathcal{F}$ satisfy the locality property in (8.1). Then as $N \to \infty$, the upper and lower bounds on performance scale asymptotically as*

1. Suppose that absolute velocity feedback is present, i.e. $f_o > 0$.

(a) Absolute Position and Absolute Velocity Feedback

$$P_{loc} \sim 1,$$
$$P_{dav} \sim 1,$$

(b) Relative Position and Absolute Velocity Feedback

$$P_{loc} \sim 1,$$
$$P_{dav} \sim 1.$$

2. Absolute (but no relative) Position ($g_o > 0$ and $\gamma_g = 0$) and Relative Velocity Feedback

$$P_{loc} \sim 1,$$
$$P_{dav} \sim \begin{cases} M & d = 1 \\ \ln(M) & d = 2 \\ 1 & d \geq 3 \end{cases}.$$

Here the quantities are given up to a multiplicative factor that is independent of M.

The preliminary results in conjectures 8.1 and 8.2 can be respectively summarized in tables 8-I and 8-II. We note that when the performance output is position-based, the same asymptotic scaling of bounds on both local and global degrees of disorder

in networks with uni-directional feedback, which are given in Theorem 7.1, hold for more general directed feedback operators that satisfy the locality property in (8.1). Comparing the position and velocity-based performance metrics shows that their asymptotic behavior differs only in the case of global disorder P_{dav} and relative position and absolute velocity feedback. This feedback strategy can uniformly bound the asymptotic scaling of global network disorder in terms of the velocity states. We do not consider the cases of absolute (with relative) position and relative velocity feedback and relative position and relative velocity feedback; as directed interconnections over toric lattices lead to instability with these feedback strategies for sufficiently large but finite network size [88].

Table 8-I. In systems with directed feedback, asymptotic scalings of upper and lower bounds on position-based performance metrics with respect to network size M in finite spatial dimension d. Quantities are up to a multiplicative factor that is independent of M.

	P_{loc}	P_{dav}
abs. pos. & abs. vel.	1	1
rel. pos. & abs. vel.	1	M $d=1$ $\ln(M)$ $d=2$ 1 $d\geq 3$
abs. pos. & rel. vel. ($\gamma_g = 0$)	1	M $d=1$ $\ln(M)$ $d=2$ 1 $d\geq 3$

Table 8-II. In systems with directed feedback, asymptotic scalings of upper and lower bounds on velocity-based performance metrics with respect to network size M in finite spatial dimension d. Quantities are up to a multiplicative factor that is independent of M.

	P_{loc}	P_{dav}
abs. pos. & abs. vel.	1	1
rel. pos. & abs. vel.	1	1
abs. pos. & rel. vel. ($\gamma_g = 0$)	1	M $d=1$ $\ln(M)$ $d=2$ 1 $d\geq 3$

References

[1] B. Bamieh, M. R. Jovanović, P. Mitra, and S. Patterson, "Coherence in large-scale networks: Dimension-dependent limitations of local feedback," *IEEE Trans. Autom. Control*, vol. 57, no. 9, pp. 2235–2249, Sep. 2012.

[2] F. Dörfler, M. Chertkov, and F. Bullo, "Synchronization in complex oscillator networks and smart grids," *Proceedings of the National Academy of Sciences*, vol. 110, no. 6, pp. 2005–2010, 2013.

[3] M. H. Degroot, "Reaching a consensus," *Journal of the American Statistical Association*, vol. 69, no. 345, pp. 118–121, 1974.

[4] A. R. Bergen and D. J. Hill, "A structure preserving model for power system stability analysis," *IEEE Transactions on Power Apparatus and Systems*, vol. PAS-100, no. 1, pp. 25–35, 1981.

[5] L. Moreau, "Stability of continuous-time distributed consensus algorithms," in *2004 43rd IEEE Conference on Decision and Control (CDC)*, vol. 4, 2004, pp. 3998–4003 Vol.4.

[6] R. Olfati-Saber and R. M. Murray, "Consensus protocols for networks of dynamic agents," in *Proceedings of the 2003 American Control Conference, 2003.*, vol. 2, 2003, pp. 951–956.

[7] W. Ren and E. Atkins, "Second-order consensus protocols in multiple vehicle systems with local interactions," in *AIAA Guidance, Navigation, and Control Conf. and Exhibit*, Aug. 2005, pp. 6238–6251.

[8] W. Ren and R. W. Beard, "Consensus seeking in multiagent systems under dynamically changing interaction topologies," *IEEE Transactions on Automatic Control*, vol. 50, no. 5, pp. 655–661, 2005.

[9] J. Zhu, Y. Tian, and J. Kuang, "On the general consensus protocol of multi-agent systems with double-integrator dynamics," *Linear Algebra Appl.*, vol. 431, no. 5, pp. 701–715, 2009.

[10] W. Yu, G. Chen, and M. Cao, "Some necessary and sufficient conditions for second-order consensus in multi-agent dynamical systems," *Automatica*, vol. 46, no. 6, pp. 1089–1095, 2010.

[11] F. Dörfler and F. Bullo, "Synchronization and transient stability in power networks and nonuniform kuramoto oscillators," *SIAM Journal on Control and Optimization*, vol. 50, no. 3, pp. 1616–1642, 2012.

[12] J. W. Simpson-Porco, F. Dörfler, and F. Bullo, "Synchronization and power sharing for droop-controlled inverters in islanded microgrids," *Automatica*, vol. 49, no. 9, pp. 2603 – 2611, 2013.

[13] N. E. Leonard and E. Fiorelli, "Virtual leaders, artificial potentials and coordinated control of groups," in *Proceedings of the 40th IEEE Conference on Decision and Control*, vol. 3, 2001, pp. 2968–2973 vol.3.

[14] H. G. Tanner, A. Jadbabaie, and G. J. Pappas, "Stable flocking of mobile agents, part i: fixed topology," in *42nd IEEE International Conference on Decision and Control*, vol. 2, 2003, pp. 2010–2015 Vol.2.

[15] ——, "Stable flocking of mobile agents part ii: dynamic topology," in *42nd IEEE International Conference on Decision and Control*, vol. 2, 2003, pp. 2016–2021 Vol.2.

[16] ——, "Flocking in fixed and switching networks," *IEEE Transactions on Automatic Control*, vol. 52, no. 5, pp. 863–868, 2007.

[17] Z. Lin, B. Francis, and M. Maggiore, "Necessary and sufficient graphical conditions for formation control of unicycles," *IEEE Transactions on Automatic Control*, vol. 50, no. 1, pp. 121–127, 2005.

[18] R. Olfati-Saber, "Flocking for multi-agent dynamic systems: algorithms and theory," *IEEE Transactions on Automatic Control*, vol. 51, no. 3, pp. 401–420, 2006.

[19] J. Schiffer, R. Ortega, A. Astolfi, J. Raisch, and T. Sezi, "Conditions for stability of droop-controlled inverter-based microgrids," *Automatica*, vol. 50, no. 10, pp. 2457 – 2469, 2014.

[20] B. Gentile, J. W. Simpson-Porco, F. Dörfler, S. Zampieri, and F. Bullo, "On reactive power flow and voltage stability in microgrids," in *2014 American Control Conference*, 2014, pp. 759–764.

[21] J. Schiffer, T. Seel, J. Raisch, and T. Sezi, "Voltage stability and reactive power sharing in inverter-based microgrids with consensus-based distributed voltage control," *IEEE Transactions on Control Systems Technology*, vol. 24, no. 1, pp. 96–109, 2016.

[22] T. Vicsek, A. Czirók, E. Ben-Jacob, I. Cohen, and O. Shochet, "Novel type of phase transition in a system of self-driven particles," *Phys. Rev. Lett.*, vol. 75, pp. 1226–1229, Aug 1995.

[23] L. Moreau, "Leaderless coordination via bidirectional and unidirectional time-dependent communication," in *42nd IEEE International Conference on Decision and Control*, vol. 3, 2003, pp. 3070–3075 Vol.3.

[24] A. Jadbabaie, Jie Lin, and A. S. Morse, "Coordination of groups of mobile autonomous agents using nearest neighbor rules," *IEEE Transactions on Automatic Control*, vol. 48, no. 6, pp. 988–1001, 2003.

[25] J. A. Fax and R. M. Murray, "Information flow and cooperative control of vehicle formations," *IEEE Transactions on Automatic Control*, vol. 49, no. 9, pp. 1465–1476, 2004.

[26] R. Olfati-Saber, J. A. Fax, and R. M. Murray, "Consensus and cooperation in networked multi-agent systems," *Proceedings of the IEEE*, vol. 95, no. 1, pp. 215–233, 2007.

[27] M. C. Chandorkar, D. M. Divan, and R. Adapa, "Control of parallel connected inverters in standalone ac supply systems," *IEEE Transactions on Industry Applications*, vol. 29, no. 1, pp. 136–143, 1993.

[28] K. De Brabandere, B. Bolsens, J. Van den Keybus, A. Woyte, J. Driesen, and R. Belmans, "A voltage and frequency droop control method for parallel inverters," *IEEE Transactions on Power Electronics*, vol. 22, no. 4, pp. 1107–1115, 2007.

[29] P. Vorobev, P. Huang, M. Al Hosani, J. L. Kirtley, and K. Turitsyn, "A framework for development of universal rules for microgrids stability and control," in *2017 IEEE 56th Annual Conference on Decision and Control (CDC)*, 2017, pp. 5125–5130.

[30] K. K. Oh, M. C. Park, and H. S. Ahn, "A survey of multi-agent formation control," *Automatica*, vol. 53, pp. 424 – 440, 2015.

[31] A. Arenas, A. Díaz-Guilera, J. Kurths, Y. Moreno, and C. Zhou, "Synchronization in complex networks," *Physics Reports*, vol. 469, no. 3, pp. 93 – 153, 2008.

[32] F. Dörfler and F. Bullo, "Synchronization in complex networks of phase oscillators: A survey," *Automatica*, vol. 50, no. 6, pp. 1539 – 1564, 2014.

[33] J. C. Doyle, K. Glover, P. P. Khargonekar, and B. A. Francis, "State-space solutions to standard h_2 and h_∞ control problems," *IEEE Transactions on Automatic Control*, vol. 34, no. 8, pp. 831–847, 1989.

[34] B. A. Francis and J. C. Doyle, "Linear control theory with an h_∞ optimality criterion," *SIAM Journal on Control and Optimization*, vol. 25, no. 4, pp. 815–844, 1987.

[35] M. Siami and N. Motee, "Fundamental limits and tradeoffs on disturbance propagation in linear dynamical networks," *IEEE Trans. Autom. Control*, vol. 61, no. 12, pp. 4055–4062, Dec. 2016.

[36] G. F. Young, L. Scardovi, and N. E. Leonard, "Robustness of noisy consensus dynamics with directed communication," in *Proc. of the American Ctrl. Conf.*, Jun. 2010, pp. 6312–6317.

[37] S. Dezfulian, Y. Ghaedsharaf, and N. Motee, "On performance of time-delay linear consensus networks with directed interconnection topologies," in *Proc. of the American Ctrl. Conf.*, Jun. 2018.

[38] T. Sarkar, M. Roozbehani, and M. A. Dahleh, "Asymptotic robustness in consensus networks," in *2018 Annual American Control Conference (ACC)*, June 2018, pp. 6212–6217.

[39] X. Ma and N. Elia, "Mean square performance and robust yet fragile nature of torus networked average consensus," *IEEE Trans. on Ctrl. of Network Systems*, vol. 2, no. 3, pp. 216–225, Sep. 2015.

[40] F. Lin, M. Fardad, and M. R. Jovanović, "Performance of leader-follower networks in directed trees and lattices," in *in Proc. of the 51st IEEE Conf. on Dec. and Ctrl.*, Dec. 2012, pp. 734–739.

[41] F. Lin, "Performance of leader–follower multi-agent systems in directed networks," *Systems and Control Letters*, vol. 113, pp. 52 – 58, 2018.

[42] T. W. Grunberg and D. F. Gayme, "Performance measures for linear oscillator networks over arbitrary graphs," *IEEE Trans. on Ctrl. of Network Systems*, vol. 5, no. 1, pp. 456–468, Mar. 2018.

[43] E. Tegling, P. Mitra, H. Sandberg, and B. Bamieh, "On fundamental limitations of dynamic feedback control in regular large-scale networks," *IEEE Transactions on Automatic Control*, Apr. 2019, doi: 10.1109/TAC.2019.2909811.

[44] R. Pates, C. Lidström, and A. Rantzer, "Control using local distance measurements cannot prevent incoherence in platoons," in *In Proc. of the 56th IEEE Conf. on Dec. and Ctrl.*, Dec. 2017, pp. 3461–3466.

[45] H. Hao and P. Barooah, "Stability and robustness of large platoons of vehicles with double-integrator models and nearest neighbor interaction," *International Journal of Robust and Nonlinear Control*, vol. 23, no. 18, pp. 2097–2122, Dec. 2013.

[46] F. Lin, M. Fardad, and M. R. Jovanović, "Optimal control of vehicular formations with nearest neighbor interactions," *IEEE Trans. Autom. Control*, vol. 57, no. 9, pp. 2203–2218, Sep. 2012.

[47] H. G. Oral, E. Mallada, and D. F. Gayme, "Performance of first and second order linear networked systems over digraphs," in *Proc. of the 56th IEEE Conf. on Dec. and Ctrl.*, Dec. 2017, pp. 1688–1694.

[48] E. Tegling and H. Sandberg, "On the coherence of large-scale networks with distributed pi and pd control," *IEEE Ctrl. Systems Lett.*, vol. 1, no. 1, pp. 170–175, Jul. 2017.

[49] B. Bamieh and D. F. Gayme, "The price of synchrony: Resistive losses due to phase synchronization in power networks," in *Proc. of the American Ctrl. Conf.*, Jun. 2013, pp. 5815–5820.

[50] E. Tegling, B. Bamieh, and D. F. Gayme, "The price of synchrony: Evaluating the resistive losses in synchronizing power networks," *IEEE Transactions on Control of Network Systems*, vol. 2, no. 3, pp. 254–266, Sep. 2015.

[51] E. Tegling, D. F. Gayme, and H. Sandberg, "Performance metrics for droop-controlled microgrids with variable voltage dynamics," in *Proc. of the 54th IEEE Conf. on Dec. and Ctrl.*, Dec. 2015, pp. 7502–7509.

[52] E. Mallada, "iDroop: A dynamic droop controller to decouple power grid's steady-state and dynamic performance," in *55th IEEE Conference on Decision and Control (CDC)*, Dec. 2016, pp. 4957–4964.

[53] Y. Jiang, R. Pates, and E. Mallada, "Performance tradeoffs of dynamically controlled grid-connected inverters in low inertia power systems," in *56th IEEE Conference on Decision and Control (CDC)*, Dec. 2017, pp. 5098–5105.

[54] E. Weitenberg, Y. Jiang, C. Zhao, E. Mallada, C. De Persis, and F. Dörfler, "Robust decentralized secondary frequency control in power systems: Merits and trade-offs," *IEEE Transactions on Automatic Control*, Dec. 2018, doi: 10.1109/TAC.2018.2884650.

[55] X. Wu, F. Dörfler, and M. R. Jovanović, "Input-output analysis and decentralized optimal control of inter-area oscillations in power systems," *IEEE Transactions on Power Systems*, vol. 31, no. 3, pp. 2434–2444, May 2016.

[56] J. W. Simpson-Porco, B. K. Poolla, N. Monshizadeh, and F. Dörfler, "Quadratic performance of primal-dual methods with application to secondary frequency control of power systems," in *2016 IEEE 55th Conference on Decision and Control (CDC)*, Dec 2016, pp. 1840–1845.

[57] H. G. Oral and D. F. Gayme, "Performance of droop-controlled microgrids with heterogeneous inverter ratings," in *Proc. of the European Ctrl. Conf.*, Jun. 2019, pp. 1398–1405.

[58] M. Pirani, J. W. Simpson-Porco, and B. Fidan, "System-theoretic performance metrics for low-inertia stability of power networks," in *2017 IEEE 56th Annual Conference on Decision and Control (CDC)*, 2017, pp. 5106–5111.

[59] F. Paganini and E. Mallada, "Global performance metrics for synchronization of heterogeneously rated power systems: The role of machine models and inertia," in *2017 55th Annual Allerton Conference on Communication, Control, and Computing (Allerton)*, Oct 2017, pp. 324–331.

[60] ——, "Global analysis of synchronization performance for power systems: bridging the theory-practice gap," *arXiv preprint*, May 2019, arXiv:1905.06948.

[61] E. Sjödin and D. Gayme, "Transient losses in synchronizing renewable energy integrated power networks," in *Proc. of the American Ctrl. Conf.*, Jun. 2014, pp. 5217–5223.

[62] T. W. Grunberg and D. F. Gayme, "Minimizing interactions in mixed oscillator networks," in *53rd IEEE Conference on Decision and Control*, 2014, pp. 3209–3215.

[63] B. K. Poolla, S. Bolognani, and F. Dörfler, "Optimal placement of virtual inertia in power grids," *IEEE Transactions on Automatic Control*, vol. 62, no. 12, pp. 6209–6220, 2017.

[64] E. Tegling, M. Andreasson, J. W. Simpson-Porco, and H. Sandberg, "Improving performance of droop-controlled microgrids through distributed pi-control," in *2016 American Control Conference (ACC)*, 2016, pp. 2321–2327.

[65] Y. Jiang, R. Pates, and E. Mallada, "Dynamic droop control in low-inertia power systems," *arXiv preprint*, Aug. 2019, arXiv:1908.10983.

[66] L. Guo, C. Zhao, and S. H. Low, "Graph laplacian spectrum and primary frequency regulation," in *2018 IEEE Conference on Decision and Control (CDC)*, 2018, pp. 158–165.

[67] M. Tyloo and P. Jacquod, "Global robustness versus local vulnerabilities in complex synchronous networks," *Phys. Rev. E*, vol. 100, p. 032303, Sep. 2019.

[68] S. Patterson, Y. Yi, and Z. Zhang, "A resistance-distance-based approach for optimal leader selection in noisy consensus networks," *IEEE Transactions on Control of Network Systems*, vol. 6, no. 1, pp. 191–201, March 2019.

[69] W. Ellens, F. M. Spieksma, P. V. Mieghem, A. Jamakovic, and R. E. Kooij, "Effective graph resistance," *Linear Algebra Appl.*, vol. 435, no. 10, pp. 2491–2506, Nov. 2011.

[70] H. G. Oral and D. F. Gayme, "Disorder in large-scale networks with uni-directional feedback," in *Proc. of the American Ctrl. Conf.*, Jul. 2019, pp. 3394–3401.

[71] M. Siami and N. Motee, "New spectral bounds on h2-norm of linear dynamical networks," *Automatica*, vol. 80, pp. 305–312, Jun. 2017.

[72] G. F. Young, L. Scardovi, and N. E. Leonard, "A new notion of effective resistance for directed graphs– part i: Definition and properties," *IEEE Trans. Autom. Control*, vol. 61, no. 7, pp. 1727–1736, Jul. 2016.

[73] ——, "A new notion of effective resistance for directed graphs– part ii: Computing resistances," *IEEE Trans. Autom. Control*, vol. 61, no. 7, pp. 1737–1752, Jul. 2016.

[74] T. Coletta and P. Jacquod, "Performance measures in electric power networks under line contingencies," *IEEE Transactions on Control of Network Systems*, Apr. 2019, doi: 10.1109/TCNS.2019.2913554.

[75] C. Ji, E. Mallada, and D. F. Gayme, "Evaluating robustness of consensus algorithms under measurement error over digraphs," in *2018 IEEE Conference on Decision and Control (CDC)*, Dec 2018, pp. 1238–1244.

[76] T. Kailath, *Linear Systems*. NJ: Prentice-Hall, 1980.

[77] H. K. Khalil, *Nonlinear Systems*. NJ: Prentice-Hall, 2002.

[78] J. Doyle, B. Francis, and A. Tannenbaum, *Feedback Control Theory*. Macmillan Publishing Co, 1990.

[79] F. Bullo, "Lectures on network systems," *Online at http://motion.me.ucsb.edu/book-lns, with contributions by J. Cortes, F. Dörfler and S. Martinez*, 2016.

[80] F. Dörfler and F. Bullo, "Kron reduction of graphs with applications to electrical networks," *IEEE Transactions on Circuits and Systems I: Regular Papers*, vol. 60, no. 1, pp. 150–163, 2013.

[81] A. E. Motter, S. A. Myers, M. Anghel, and T. Nishikawa, "Spontaneous synchrony in power-grid networks," *Nature Physics*, vol. 9, p. 191–197, 2013.

[82] R. A. Horn and C. R. Johnson, *Matrix Analysis*. Cambridge University Press, 2012.

[83] H. G. Oral, E. Mallada, and D. F. Gayme, "Performance of single and double-integrator networks over directed graphs," *arXiv preprint*, Nov. 2019, arXiv:1911.00791.

[84] C. Cantos, J. Veerman, and D. Hammond, "Signal velocity in oscillator arrays," *Eur. Phys. J. Spec. Top.*, vol. 225, p. 1115–1126, 2016.

[85] I. Herman, D. Martinec, J. Veerman, and M. Sebek, "Stability of a circular system with multiple asymmetric laplacians," *IFAC-PapersOnLine*, vol. 48, no. 22, pp. 162 – 167, 2015, 5th IFAC Workshop on Distributed Estimation and Control in Networked Systems NecSys 2015.

[86] A. A. Peters, R. H. Middleton, and O. Mason, "Cyclic interconnection for formation control of 1-d vehicle strings," *European Journal of Control*, vol. 27, pp. 36 – 44, 2016.

[87] S. Stüdli, M. M. Seron, and R. H. Middleton, "Vehicular platoons in cyclic interconnections," *Automatica*, vol. 94, pp. 283 – 293, 2018.

[88] E. Tegling, "Fundamental limitations of distributed feedback control in large-scale networks," *Ph.D. dissertation, KTH Royal Institute of Technology*, Dec 2018.

[89] B. Bamieh, F. Paganini, and M. A. Dahleh, "Distributed control of spatially invariant systems," *IEEE Transactions on Automatic Control*, vol. 47, no. 7, pp. 1091–1107, 2002.

[90] H. Hao and P. Barooah, "On achieving size-independent stability margin of vehicular lattice formations with distributed control," *IEEE Trans. Autom. Control*, vol. 57, no. 10, pp. 2688–2694, Oct. 2012.

[91] H. Nina, R. L. Soto, and D. M. Cardoso, "The jordan canonical form for a class of weighted directed graphs," *Linear Algebra and its Applications*, vol. 438, no. 1, pp. 261 – 268, 2013.

Biographical Sketch

Hasan Giray Oral received the Ph.D. degree in Mechanical Engineering from the Johns Hopkins University in 2020. Prior to his studies at the Johns Hopkins University, he was with GE Aviation Turkey Technology Center from 2013 to 2014. He earned his B.S. degree from Koc University, Turkey in 2009 and M.S. degrees from Georgia Institute of Technology and the Johns Hopkins University in respectively 2012 and 2019, all in Mechanical Engineering. He graduated with the highest academic record in his mechanical engineering class at Koc University; was a recipient of a Fulbright Scholarship in 2009 for his M.S. studies at Georgia Tech and a Croft Fellowship at Hopkins. His research interests are in control theory and networked dynamical systems. During his Ph.D. studies, he was a graduate teaching assistant for a graduate level engineering mathematics class and an upper level undergraduate class on feedback control systems.